STUDIES OF ROTAXANES CONSISTING OF 1,10-PHENANTHROLINE-BASED MACROCYCLES AND PLATINUM-CAPPED POLYYNEDIYL COMPLEXES: A STERIC AND DYNAMIC APPROACH TO INSULATED MOLECULAR WIRES

A Dissertation

by

ZUZANA BARANOVÁ

Submitted to the Office of Graduate and Professional Studies of
Texas A&M University
in partial fulfillment of the requirements for the degree of

DOCTOR OF PHILOSOPHY

Chair of Committee,	John A. Gladysz
Committee Members,	Donald J. Darensbourg
	John P. Fackler
	François P. Gabbaï
	Timothy Jacobs
Head of Department,	Simon W. North

December 2017

Major Subject: Chemistry

ABSTRACT

The objective of this dissertation is the steric insulation of diplatinum polyynediyl complexes through the assembly of [2]rotaxanes, a class of mechanically interlocked molecules (MIMs). The synthetic approach to these MIMs takes advantage of the active metal template employing a copper(I) iodide macrocycle complex as the site of an oxidative homocoupling of two terminal alkynes. Various structural modifications to the macrocyclic precursors are explored.

Firstly the chemistry of polyynes emphasizing diplatinum polyynediyl complexes as model compounds for molecular wires is presented. Previous studies have revealed a need for steric insulation of these unsaturated linkers and earlier attempts in this direction are introduced. Here, a new approach to the steric insulation employing rotaxanes will be discussed.

Following, a series of macrocyclic precursors to rotaxanes equipped with a 1,10-phenanthroline moiety available for coordination with copper(I) iodide are described. These complexes serve as active templates in the syntheses of rotaxanes. Various α,ω-bis(bromoalkoxy)aryl precursors are prepared via Williamson ether synthesis. These dibromides are condensed with 2,9-bis(4-hydroxyphenyl)-1,10-phenanthroline in the presence of K_2CO_3 to give the corresponding 31- to 35-membered macrocycles. When the macrocycles are treated with copper(I) iodide, mononuclear 1:1 complexes form in which the metal cation chelates to the nitrogen donor atoms of the phenanthroline moiety. The crystal structures of the synthesized macrocycles and their corresponding complexes are determined and analyzed in the context of DFT calculations and rotaxanes that can be formed by treatment of the copper(I) iodide macrocycle complexes with terminal alkynes (e.g., macrocycle dimensions, void volumes). The copper and

iodide atoms significantly protrude from the least squares plane of the phenanthroline moiety (0.46-0.63 Å and 1.65-2.07 Å).

Lastly, the syntheses of various platinum-capped polyynediyl containing rotaxanes by the oxidative homocoupling of the monoplatinum polyynyl complexes *trans*-$(C_6F_5)(p\text{-}tol_3P)_2Pt(C{\equiv}C)_{n/2}H$ in the presence of copper(I) iodide adducts of the 1,10-phenanthroline-based macrocycles 2,9-(1,10-phenanthrolinediyl)(*p*-$C_6H_4O(CH_2)_6O)_2$(1,3-C_6H_4) or 2,9-(1,10-phenanthrolinediyl)(*p*-$C_6H_4O(CH_2)_6O)_2$(2,7-naphthdiyl) are described. All of these MIMs feature a $Pt(C{\equiv}C)_nPt$ unit (n = 4, 6, 8) that is threaded through the macrocycle. Crystal structures of three rotaxanes are determined and analyzed in detail, particularly in regards to geometric perturbations and the degree of steric C_{sp} chain insulation. The ^1H NMR spectra show a number of noteworthy shielding effects. UV-visible spectra exhibit negligible electronic interactions between the $Pt(C{\equiv}C)_nPt$ axles and macrocycles, although cyclic voltammetry data suggest rapid reactions following oxidation. Finally, the findings of this work are summarized and a perspective on potential future studies in this area is offered.

DEDICATION

To my grandparents

ACKNOWLEDGEMENTS

I would like to thank my committee chair, Dr. John A. Gladysz, for allowing me to work in this stunning field of chemistry and for setting an example. I am grateful to my committee members, Dr. Donald J. Darensbourg, Dr. John P. Fackler, Jr., Dr. François P. Gabbaï, and Dr. Timothy Jacobs for the questions that encouraged my deeper understanding and curiosity in the topic and for an overall support of my growth in the direction I chose. To Dr. Fackler goes an extra special thank you that dates back to my summer undergraduate research experience in his laboratory which set me strong for this journey; I appreciate his long-lasting support since. To the committee member substitute, Dr. Edward Vargo, thank you for his precious time and quick response.

Thanks also go to my friends and colleagues in the Department of Chemistry. An immense gratitude goes to all those who made my time at Texas A&M University an enriching experience of personal and professional growth and who let me be part of this great community. Thank you to Dr. Sebastien Gauthier for making the first successful stab at this project and leaving the promising field to me for further explorations and to Dr. Nancy Weisbach for her ready help and expertise when the project was swimming in shallow waters. To Andreas Ehnbom, thank you for enriching this project with his computational skills. Special appreciation goes to my immediate collaborators who contributed to this dissertation with the fruits of their labor and who allowed me to practice my early mentoring skills: Madhav Neupane, J. Scott Villalpando, Hashem Amini, Sydney C. Garrett, and Alex J. Kalin.

Thanks to the many instrumental scientists for their assistance: Dr. Joseph Reibenspies and Dr. Nattamai Bhuvanesh (crystallography); Dr. Howard Williams, Dr.

Greg Wylie, and Dr. Doug Elliott (NMR); Dr. Vanessa Santiago (MS). I am also grateful to Bryan Stewart whose versatile help was instrumental throughout these times.

My profound gratitude goes also to the teaching labs of FYP and OCLP and all my teaching mentors, staff, fellow TAs, and my students who have taught me more than any textbooks could. You were a crucial catalyst in this academic reaction mixture and a constant reminder of my desired product.

To the many groupmates who have shared with me various amounts of time, laughter, language lessons, cross-cultural stories … NMR tubes … in and out of the lab, thank y'all; in chronological order: Rodrigo Ramírez, Dr. José Nuñez, Bret Macha, Jan Breitenfeld, Mario Babuněk, Dr. Yoshi Kobayashi, Roy Herrmann, Brett Anderson, Dr. Sandip Dey, Chon Qiu, Dr. Zhiqiang Liu, Dr. Bjoern Beele, Diego Sierra-Castro, Michael Williams, Christian Sindlinger, Dr. Debaprasad Mandal, Yi Shu, Dr. Juan Guerrero-Leal, Ann Sullivan, Paul Zeits, Xi Wang, Tiezheng Jia, Dr. Markus Jurisch, Adebomi Ikotun, Ryan Laddusaw, Dr. Fazlur Rahman, Laura Ramirez, Robert Tuba, Melissa Clough, Alejandra Gómez, Yiwei Zhu, Sri Moturu, Eric Kleihege, Elham Tabei, Casie Hilliard, Kyle Lewis, Katherine Cude, Dr. Coralie Thomas, Dr. Hamid Safaei, Lauren Freeman, Dr. Cheng-Pan Zhang, Dr. Deeb Taher, Matthew Wesson, Dr. Zhuoqiang Zhou, Ryan Sarkisian, Dr. Zhenxing Xi, Tathagata Mukherjee, Dr. Michael Stollenz, Prasmit Devkota, Ayush Upreti, Dr. Soumik Biswas, Ashley Cardenal, Dr. Anil Kumar, Georgette Lang, Stephen Bierschenk, Tianyi Zhang, Che Wu, Amartya Sharma, Anik Banerjee, Subrata Ghosh, Sugam Kharel, Alex Estrada, Dr. Hemant Joshi, Quang Luu, Billy Maximuck, Scheherzad Alvi, Dr. Gong Chu.

Tobias, I am forever grateful for your patience, love and understanding. Your encouragement and windshield kept me upright through the crosswinds with a perfect lead out to that uphill sprint finish.

Finally, thank you to my parents, Ľubica Baranová and Peter Baran, for your love and encouragement. You have instilled in me the sense of curiosity and perseverance and provided me with plenty of opportunities for discovery. You raised me surrounded by our big loving family sharing the most important powers across four generations. Thank you also to my brother Matej, specially for teaching me to see the brighter side in everything and everyone.

To all whose names are inscribed on these pages as well as the many whose names are not spelled out here please know that your kindness has left a longer-lasting impact on me than these visible ink prints.

CONTRIBUTORS AND FUNDING SOURCES

Contributors

This work was supervised by a dissertation committee consisting of Dr. John A. Gladysz (advisor), Dr. Donald J. Darensbourg, Dr. John P. Fackler, Jr., and Dr. François P. Gabbaï of the Department of Chemistry, and Dr. Timothy Jacobs of the Department of Mechanical Engineering.

The work presented in section 2 was completed by the student, in collaboration with Hashem Amini, Madhav Neupane, Sydney C. Garrett, and Andreas Ehnbom of the Department of Chemistry.

The work presented in section 3 was completed by the student, in collaboration with Hashem Amini, Dr. Nancy Weisbach, Dr. Sébastien Gauthier of the Department of Chemistry.

The computational data referenced in section 3 was completed in collaboration with Hiba Sahnoune and Dr. Jean-François Halet of the Institut des Sciences Chimiques de Rennes, UMR 6226, CNRS-Université de Rennes 1, F-35042 Rennes, France.

All crystal structures were determined by the crystallographers (Dr. Nattamai Bhuvanesh or Dr. Joseph H. Reibenspies of the Department of Chemistry), although all crystallographic data were interpreted by the student.

Funding Sources

This work was made possible in part by the US National Science Foundation under the Grant Numbers CHE-0719267, CHE-1153085, and CHE-1566601.

NOMENCLATURE

δ	chemical shift
ε	molar extinction coefficient
λ	wavelength
ν	stretching mode (IR)
ρ	density
$\{^1H\}$	proton decoupled
Å	Angstrom
Anal.	Analysis
Ar	aryl
aq	aqueous
br	broad
Bu	butyl
Calcd.	Calculated
d	doublet (NMR), days
dec	decomposition
DMSO	dimethylsulfoxide
Et	ethyl
EtOAc	ethyl acetate
equiv	equivalent
h	hour
Hz	hertz
i	*ipso*

$^{i}J_{jk}$	scalar coupling constant for coupling of nucleus j with nucleus k through i bonds
IR	infrared
K	Kelvin
kcal	kilocalorie
M	mol/Liter
m	multiplet (NMR), medium (IR)
m	*meta*
Me	methyl
MeOH	methanol
mg	milligram
min	minutes
mol	mole
mmol	millimole
mp	melting point
NMR	nuclear magnetic resonance
o	*ortho*
p	*para*
Ph	phenyl
phen	1,10-phenanthroline
ppm	parts per million
q	quartet
R	organic group
rt	room temperature
s	singlet (NMR), strong (IR)

t	triplet
temp	temperature
TLC	thin layer chromatography
tol	tolyl
THF	tetrahydrofuran
TMEDA	tetramethylethylenediamine
UV	ultraviolet
v/v	volume/volume
vis	visible
w	weak

TABLE OF CONTENTS

LIST OF FIGURES

LIST OF SCHEMES

LIST OF TABLES

1. INTRODUCTION

1.1 Polyynes

The chemistry of carbon and its many allotropes shown in Figure 1.1 has always fascinated scientists and also the general population (e.g. diamonds, buckyballs). Studies of fullerenes and more recently graphene have been recognized with two Nobel Prizes: in 1996 for chemistry to Curl,[1] Kroto,[2] and Smalley[3] and in 2010 for physics to Geim[4] and Novoselov,[5] respectively. Besides these captivating allotropes of sp^3 and sp^2 hybridized carbon, a sp hybridized analogue, namely carbyne, was proposed in 1885 by Adolf von Baeyer.[6]

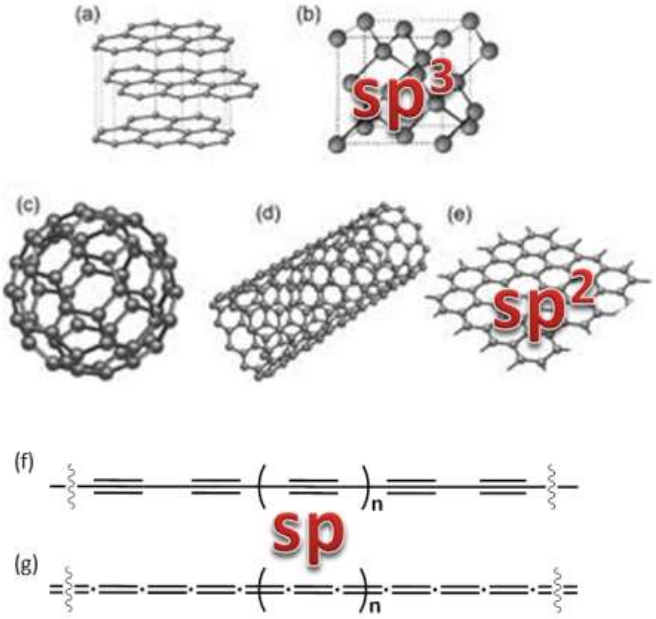

Figure 1.1. Allotropes of carbon are portrayed with their corresponding hybridization: (a) graphite, (b) diamond, (c) buckminsterfullerene, (d) carbon nanotube (CNT), (e) graphene, (f) carbyne, (g) cumulene.

Carbyne, being still somewhat of an elusive compound, is the protagonist of numerous interdisciplinary studies. From theoreticians to material scientists, claims of the mythical carbyne have been coming from all directions. Geologists claimed the presence of carbyne in a form of a natural mineral (chaoite) in the Ries crater in Bavaria while astronomers claimed the detection carbyne in interstellar dust. Physicists and material/condensed matter scientists have made predictions about the properties of carbyne through models and calculations.[7] Although scarce in nature, polyynyl substructures have been found even in biological species. The first report of what is today recognized as an acetylenic compound (Figure 1.2, left) dates back to 1826.[8] However, it was Arnaud in 1892[9] who got the credit for the first characterization of a natural acetylene, namely tariric acid (Figure 1.2, right).[10]

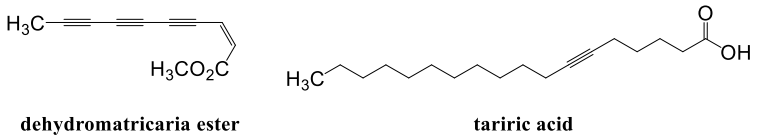

dehydromatricaria ester **tariric acid**

Figure 1.2. The first reports of naturally occurring acetylenic compounds: dehydromatricaria ester (left; extracted from the essential oil of *Artemisia vulgaris*) and tariric acid (right).

Recently, a multidisciplinary group of researchers reported the formation of linear carbon chains inside carbon nanotubes (CNTs) of up to 6,000 consecutive atoms (Figure 1.3).[11] Chemists have taken to studies of synthetically accessible polyynyl and cumulenic containing structures as finite approximations to the mythical carbyne.[12]

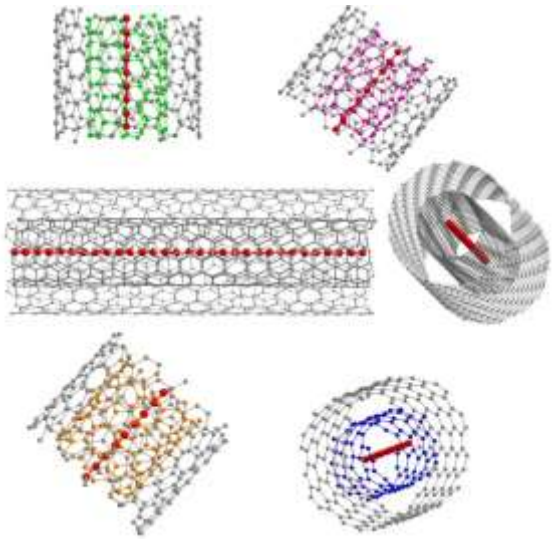

Figure 1.3. Carbynes of finite lengths have been incorporated into CNTs through a high temperature and high vacuum annealing procedure.[11]

The field of acetylene compounds was inscribed into the synthetic chemistry literature as early as 1869 by an early pioneer Carl Glaser who discovered the coupling reaction of terminal acetylenes in the presence of copper(I) chloride/ammonia species and oxygen as depicted in Scheme 1.1 (top).[13] In 1962, Hay reported a practical modification introducing a more universally soluble copper(I) species[14] (Scheme 1.1 bottom) and numerous alternative methods of alkyne coupling have been described since.[15]

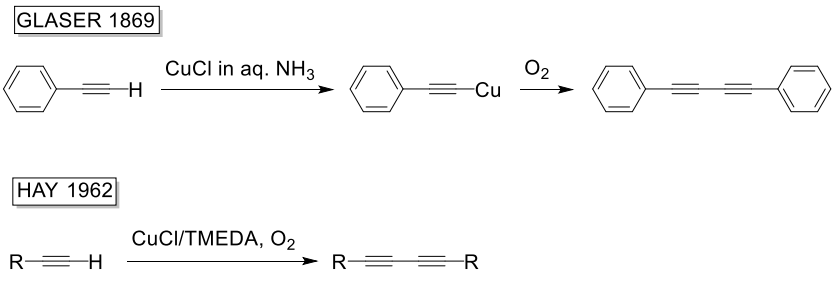

Scheme 1.1. Some of the commonly used alkyne homocoupling methods.

Inherently, the stabilities of polyynyl and polyynediyl compounds decrease with increasing length of the alkynyl fragment.[16] It has been established though that there is a dependence between the stability and the nature or bulkiness of the endgroup of polyynediyls. Earlier studies of polyynes featured endgroups with a tetrahedral geometry, such as quaternary carbon or silicon derivatives. As shown in Figure 1.4, polyynes of up to 24 *sp* carbons with *t*-Bu endgroups (**(*t*-Bu)C_{24}(*t*-Bu)**) were synthesized by Walton in 1972; a longer, 32 *sp* carbon molecule capped with Et_3Si (TES) (**TESC_{32}TES**) was partially characterized in the presence of impurities from the starting material.[17] Other notable endgroups included dendrimers (Hirsch; **[D3]C_{20}[D3]**) and adamantyl (Tykwinski; **AdC_{20}Ad**). The longest polyynediyl to date, reported by Tykwinski, is a purely organic molecule consisting of 44 consecutive *sp* carbons and the supertrityl engroups (Tr*, tris(3,5-di-(*t*-butyl)phenyl)methyl; **Tr*C_{44}Tr***; Figure 1.4 bottom).[18]

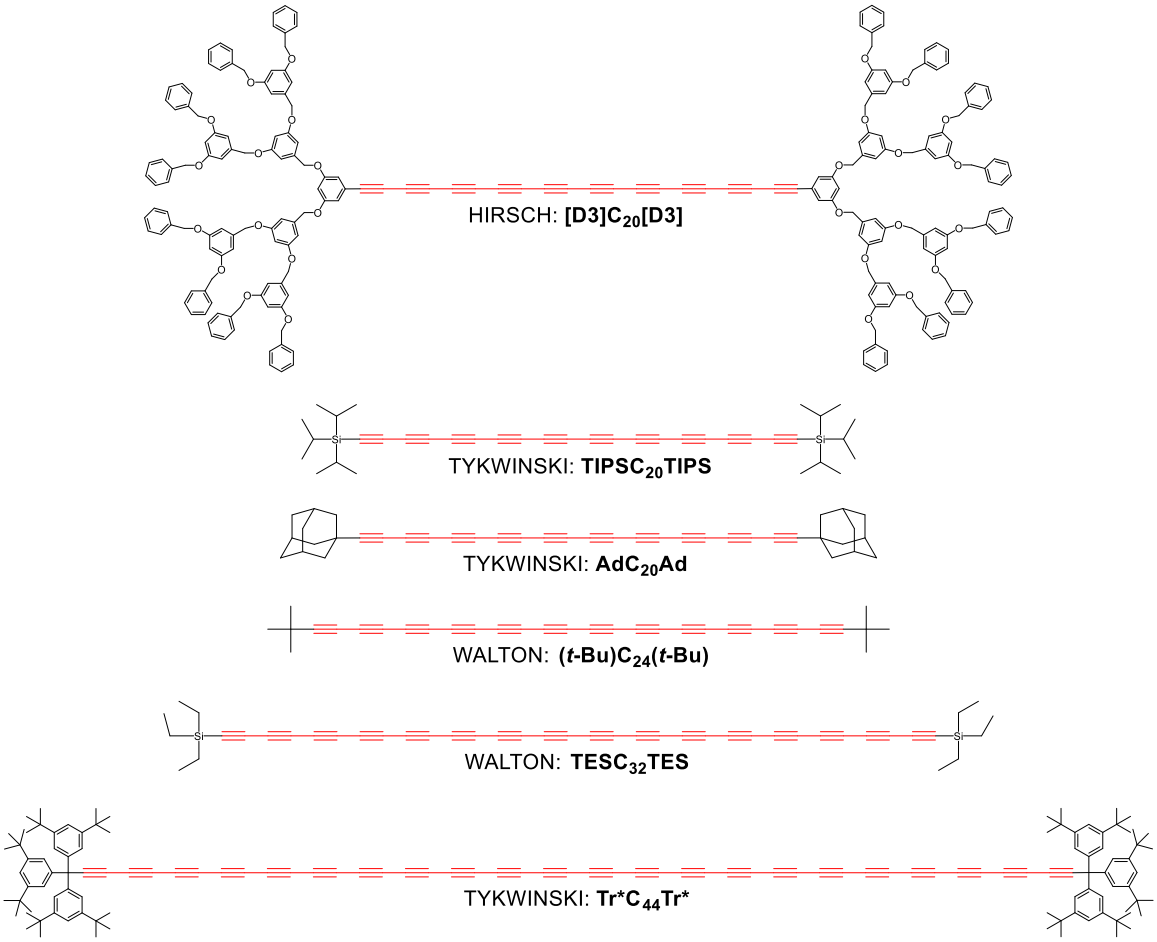

Figure 1.4. Polyynes with various organic and silyl endgroups.

The electronegative nature of the polyynediyl linker sets it up for high affinity to even larger electropositive endgroups, such as metal cations. The introduction of organometallic endgroups by Gladysz[16] and others[19] has proved to increase the stabilities of the polyynediyl spacer versus their organic analogues, in part due to the typically larger coordination sphere of the metal cation versus its carbon or silicon analogues. Electrochemical studies of these systems, commonly termed molecular wires,[20] have revealed many interesting phenomena.

Further insulation of these unsaturated linkers was sought and Gladysz has employed two strategies to this task: 1. steric insulation[21] and 2. phase separation,[22] as depicted by the structures **I** and **II**, respectively, in Figure **1.6**. This dissertation work took on yet another approach to sterically insulate such compounds by threading a platinum-capped polyynediyl complex through a macrocycle resulting in an assembly termed a rotaxane.

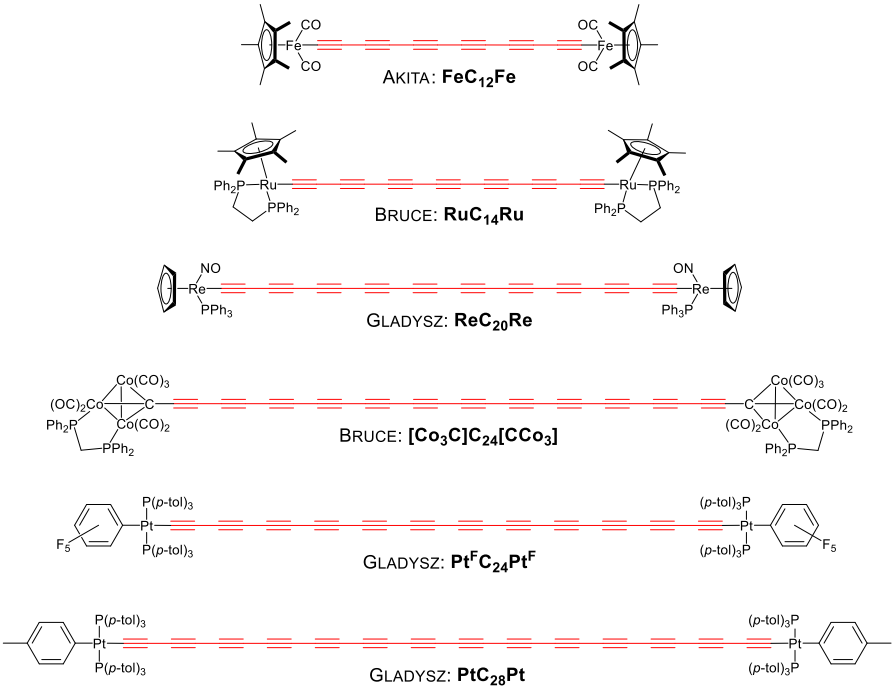

Figure 1.5. Polyynes with various transition metal endgroups.

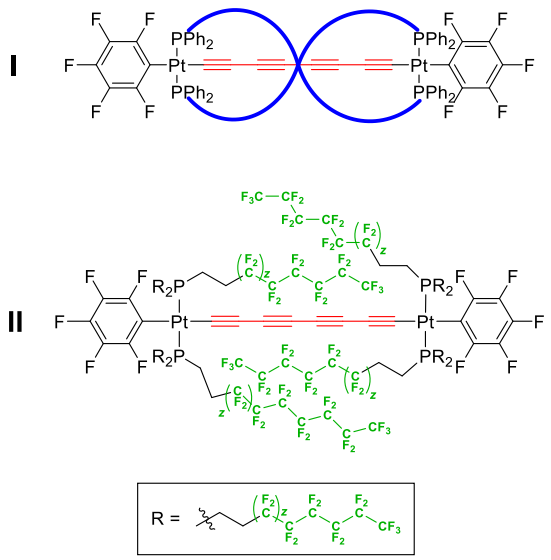

Figure 1.6. Different steric approaches to increasing the stabilities of polyynes: sterically demanding double helix as a result of termini spanning diphosphine alkyl ligands (**I**) and biphasic separation from perfluoroalkyl phosphine containing endgroups (**II**).

1.2 Rotaxanes

A rotaxane, derived from Latin words rota (wheel) and axis (axle), consists of a dumbbell like axle with large endgroups (stoppers) threaded through a ring shaped entity. The voluminous endgroups, relative to the size of the ring cavity, prevent the axle from slipping out. Thus, these building blocks of the rotaxane are restrained within each other's vicinity through non-covalent bonding, also termed mechanically interlocked molecules (MIMs).[23] These molecules are dynamic in the sense of various motions of the ring along the axle (translation), or around the axle (pirouetting) as illustrated in Figure 1.7.

The larger field of MIMs, which includes other intriguing architectures, such as catenanes or knots, resembles a molecular playground filled with tiny machinery. The foundation for this field was laid down by the Nobel Laureates of 1987 (Donald J. Cram, Jean-Marie Lehn, and Charles J. Pedersen)[24,2526] and more recently Nobel Prizes

awarded to Jean-Pierre Sauvage, Sir J. Fraser Stoddart, and Bernard L. Feringa in 2016 celebrating "the design and synthesis of molecular machines".[27,28,29]

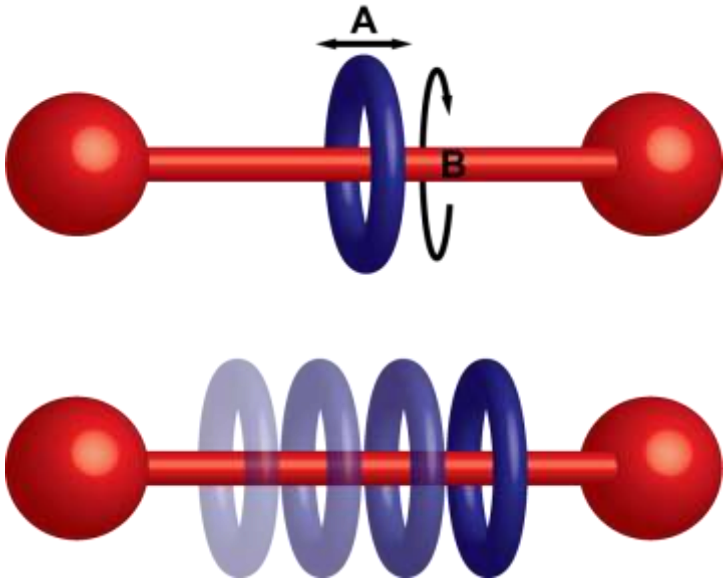

Figure 1.7. Rotaxanes can experience two types of motion: (A) longitudinal displacement and (B) pirouetting.

Four strategies are commonly employed in the synthesis of rotaxanes: 1. capping, 2. clipping, 3. slipping, and 4. active metal template (Scheme 1.2). The capping and clipping routes rely on a molecular recognition between the axle and the rotor (or a fragment of either one). Weak intermolecular forces of those reactants and the law of entropy keep the reactants in equilibrium with the prearranged pseudorotaxane (an incomplete rotaxane mechanically able to dissociate). Upon the addition of the missing link, either the stoppers/endgroups of the axle (capping) or the missing segment of the rotor (clipping), the preassembled species proceed towards the completion of the interlocked structure. Alternatively, one can combine the fully assembled axle and the rotor and heat the mixture just enough to allow for an expansion of the rotor which can

then slip over the stoppers of the axle. Then, upon cooling of the threaded species, the rotor would be trapped in the rotaxane form. Ultimately, the active template benefits from a transition metal complex which is formed within the cavity of the macrocyclic rotor which should contain the appropriate donor atoms. This complex is then employed as a coupling agent for the two half-axles. The position of the metal cation within the macrocyclic cavity aids in directing the half-axles to thread through the macrocycle, thus resulting in an interlocked species rather than just a plain coupling product.

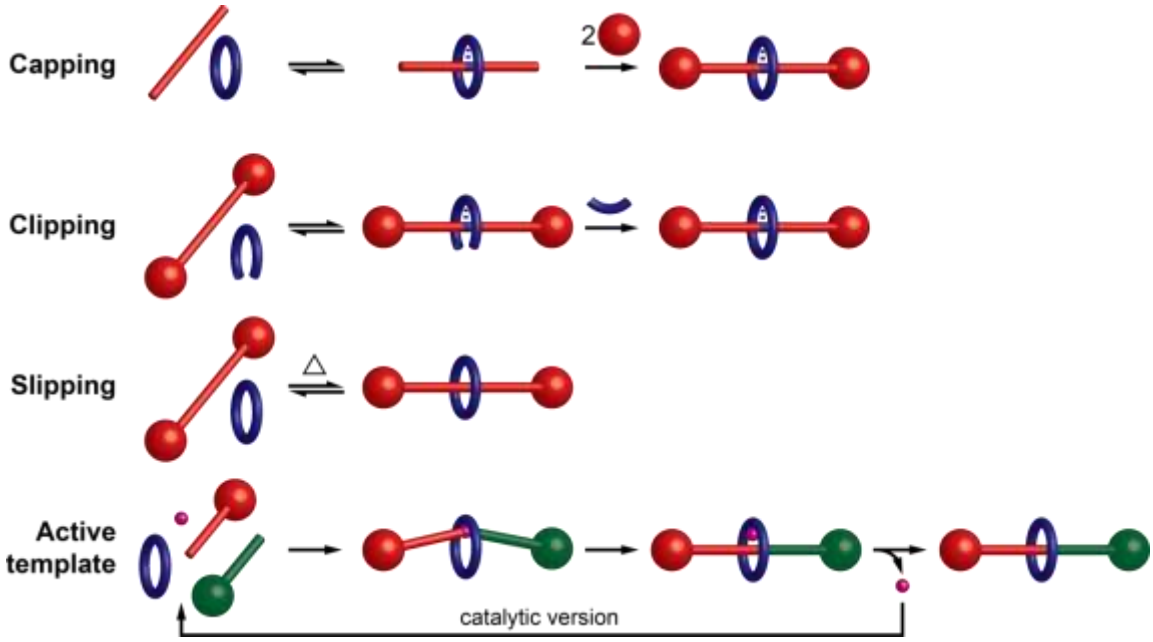

Scheme 1.2. Four synthetic approaches to the formation of rotaxanes: capping, clipping, slipping, and active template.

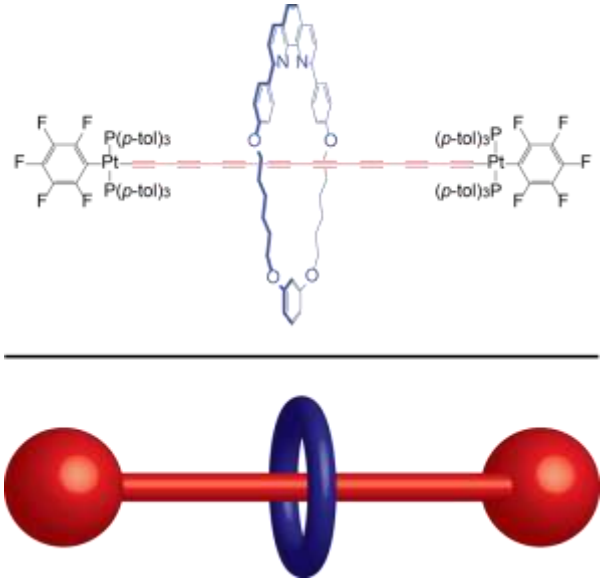

Figure 1.8. A structure (top) and a cartoon (bottom) representation of target rotaxanes.

An earlier example of a diyne-containing rotaxane by Saito and coworkers was an inspiration for our project.[30] We adopted the template approach for the formation of rotaxanes involving an alkyne homocoupling reaction under Hay conditions.[14] A macrocyclic copper(I) complex acts both as a coupling mediator and a directing point for the axle fragments threading through the rotor.

This research aims to study the formation of rotaxanes with platinum-capped polyynediyl axles (Figure 1.8) and to further understand the properties and stability of the polyynes. The construction of such supramolecular scaffolds requires (1) suitable building blocks (macrocycles, section 2 and axle, section 3) and (2) favorable reaction conditions (section 3) as presented in this work. The structural characterization of these compounds relies heavily on multinuclear NMR spectroscopy and crystallography.

1.3 References

(1) Curl, R. F. *Angew. Chem. Int. Ed. Engl.* **1997**, *36*, 1566-1576; *Angew. Chem.* **1997**, *109*, 1636–1647.

(2) Kroto, H. *Angew. Chem. Int. Ed. Engl.* **1997**, *36*, 1578-1593; *Angew. Chem.* **1997**, *109*, 1648-1664.

(3) Smalley, R. E. *Angew. Chem. Int. Ed. Engl.* **1997**, *36*, 1594-1601; *Angew. Chem.* **1997**, *109*, 1666–1673.

(4) Geim, A. K. *Angew. Chem. Int. Ed.* **2011**, *50*, 6966-6985; *Angew. Chem.* **2011**, *123*, 7100-7122.

(5) Novoselov, K. S. *Angew. Chem. Int. Ed.* **2011**, *50*, 6986-7002; *Angew. Chem.* **2011**, *123*, 7123-7141.

(6) Baeyer, A. *Ber. Dtsch. Chem. Ges.* **1885**, *18*, 2269-2281.

(7) Liu, M. J.; Artyukhov, V. I.; Lee, H.; Xu, F. B.; Yakobson, B. I. *ACS Nano* **2013**, *7*, 10075-10082.

(8) See: Gildemeister, E.; Hoffmann, F. *Die ätherischen Öle*, 3rd ed, Vol. 3; Schimmel & Co. AG: Leipzig, 1931; p 1018.

(9) Arnaud, M. A. *Compt. Rend.* **1892**, *114*, 79.

(10) (a) Shi Shun, A. L. K.; Tykwinski, R. R. *Angew. Chem. Int. Ed.* **2006**, *45*, 1034-1057; *Angew. Chem.* **2006**, *118*, 1050-1073. (b) Bohlmann, F.; Burkhardt, H.; Zdero, C. *Naturally Occurring Acetylenes*; Academic Press: New York, 1973; p 1.

(11) Shi, L.; Rohringer, P.; Suenaga, K.; Niimi, Y.; Kotakoski, J.; Meyer, J. C.; Peterlik, H.; Wanko, M.; Cahangirov, S.; Rubio, A.; Lapin, Z. J.; Novotny, L.; Ayala, P.; Pichler, T. *Nature Mater.* **2016**, *15*, 634-640.

(12) Diederich, F. *Nature* **1994**, *369*, 199-207.

(13) Glaser, C. *Ber. Dtsch. Chem. Ges.* **1869**, *2*, 422-424.

(14) Hay, A. S. *J. Org. Chem.* **1962**, *27*, 3320-3321.

(15) (a) Eglinton, G.; Galbraith, A. R. *J. Chem. Soc.* **1959**, 889-896. (b) Cadiot, P.; Chodkiewicz, W. in *Chemistry of Acetylenes*; Viehe, H. G., Ed.; Marcel Dekker: New York, 1969, 597-647. (c) Armitage, J. B.; Jones, E. R. H.; Whiting, M. C. *J. Chem. Soc.* **1951**, 44-47. (d) Bohlmann, F. *Chem. Ber.* **1951**, *84*, 785-794. (e) Armitage, J. B.; Cook, C. L.; Jones, E. R. H.; Whiting, M. C. *J. Chem. Soc.* **1952**, 2010-2014. (f) Cook, C. L.; Jones, E. R. H.; Whiting, M. C. *J. Chem. Soc.* **1952**, 2883-2891.

(16) (a) Dembinski, R.; Bartik, T.; Bartik, B.; Jaeger, M.; Gladysz, J. A. *J. Am. Chem. Soc*. **2000**, *122*, 810-822. (b) Mohr, W.; Stahl, J.; Hampel, F.; Gladysz, J. A. *Chem. Eur. J.* **2003**, *9*, 3324-3340. (c) Zheng, Q.; Bohling, J. C.; Peters, T. B.; Frisch, A. C.; Hampel, F.; Gladysz, J. A. *Chem. Eur. J.* **2006**, *12*, 6486-6505.

(17) (a) Eastmond, R.; Walton, D. R. M.; Johnson, T. R. *Tetrahedron* **1972**, *28*, 4601-4616. (b) Johnson, T. R.; Walton, D. R. M. *Tetrahedron* **1972**, *28*, 5221-5236.

(18) Chalifoux, W. A.; Tykwinski, R. R. *Nature Chem.* **2010**, *2*, 967-971.

(19) Representative literature since 2013 involving polyynediyl complexes: (a) Burgun, A.; Gendron, F.; Sumby, C. J.; Roisnel, T.; Cador, O.; Costuas, K.; Halet, J.-F.; Bruce, M. I.; Lapinte, C. *Organometallics* **2014**, *33*, 2613-2627. (b) Lissel, F.; Schwarz, F.; Blacque, O.; Riel, H.; Lörtscher, E.; Venkatesan, K.; Berke, H. *J. Am. Chem. Soc.* **2014**, *136*, 14560-14569. (c) Hau, S. C. K.; Mak, T. C. W. *J. Am. Chem. Soc.* **2014**, *136*, 902-905. (d) Bruce, M. I.; Cole, M. L.; Ellis, B. G.; Gaudio, M.; Nicholson, B. K.; Parker, C. R.; Skelton, B. W.; White, A. H. *Polyhedron* **2015**, *86*, 43-56. (e) Oerthel, M.-C.; Yufit, D. S.; Fox, M. A.; Bryce, M. R.; Low, P. J. *Organometallics* **2015**, *34*, 2395-

2405. (f) Cook, T. D.; Natoli, S. N.; Fanwick, P. E.; Ren, T. *Organometallics* **2016**, *35*, 1329-1338.

(20) (a) *Molecular Wires: From Design to Properties;* de Cola, L., Ed.; Topics in Current Chemistry, Vol. 257; Springer: Berlin, 2005. (b) Lehn, J.-M. *Supramolecular Chemistry*; VCH: Weinheim, 1995; p 106.

(21) (a) Stahl, J.; Mohr, W.; de Quadras, L.; Peters, T. B.; Bohling, J. C.; Martín-Alvarez, J. M.; Owen, G. R.; Hampel, F.; Gladysz, J. A. *J. Am. Chem. Soc.* **2007**, *129*, 8282-8295. (b) de Quadras, L.; Bauer, E. B.; Mohr, W.; Bohling, J. C.; Peters, T. B.; Martín-Alvarez, J. M.; Hampel, F.; Gladysz, J. A. *J. Am. Chem. Soc.* **2007**, *129*, 8296-8309. (c) de Quadras, L.; Bauer, E. B.; Stahl, J.; Zhuravlev, F.; Hampel, F.; Gladysz, J. A. *New. J. Chem.* **2007**, *31*, 1594-1604. (d) Owen, G. R.; Stahl, J.; Hampel, F.; Gladysz, J. A. *Chem. Eur. J.* **2008**, *14*, 73-87. (e) Horn, C. R.; Martín-Alvarez, J. M.; Gladysz, J. A. *Organometallics* **2002**, *21*, 5386-5393.

(22) Clough, M. C.; Fiedler, T.; Bhuvanesh, N.; Gladysz, J. A. *J. Organomet. Chem.* **2015**, *812*, 34-42.

(23) Bruns, C. J.; Stoddart, J. F. *The Nature of the Mechanical Bond: From Molecules to Machines*; John Wiley & Sons, Inc.: Hoboken, NJ, 2017.

(24) Cram, D. J. *Angew. Chem. Int. Ed. Engl.* **1988**, *27*, 1009-1020; *Angew. Chem.* **1988**, *100*, 1041-1052.

(25) Lehn, J.-M. *Angew. Chem. Int. Ed. Engl.* **1988**, *27*, 89-112; *Angew. Chem.* **1988**, *100*, 91-116.

(26) Pedersen, C. J. *Angew. Chem. Int. Ed. Engl.* **1988**, *27*, 1021-1027; *Angew. Chem.* **1988**, *100*, 1053-1059.

(27) Sauvage, J.-P. *Nobel Prize Lecture* **2016**, http://www.nobelprize.org/nobel_ prizes/chemistry/laureates/2016/sauvage-facts.html

(28) Stoddart, Sir J. F. *Nobel Prize Lecture* **2016**, https://www.nobelprize.org/ nobel_ prizes/chemistry/laureates/2016/stoddart-facts.html

(29) Feringa, B. *Nobel Prize Lecture* **2016**, https://www.nobelprize.org/nobel_ prizes/chemistry/laureates/2016/feringa-facts.html

(30) Saito, S.; Takahashi, E.; Nakazono, K. *Org. Let.* **2006**, *8*, 5133-5136.

2. SYNTHESES, STRUCTURAL STUDIES, AND COPPER IODIDE COMPLEXES OF MACROCYCLES DERIVED FROM WILLIAMSON ETHER SYNTHESES INVOLVING 2,9-BIS(4-HYDROXYPHENYL)-1,10-PHENANTHROLINE, α,ω-DIBROMIDES, AND RESORCINOL OR 2,7-DIHYDROXYNAPHTHALENE*

2.1 Introduction

Macrocycles and metal complexes thereof play ubiquitous roles in supramolecular chemistry and particularly the syntheses of mechanically interlocked molecules (MIMs),[1] a descriptor that encompasses catenanes, rotaxanes, and knots.[2,3] Variables such as shape, conformational flexibility, and the nature and position of any functional groups can influence the efficacy of these processes and the properties of the topologically novel products.[4]

In ongoing efforts, we have sought to synthesize rotaxanes derived from diplatinum polyynediyl axles and 2,9-disubstituted 1,10-phenanthroline based macrocycles, as exemplified by **III** in Scheme 2.1.[5,6] The former building blocks have been the subject of extensive studies in our laboratory.[7] Such complexes are normally accessed by oxidative homocouplings of the corresponding monoplatinum polyynyl complexes under "Hay conditions" (O_2, CuCl/TMEDA).[8]

* Reprinted with permission from "Syntheses, Structural Studies, and Copper Iodide Complexes of Macrocycles Derived from Williamson Ether Syntheses Involving 2,9-Bis(4-hydroxyphenyl)-1,10-phenanthroline, α,ω-Dibromides, and Resorcinol or 2,7-Dihydroxynaphthalene" Baranová, Z.; Amini, H.; Neupane, M.; Garrett, S. C.; Ehnbom, A.; Bhuvanesh, N.; Reibenspies, J. H.; Gladysz, J. A. *Aust. J. Chem.* **2017**, *70*, 373-386. Copyright 2017 by CSIRO Publishing.

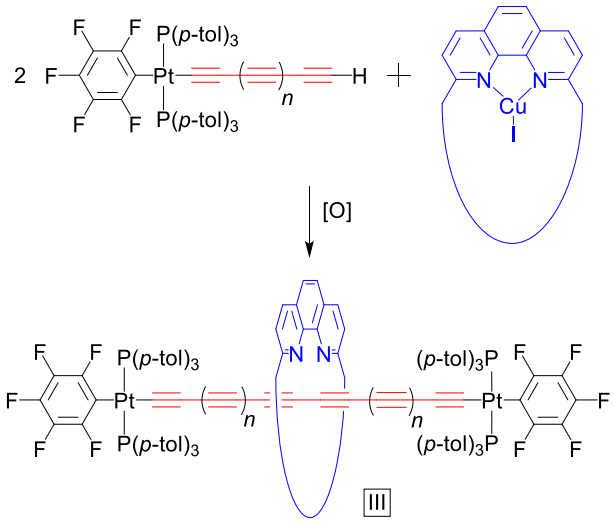

Scheme 2.1. Rotaxanes derived from diplatinum polyynediyl axles and 1,10-phenanthroline based macrocycles (**III**).

The latter building blocks have been applied to MIMs by several groups.[4d,9,10,11] The inspiration for our studies came from Saito, who employed CuI complexes with polyether $O(CH_2)_mO$ (m = 6, 8) and m-C_6H_4 linkages to prepare rotaxanes with organic 1,3-butadiyne axles, as exemplified by **IV** in Figure 2.1.[10] The copper(I) 1,10-phenanthroline precursors represent an embodiment of the "active metal template" strategy popularized by Leigh.[4d,e,g,12] In this scenario, the copper is believed to template the coupling partners onto opposite faces of the macrocycle complex, facilitating subsequent elimination to a rotaxane topology.

Accordingly, in this paper we describe (1) the preparations of three new and one previously reported 2,9-disubstituted 1,10-phenanthroline based macrocycles, (2) syntheses of the corresponding CuI complexes, (3) crystallographic and density functional theory (DFT) characterization of the macrocycles and complexes, and (4) analyses of their geometries, particularly features relevant to the derived rotaxanes and their proposed mechanism of formation. Portions of the preparative chemistry, and one

crystal structure, have been described in the supporting information of preliminary communications.[5,6] The resulting rotaxanes will be the subject of a subsequent full paper.[13]

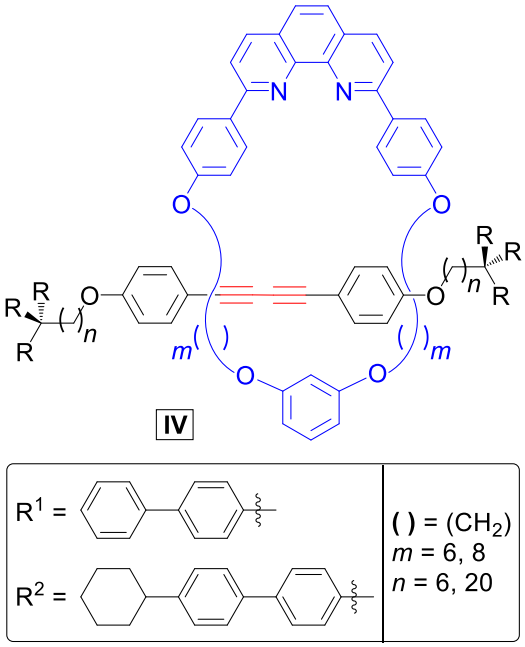

Figure 2.1. Rotaxanes synthesized by Saito via oxidative homocouplings of organic terminal monoalkynes using CuI complexes of 1,10-phenanthroline containing macrocycles.[10e,f,14]

2.2 Results

2.2.1. Syntheses of Macrocycles. We sought a family of polyether macrocycles based upon a 2,9-disubstituted 1,10-phenanthroline "northern hemisphere" and a dihydroxyarene derived "southern hemisphere" with a gradation of dimensions and conformational degrees of freedom. The first target molecule had been previously reported by Saito as part of his study in Figure 2.1,[10a] and his route is summarized in

Scheme 2.2 (top).[14] The "northern" precursor **1** was easily accessed via a two step sequence starting with 1,10-phenanthroline and 4-lithioanisole.[9a,15]

As with all of the preparations described below, the "southern" precursor was accessed by a classical Williamson ether synthesis. Thus, resorcinol, 1,6-dibromohexane, and K_2CO_3 were allowed to react in acetone (1.0:3.0:2.5 mol ratio). A chromatographic workup gave the diether **2a**[16] as a white solid in 47% yield. Next **1**, **2a**, and K_2CO_3 were combined in wet DMSO (1.0:1.0:14.0 mol ratio). Workup gave **3a**, which features a thirty three membered ring, in 59% yield as an air stable white solid (lit: 41%).[14] In cases where we improved on reported yields and/or acquired new NMR data, experimentals are provided in the appendix A.

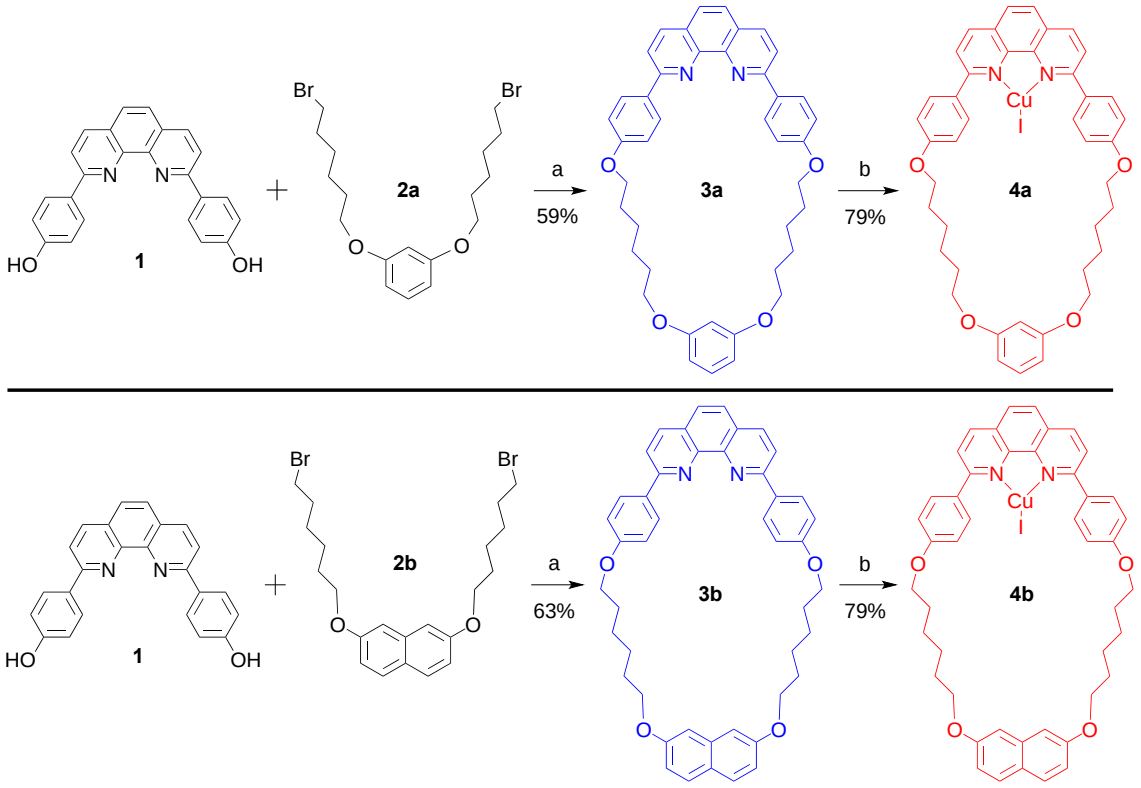

Scheme 2.2. Syntheses of macrocycles containing $O(CH_2)_6O$ tethers and copper complexes thereof: (a) K_2CO_3, wet DMSO; (b) CuI, CH_3CN/CH_2Cl_2.

In the second target molecule, the previously unknown **3b** (Scheme 2.2, bottom), the resorcinol unit of **3a** was replaced by a 2,7-dihydroxynaphthalene moiety, thereby expanding the macrocycle cavity to a thirty five membered ring. A reaction of 2,7-dihydroxynaphthalene, 1,6-dibromohexane, and K_2CO_3 (1.0:3.0:2.5 mol ratio) in acetone gave the "southern" precursor **2b** as a white solid in 41% yield. A condensation of **1**, **2b**, and K_2CO_3 (1.0:1.0:14.0 mol ratio) then afforded **3b** as a white solid in 63% yield. The products **2b**, **3b**, and all other new compounds below, were characterized by NMR spectroscopy (^1H and $^{13}C\{^1H\}$) and microanalyses, as summarized in the experimental section.

In the third target molecule, the previously unknown **3c** (Scheme 2.3, top), the $(CH_2)_6$ linker of **3a** was replaced by a more rigid *p*-xylylyl moiety, which maintains a thirty three membered ring. A reaction of resorcinol, 1,4-bis(bromomethyl)benzene, and K_2CO_3, similar to the analogous condensations above, gave the "southern" precursor **2c** in 21% yield. This was followed by a reaction of **1**, **2c**, and K_2CO_3 (1.0:1.0:3.0 mol ratio), which afforded **3c** in 39% yield. In the final target molecule, **3d** (Scheme 2.3, bottom), the *p*-xylylyl moiety of **3c** was replaced by a *m*-xylylyl linkage, reducing the ring size to thirty one. An analogous sequence gave **2d** in 38% yield, and **3d** in 22% yield. All of the new organic compounds in Scheme 2.3 were white or pale yellow solids.

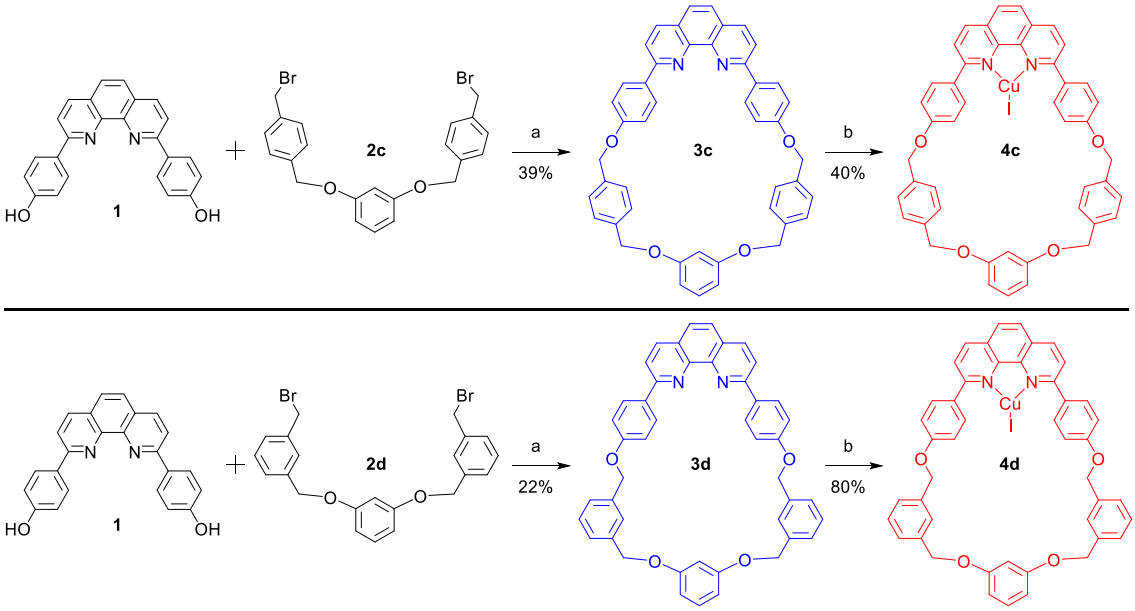

Scheme 2.3. Syntheses of macrocycles containing $OCH_2C_6H_4CH_2O$ tethers and copper complexes thereof: (a) K_2CO_3, wet DMSO; (b) CuI, CH_3CN/CH_2Cl_2.

A number of related macrocyclic targets were contemplated. In the course of a vigorous program involving undergraduate research students, additional "southern" precursors were prepared (e.g., analogs of **2c**,**d** derived from 2,7-dihydroxynaphthalene). For a variety of reasons, the macrocycle syntheses were not consummated. Nonetheless, new compounds that were completely characterized are included in the SI.

2.2.2. Copper(I) Complexes. In accord with the preparative goals in the introduction, copper(I) complexes of the macrocycles were sought. Various copper halides were screened, and copper(I) iodide proved to be optimal in terms of yield and product stability. Thus, as shown in Schemes 2.2 and 2.3, CH_2Cl_2 solutions of the macrocycles **3a-d** were combined with acetonitrile solutions of CuI. Workups gave the 1:1 adducts **4a-d** in 40-80% yields as orange to yellow crystals or solids that were stable to >100 °C.[17]

2.2.3. Spectroscopic and Structural Characterization. The NMR properties of the macrocycles (experimental section) were routine, but nonetheless important in providing baselines for shielding effects in the corresponding rotaxanes.[5,13] The CuI complexes with the xylylyl linkers, **4c**,**d**, were poorly soluble, and good quality spectra could not be obtained. With **4a**,**b**, some of the phenanthroline ^{1}H NMR signals were 0.1-0.2 ppm downfield from those of **3a**,**b**. In contrast, the *p*-C_6H_4 protons that were *ortho* to the phenanthroline shifted upfield by 0.27-0.34 ppm. Some signals also broadened.

Crystals of **3a** and the solvates **3b**·2$CHCl_3$ and **3c**·CH_2Cl_2 could be grown as described in the experimental section. The crystal structures were solved as summarized in Table 1 and the experimental section. Out of all the solvate molecules, only one of the two associated with **3b** could be accurately modeled. The others were removed during refinement using standard protocols, and thus do not appear in the headers in the tables. Key metrical parameters are given in Table 3.[18]

Table 2.1. Crystallographic data for **3a-c**.

	3a[a]	**3b**·$CHCl_3$[b]	**3c**[b]
empirical formula	$C_{42}H_{42}N_2O_4$	$C_{47}H_{45}Cl_3N_2O_4$	$C_{46}H_{34}N_2O_4$
formula weight	638.78	808.20	678.75
Temperature [K]	110(2)	110(2)	110(2)
Wavelength [Å]	1.54178	1.54178	0.71073
diffractometer	Bruker D8 GADDS	Bruker D8 GADDS	Bruker APEX 2
crystal system	Monoclinic	Triclinic	Orthorhombic
space group	*Pn*	*P*-1	*Pnma*
unit cell dimensions			
a [Å]	10.8861(9)	8.4044(4)	11.058(4)
b [Å]	15.6003(14)	14.7638(6)	23.613(8)
c [Å]	11.1600(10)	18.7247(8)	14.049(5)
α [°]	90	73.146(3)	90
β [°]	112.189(4)	85.741(3)	90
γ [°]	90	81.873(3)	90
volume [$Å^3$]	1754.9(3)	2199.89(17)	3668(2)
Z	2	2	4
ρ_{calcd} [Mg/m^3]	1.209	1.220	1.229
μ [mm^{-1}]	0.611	2.231	0.078
F (000)	680	848	1424
crystal size [mm^3]	0.11 × 0.10 × 0.03	0.12 × 0.06 × 0.04	0.12 × 0.10 × 0.07
range for data collection	2.83 to 59.99	2.47 to 60.00	2.34 to 24.99

Table 2.1 continued

	3a[a]	**3b**·$CHCl_3$[b]	**3c**[b]
index ranges	$-12 \le h \le 12$	$-9 \le h \le 9$	$-13 \le h \le 13$
	$-17 \le k \le 17$	$-16 \le k \le 16$	$-28 \le k \le 28$
	$-12 \le l \le 12$	$-21 \le l \le 21$	$-16 \le l \le 16$
reflections collected	24948	43282	33095
independent reflections	4608 [R(int) = 0.0499]	6414 [R(int) = 0.0526]	3286 [R(int) = 0.0504]
max. and min. transmission	0.9819 and 0.9358	0.9161 and 0.7756	0.9945 and 0.9906
data / restraints / parameters	4608 / 2 / 434	6414 / 6 / 525	3286 / 0 / 239
goodness-of-fit on F^2	0.990	1.064	1.032
final R indices [$I>2\sigma(I)$]	R1 = 0.0364	R1 = 0.0519	R1 = 0.0401
	wR2 = 0.0832	wR2 = 0.1416	wR2 = 0.1031
R indices (all data)	R1 = 0.0459	R1 = 0.0619	R1 = 0.0486
	wR2 = 0.0900	wR2 = 0.1477	wR2 = 0.1073
largest diff. peak & hole [$eÅ^{-3}$]	0.208 and –0.193	0.605 and –0.553	0.169 and –0.155

[a]This structure was described earlier in reference 6. [b]Some or all of the solvate molecules were removed during refinement as described in the experimental section.

Table 2.2. Key crystallographic distances [Å], angles [°] and void volumes [Å^3] for **3a-c** and **4a-c**.

	3a[a]	**3b**·$CHCl_3$[b]	**3c**[b]	**4a**·CH_2Cl_2	**4b**·$2CHCl_3$	**4c**·CH_2Cl_2
Cu-N1	-	-	-	2.077(3)	2.053(3)	2.059(3)
Cu-N2	-	-	-	2.051(4)	2.054(2)	2.072(3)
Cu-I	-	-	-	2.4306(7)	2.4347(8)	2.4325(5)
C1-N1	1.330(3)	1.332(3)	1.321(2)	1.346(6)	1.346(6)	1.338(4)
N1-C5	1.357(3)	1.358(3)	1.3581(19)	1.373(6)	1.373(6)	1.369(5)
C5-C9	1.448(4)	1.457(4)	1.450(3)	1.437(6)	1.437(6)	1.443(5)
C9-N2	1.356(3)	1.364(3)	1.3581(19)	1.370(5)	1.370(5)	1.358(5)
N2-C12	1.338(3)	1.336(3)	1.321(2)	1.349(5)	1.349(5)	1.344(5)
C12-C13	1.481(4)	1.483(4)	1.492(2)	1.478(6)	1.473(5)	1.474(6)
C16-O1	1.373(3)	1.365(3)	1.3808(18)	1.364(5)	1.361(4)	1.375(5)
O1-C19	1.438(3)	1.442(3)	1.432(2)	1.443(5)	1.433(4)	1.427(5)
C19-C20	1.501(4)	1.505(4)	1.507(2)	1.494(6)	1.493(5)	1.506(6)
C20-C21	1.511(4)	1.529(4)	1.390(2) / 1.382(2)[c]	1.530(6)	1.521(5)	1.390(6) / 1.390(6)[c]
C21-C22	1.508(4)	1.533(4)	1.386(2) / 1.393(2)[c]	1.528(6)	1.515(5)	1.387(6) / 1.383(6)[c]
C22-C23	1.533(4)	1.528(4)	1.390(2) / 1.389(2)[c]	1.528(6)	1.522(4)	1.394(6) / 1.391(6)[c]
C23-C24	1.503(4)	1.505(4)	1.513(2)	1.501(6)	1.509(4)	1.495(6)
C24-O2	1.435(3)	1.445(3)	1.4243(18)	1.439(5)	1.431(4)	1.432(5)
O2-C25	1.385(3)	1.367(3)	1.3761(17)	1.376(5)	1.367(4)	1.381(5)
C29-O3	1.376(3)	1.372(3)	1.3761(17)	1.374(5)	1.365(4)	1.368(5)
O3-C31	1.440(3)	1.431(3)	1.4243(18)	1.445(5)	1.427(4)	1.445(5)
C31-C32	1.505(4)	1.507(4)	1.513(2)	1.513(6)	1.516(5)	1.505(6)
C32-C33	1.521(3)	1.534(4)	1.390(2) / 1.389(2)[c]	1.516(6)	1.517(4)	1.399(6) / 1.371(6)[c]
C33-C34	1.528(4)	1.516(4)	1.386(2) / 1.393(2)[c]	1.528(6)	1.528(4)	1.374(6) / 1.398(6)[c]
C34-C35	1.524(3)	1.521(4)	1.390(2) / 1.382(2)[c]	1.526(6)	1.502(4)	1.408(6) / 1.366(6)[c]
C35-C36	1.500(4)	1.501(4)	1.507(2)	1.524(6)	1.520(4)	1.503(6)
C36-O4	1.437(3)	1.439(3)	1.432(2)	1.437(5)	1.451(3)	1.440(5)

Table 2.2 continued

	3a[a]	**3b**·$CHCl_3$[b]	**3c**[b]	**4a**·CH_2Cl_2	**4b**·$2CHCl_3$	**4c**·CH_2Cl_2
O4-C37	1.375(3)	1.364(3)	1.3808(18)	1.369(5)	1.363(3)	1.359(5)
C1-C40	1.485(4)	1.485(4)	1.492(2)	1.478(6)	1.484(4)	1.479(5)
N1-Cu-I	-	-	-	134.06(10)	136.54(7)	139.10(8)
N2-Cu-I	-	-	-	140.52(10)	137.40(8)	133.86(8)
N1-Cu-N2	-	-	-	82.46(14)	83.17(10)	82.55(12)
C1-N1-Cu	-	-	-	131.5(3)	131.5(2)	131.3(3)
C5-N1-Cu	-	-	-	107.6(3)	109.0(2)	108.0(2)
C9-N2-Cu	-	-	-	108.8(3)	109.3(2)	108.0(2)
C12-N2-Cu	-	-	-	131.0(3)	130.7(2)	130.4(3)
C1-N1-Cu	-	-	-	131.5(3)	131.5(2)	131.3(3)
C5-N1-Cu	-	-	-	107.6(3)	109.0(2)	108.0(2)
C9-N2-Cu	-	-	-	108.8(3)	109.3(2)	108.0(2)
C12-N2-Cu	-	-	-	131.0(3)	130.7(2)	130.4(3)
C1-N1-C5	118.8(2)	118.7(2)	119.25(12)	119.1(4)	118.3(3)	119.1(3)
C9-N2-C12	118.9(2)	118.6(2)	119.25(12)	118.6(4)	118.5(3)	119.4(3)
C16-O1-C19	118.8(2)	119.55(19)	117.72(12)	118.1(3)	118.7(3)	117.8(3)
C24-O2-C25	117.1(2)	117.10(19)	118.10(11)	117.7(3)	116.7(2)	116.2(3)
C29-O3-C31	117.5(2)	116.59(19)	118.10(11)	116.6(3)	118.7(2)	117.6(3)
C36-O4-C37	117.4(2)	117.89(19)	117.72(12)	118.7(3)	116.7(2)	120.8(3)
sum of angles N-Cu-N/I	-	-	-	357.04	357.11	355.51
Cu···phen[d]	-	-	-	0.630	0.462	0.603
I···phen[d]	-	-	-	1.989	1.651	2.067
CuIN1N2 vs. phen[e]	-	-	-	29.14	24.33	30.97

Table 2.2 continued

	3a[a]	**3b**·$CHCl_3$[b]	**3c**[b]	**4a**·CH_2Cl_2	**4b**·$2CHCl_3$	**4c**·CH_2Cl_2
N1-C1-C40-C41	–29.24	–19.32	–19.97	26.05	37.92	21.94
N2-C12-C13-C18	–18.75	10.67	19.97	–26.01	–32.40	–24.83
Plane A vs. phen[f]	19.04	9.59	20.97	23.09	32.67	26.65
Plane B vs. phen[f]	59.62	25.29	1.09	33.50	2.28	44.68
Plane C vs. phen[f]	30.43	19.59	20.97	–22.78	–36.02	–20.48
O1···O4	10.365	11.136	10.372	10.747	10.850	10.746
O2···O3	4.768	7.316	4.634	4.758	7.350	4.849
N1···O3	10.746	13.105	10.223	10.670	12.619	11.996
N2···O2	10.642	12.714	10.223	11.534	12.201	10.496
N1···C_{distal}[g]	10.886	12.696	9.519 (8.487)	11.618	11.955	11.953
N2···C_{distal}[g]	11.054	12.634	9.519 (8.487)	11.751	12.119	11.451
O1···O3	10.331	12.644	10.176	7.835	12.998	11.509
O2···O4	8.426	11.574	10.176	11.834	10.230	8.036
C17···C42	6.630	6.935	6.379	6.808	7.110	6.710
Void volume	20	474	354	344	482	155

[a]This structure was described earlier in reference 6. [b]Some or all of the solvate molecules were removed during refinement as described in the experimental section. [c]The second value is for the atoms C211, C221, C331, and C341 of the same arene ring. [d]The distance from the $C_{12}N_2$ least squares plane. [e]The angle defined by the CuIN1N2 least squares plane and the $C_{12}N_2$ least squares plane. [f]These represent the absolute values of the angles between the $C_{12}N_2$ least squares plane and those of the arene ring containing C13-C16 (plane A), the dihydroxyarene (plane B), and the arene ring containing C37-C40 (plane C). [g]The carbon atoms distal to N1 and N2 are taken as C29 and C25 (**3a**), C301 and C303 (**3b**), and C25 and C29 (C26 and C28, values in parenthesis) (**3c**), respectively; the analogous atoms are employed for **4a**-**c**.

Table 2.3. Crystallographic data for **4a-c**.

	4a·CH_2Cl_2	**4b**·$2CHCl_3$	**4c**·CH_2Cl_2
empirical formula	$C_{43}H_{44}Cl_2CuIN_2O_4$	$C_{48}H_{46}Cl_6CuIN_2O_4$	$C_{47}H_{36}Cl_2CuIN_2O_4$
formula weight	914.14	1118.01	954.12
Temperature [K]	110(2)	110(2)	110(2)
Wavelength [Å]	1.54178	0.71073	0.71073
diffractometer	Bruker D8 GADDS	Bruker APEX 2	Bruker APEX 2
crystal system	Monoclinic	Triclinic	Triclinic
space group	*P*2(1)/c	*P*-1	*P*-1
unit cell dimensions			
a [Å]	13.8010(10)	11.888(3)	7.5981(2)
b [Å]	8.1146(7)	14.904(4)	12.5786(2)
c [Å]	35.376(2)	14.905(4)	21.1089(4)
α [°]	90	112.140(7)	82.7280(10)
β [°]	95.820(4)	102.331(7)	88.1180(10)
γ [°]	90	91.793(6)	80.7170(10)
volume [$Å^3$]	3941.3(5)	2371.5(11)	1974.86(7)
Z	4	2	2
ρ_{calcd} [Mg/m^3]	1.541	1.566	1.605
μ [mm^{-1}]	8.536	1.495	1.519
F (000)	1856	1128	960
crystal size [mm^3]	0.13 × 0.11 × 0.02	0.18 × 0.12 × 0.12	0.20 × 0.12 × 0.03
range for data collection	3.22 to 60.00	1.767 to 27.527	2.39 to 27.56

Table 2.3 continued

	4a·CH_2Cl_2	**4b**·$2CHCl_3$	**4c**·CH_2Cl_2
index ranges	$-15 \le h \le 15$	$-15 \le h \le 15$	$-9 \le h \le 9$
	$-9 \le k \le 8$	$-19 \le k \le 19$	$-16 \le k \le 16$
	$-39 \le l \le 39$	$-19 \le l \le 19$	$-27 \le l \le 27$
reflections collected	46266	24046	43439
independent reflections	5803 [R(int) = 0.0878]	10655 [R(int) = 0.0365]	9006 [R(int) = 0.0624]
max. and min. transmission	0.8478 and 0.4033	0.7456 and 0.6326	0.9858 and 0.8325
data / restraints / parameters	5803 / 0 / 478	10655 / 0 / 559	9006 / 9 / 530
goodness-of-fit on F^2	1.038	1.051	1.034
final R indices [$I>2\sigma(I)$]	R1 = 0.0442	R1 = 0.0401	R1 = 0.0470
	wR2 = 0.1104	wR2 = 0.0856	wR2 = 0.1131
R indices (all data)	R1 = 0.0545	R1 = 0.0591	R1 = 0.0723
	wR2 = 0.1141	wR2 = 0.0948	wR2 = 0.1282
largest diff. peak & hole [$eÅ^{-3}$]	1.034 and –0.836	0.993 and –0.596	1.746 and –1.821

Thermal ellipsoid plots and space filling representations of **3a-c** are provided in Figure 2.2. The molecular structure of **3c** exhibited a mirror plane that bisected the resorcinol and central phenanthroline rings, consistent with the space group *Pnma*. In contrast, **3a**,**b** crystallized in chiral conformations with both enantiomers in the unit cell. In a break with the usual custom, the symmetry equivalent atoms of **3c** were assigned different numbers (see Figure 2.3),[18] similar to those of the analogous atoms of **3a**,**b**. This facilitates comparisons of metrical parameters (Table 3). The oxygen lone pairs in **3b**,**c**, and most of those in **3a**, were *exo* to the macrocycle cavity, analogous to the dominant orientation in the corresponding rotaxanes.[5]

Crystals of solvates of the corresponding CuI complexes – **4a**·CH_2Cl_2, **4b**·2$CHCl_3$, and **4c**·CH_2Cl_2 – were also obtained. These structures were similarly solved, giving the representations in Figure 2.3 and metrical parameters in Table 3.[18] In all cases, the solvent molecules could be accurately modeled. The oxygen lone pairs in **4b**,**c**, and most of those in **4a**, were *exo* to the macrocycle cavity, paralleling the situation with **3a-c**.

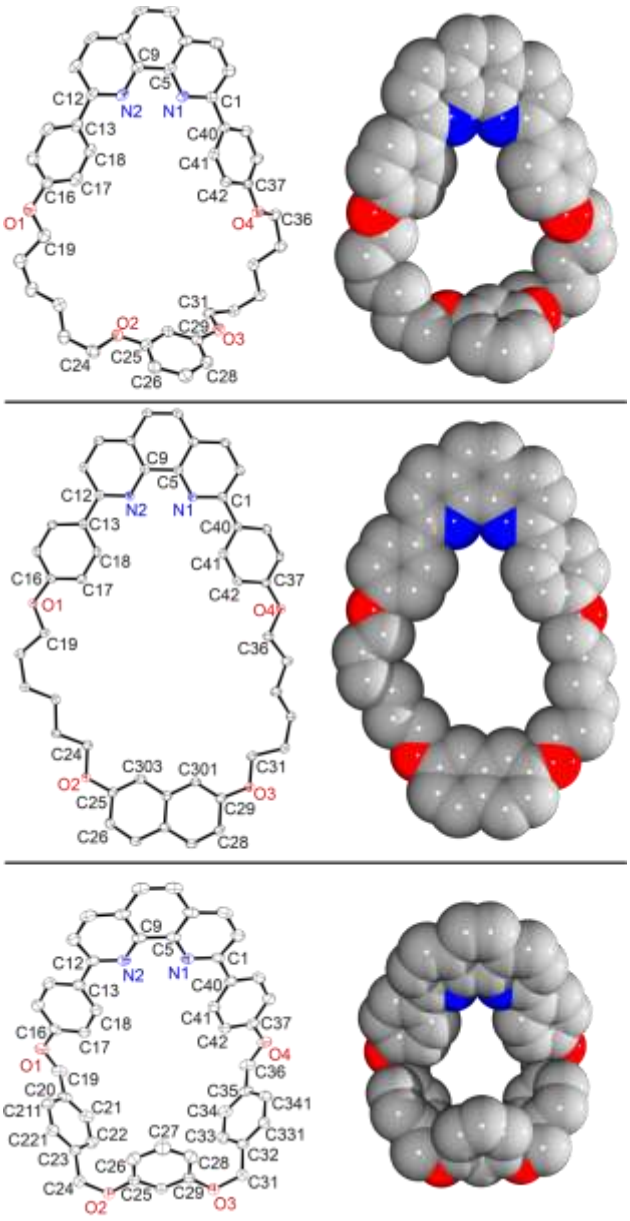

Figure 2.2. Thermal ellipsoid plots (50% probability levels) and space filling representations of the molecular structures of **3a** (top), **3b** (middle), and **3c** (bottom). With the last two, solvent molecules are either omitted or removed during refinement. Hydrogen atoms are omitted for clarity.

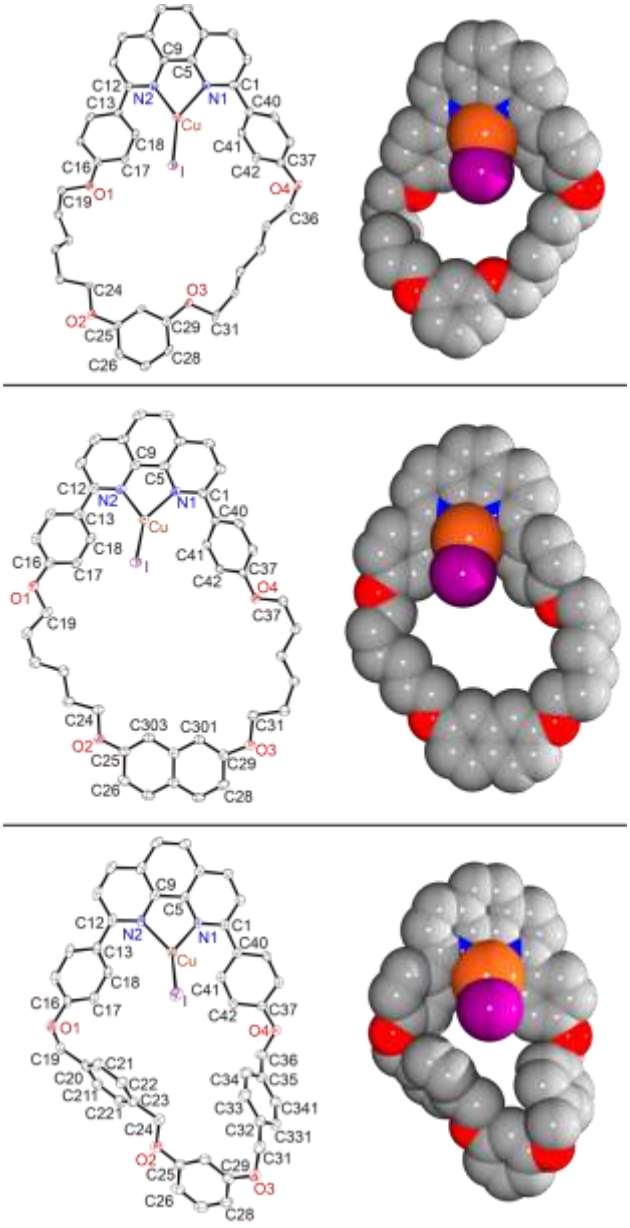

Figure 2.3. Thermal ellipsoid plots (50% probability levels) and space filling representations of the molecular structures of **4a** (top), **4b** (middle), and **4c** (bottom); solvate molecules and hydrogen atoms are omitted for clarity.

The copper atoms of **4a-c** exhibited distorted trigonal planar coordination geometries, with the N-Cu-N bond angles (82.46(14)°-83.17(10)°) much lower than the

N-Cu-I bond angles (133.86(8)°-140.52(10)°). The sums of the three bond angles (355.51°-357.11°; see Table 3) were close to 360°. In all cases, the CuI moieties markedly protruded on one side of the planar $C_{12}N_2$ 1,10-phenanthroline units. The distances of the copper and iodide atoms from the phenanthroline least squares planes ranged from 0.46 to 0.63 Å and 1.65 to 2.07 Å, respectively (Table 3). The $CuIN_2$ units were roughly planar (maximum atomic deviations from least squares planes: 0.14-0.15 Å). Thus, the folding angles with the phenanthroline least squares planes were calculated, and ranged from 24.3° to 31.0°.

In all of the solvates that could be crystallographically modeled (**3b** in part; **4a-c**), solvent was found in the macrocycle cavity. Some representative motifs are depicted in Figure 2.4. In no cases were any bonding interactions with the macrocycle or CuI moiety apparent. In **3a**, intermolecular N···HC hydrogen bonds were present, as depicted in the Appendix A (Figure A.2). In **4a-c**, π-π stacking interactions were also obvious (Figures A.3-A.5). Additional analyses of the structural data are provided in the discussion section.

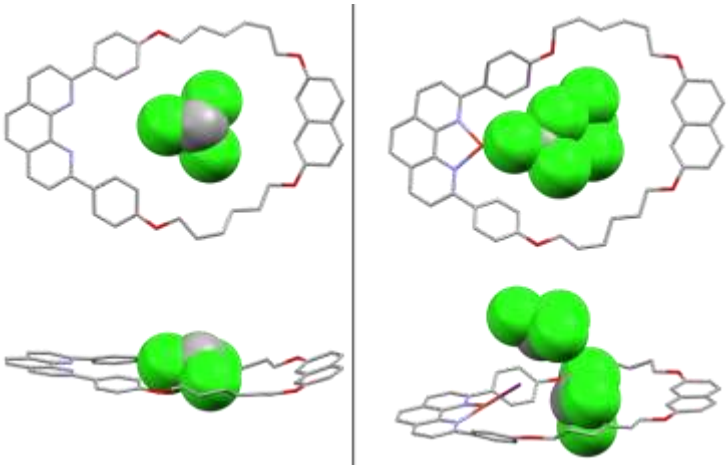

Figure 2.4. Representations of crystal structures with solvate molecules included: left, **3b** with one of two $CHCl_3$ molecules; right, **4b** with both $CHCl_3$ molecules.

The compounds in Figures 2.2 and 2.3 were also modeled by DFT calculations as described in the experimental section. In all cases, the optimized geometries very closely corresponded to those found in the crystals. The similarities were so striking that these data are simply represented by overlays in the Appendix A (Figures A.8-A.10). In particular, the CuI moieties were again displaced from the planes of the 1,10-phenanthroline units. The distances of the copper and iodide atoms from the least squares planes ranged from 0.51 to 0.57 Å and 1.69 to 1.86 Å, respectively (folding angles 24.4°-26.8°).

Analogous calculations were also carried out with **3d** and **4d**, and analogs of **3c**,**d** and **4c**,**d** in which the "southern hemispheres" were derived from 2,7-dihydroxynaphthalene as opposed to resorcinol (species not yet synthesized). Given the excellent agreement of theory and experiment with **3a-c** and **4a-c**, it can be anticipated that the optimized structures closely model those of the real compounds. These data are presented in the Appendix A.

2.3 Discussion

The syntheses of **2a-d** and **3a-d** (Schemes 2.2-2.3) illustrate the versatility of the Williamson ether synthesis for the assembly of macrocycles. With regard to **2a-d** and related bis(ethers) described in the SI, the highest yields were obtained in reactions with the aliphatic α,ω-dibromide $Br(CH_2)_6Br$ (41-47%), as opposed to xylylyl dibromides (21-38%). Possible side reactions include the participation of both primary bromide atoms in ether formation, and the generation of dimeric macrocycles derived from two molecules of **1** and two of **2a-d**. A weak peak of twice the theoretical mass (+1) was noticed in the mass spectrum of **3d**. However, no trace of a second species could be found by NMR.

The structures of **4a-c** differ significantly from those obtained from 1,10-phenanthroline and CuI. These educts react in acetonitrile to give a dimeric complex with bridging iodide ligands and a distorted tetrahedral coordination environment.[19] The copper atoms lie in the plane of the phenanthroline ligand; the Cu-I vectors define angles of 53.5°-65.6° (two different solvates) with the plane. These features are closely modeled by DFT calculations analogous to those described above (59.7° plane/Cu-I vector angle; D_{2h} symmetry). A solvothermal synthesis affords a polymeric allotrope with a zig-zag $(\text{Cu-I-Cu-I-})_n$ chain and similar tetrahedral copper coordination geometry.[20]

However, the CuI adduct of 2,9-bis(*t*-butyl)-1,10-phenanthroline crystallizes as a monomer, with the copper and iodine atoms markedly removed from the plane of the phenanthroline ligand (0.72 Å and 2.32 Å vs. 0.46-0.63 Å and 1.65-2.07 Å for **4a-c**).[21] Thus, 2,9-substituents can sterically interfere with in-plane copper coordination. This has to be a disadvantage for rotaxane syntheses, as it renders it more difficult for the two alkynyl coupling partners to effectively interact from opposite faces of the phenanthroline ring. These data suggest that macrocycles based upon 3,8-disubstituted 1,10 phenanthrolines may be more effective for "active metal template" rotaxane syntheses.[12]

Some measure of the void space available within the macrocycles of **3a-c** and **4a-c** was desired. This was quantified, *after removing all solvate molecules*, with the program Mercury,[22] using a probe volume of 7.24 $Å^3$, a probe radius of 1.2 Å, and a grid spacing of 0.7 Å. The macrocycle **3a**, the crystal of which did not incorporate any solvent, exhibited a void volume of 20 $Å^3$ (Table 3). In contrast, **3b** and **3c**, which crystallized as a disolvate and monosolvate, respectively, gave void volumes of 474 and 354 $Å^3$. With **4a-c**, the largest void volume was associated with the complex that

crystallized as a disolvate (**4b**, 482 $Å^3$). The voids in the complexes that were monosolvates were smaller (**4a**, 344 $Å^3$; **4c**, 155 $Å^3$).

Although the void volumes show a correlation to the number of solvent molecules originally present, they also reflect various geometric parameters such as the dimensions of rigid units, folding, and the efficiency of crystal packing. For example, the "southern hemisphere" of **3b** features a 2,7-dioxanaphthalene moiety, the oxygen-to-oxygen "wingspan" of which is 7.316 Å (O2···O3). Accordingly, **3b** exhibits a larger void volume than **3a**,**c**, which contain 1,3-OC_6H_4O moieties with oxygen-to-oxygen wingspans of 4.768-4.634 Å (35-37% decrease). However, the rigor of this comparison is compromised by the different number of solvent molecules present in each crystal.

Interestingly, in the "northern hemisphere", the O1···O4 wingspan associated with the C_6H_4O groups bound to the phenanthroline is 7% greater in **3b** than **3c** (11.136 vs. 10.372 Å). These and a variety of related data are compiled in the final series of entries in Table 3. For example, the distances between the nitrogen donor atoms in **3b** and opposing aromatic carbon atoms in the "southern hemisphere" are 12.696-12.634 Å. The corresponding distances for **3a**,**c** are 11.054-10.886 Å (13-14% contraction) and 9.519-8.487 Å (25-33% contraction), respectively.[23] The corresponding distances in the CuI complexes **4a-c** are much more comparable (Table 3).

In the crystal, **3c** exhibits a motif that could be likened to the perimeter of a hard taco shell (Figure 2.5, left). These stack on top of each other, thus creating extended tunnel-like voids as represented in Figure 2.6. In contrast, in the corresponding complex **4c**, which is also a monosolvate, the CuI moiety intrudes into the less severely folded macrocycle cavity. Accordingly, the void volume decreases by more than 50% (344 vs. 155 $Å^3$). Regardless, despite the intrinsically qualitative nature of these void volume comparisons, they help to define the dimensional limits that can be realized with these

macrocycles in MIMs. Additional crystallographic features of ancillary interest are illustrated in Figures in the Appendix A.

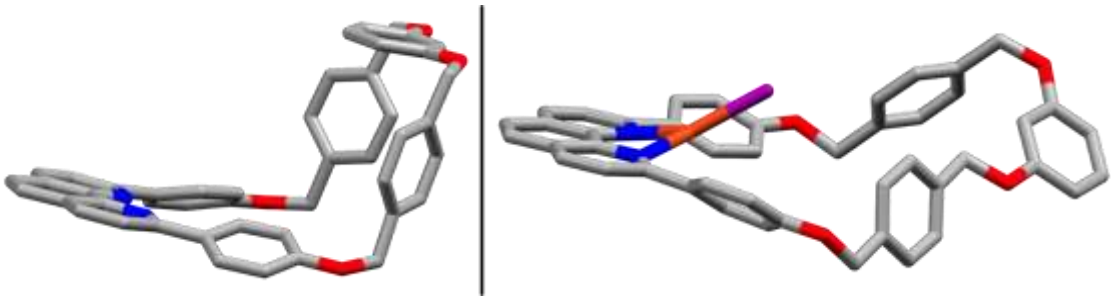

Figure 2.5. Folding of the free macrocycle **3c** (empty "taco shell", left) and the more opened conformation of the corresponding CuI complex **4c** (stuffed taco, right). Solvate molecules have been omitted in both cases.

In conclusion, this study has optimized and extended Williamson ether syntheses that enable access to a variety of macrocycles based upon the 2,9-bis(4-hydroxyphenyl)-1,10-phenanthroline building block **1**. The corresponding CuI complexes have been prepared, which as described elsewhere serve as "active metal template" precursors to rotaxanes derived from the oxidative homocoupling of terminal alkynes.[5] The structural properties of all of these compounds, as well as the NMR properties of the uncomplexed macrocycles, have been characterized in detail. These data provide a solid foundation for the analysis and interpretation of a variety of properties of the resulting rotaxanes, which include MIMs derived from diplatinum polyynediyl complexes. These efforts will soon be detailed in a comprehensive full paper.[13]

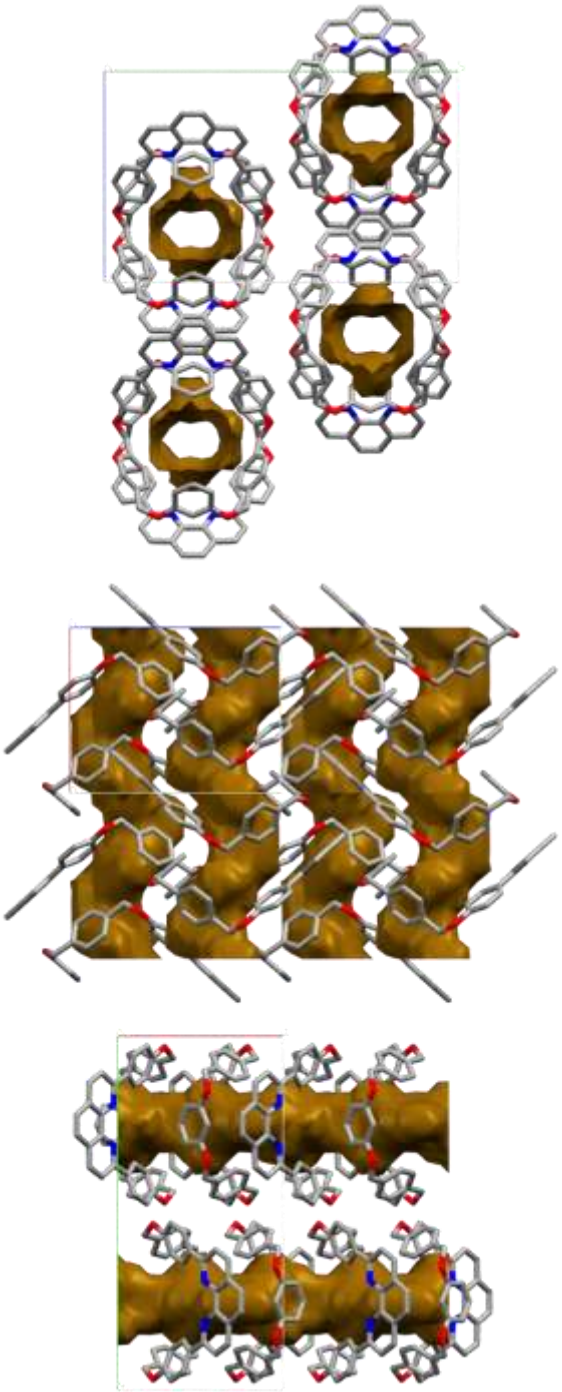

Figure 2.6. Tunnel like voids in the crystal structure of the free macrocycle **3c** after removal of solvate molecules; view along the *a* (top), *b* (middle), and *c* (bottom) axes, respectively

2.4 Experimental

General Data. Organic reactions were conducted under ambient conditions and the copper complexes were prepared under nitrogen atmospheres using Schlenk techniques. Chemicals were treated as follows: THF (Fisher Scientific), dried using a Glass Contour solvent purification system; CH_2Cl_2, $CHCl_3$, MeOH (3 × EMD), acetone, hexanes, ethyl acetate (3 × BDH), $CDCl_3$ (Cambridge Isotope Laboratories), K_2CO_3 (BDH, anhydrous), CuI (Alfa Aesar, 99.998%), 2,7-dihydroxynaphthalene (Alfa Aesar, 97%), 1,6-dibromohexane (Alfa Aesar, 97%), resorcinol (Alfa Aesar, 99%), 1,4-bis(bromomethyl)benzene (Alfa Aesar, 97%), 1,3-bis(bromomethyl)benzene (Alfa Aesar, 97%), silica (Silicycle, 40-63 μm, 230-400 mesh), and alumina (neutral, Brockmann I, 50-200 μm, Acros), used as received. Thin-layer chromatography (TLC) was carried out on EMD Silica Gel 60 F254 or EMD Aluminum Oxide 60 F254 (neutral) plates that were visualized with 254 nm or 365 nm UV light.

NMR spectra were recorded on Varian NMRS 500 MHz (ambient probe temperatures) or Bruker Avance III 500 MHz (cryoprobe conditions) spectrometers and referenced as follows (δ, ppm): ^1H, residual internal $CHCl_3$ (7.26); $^{13}C\{^1H\}$, internal $CDCl_3$ (77.16). Mass spectra were recorded on Thermo Scientific LCQ-DECA (APCI conditions) or Applied Biosystems PE SCIEX QSTAR (ESI conditions) spectrometers. Ion assignments were verified against calculated isotope patterns.[24] Melting points were determined on a Stanford Research Systems (SRS) MPA100 (Opti-Melt) automated device. Microanalyses were conducted by Atlantic Microlab.

2,7-bis(6-bromohexyloxy)naphthalene (2b). A round bottom flask was charged with acetone solutions (96 mL total) of 2,7-dihydroxynaphthalene (3.850 g, 24.04 mmol) and 1,6-dibromohexane (17.594 g, 72.112 mmol) and fitted with a condenser. Then K_2CO_3 (8.306 g, 60.09 mmol) was added with stirring. The mixture was refluxed. After

3 d, the solvent was removed by rotary evaporation. Water (250 mL) was added. The residue was extracted with CH_2Cl_2 (total 1200 mL). The extract was washed with aqueous NaOH (200 mL, 10% w/v) and brine (200 mL) and dried (Na_2SO_4). The solvent was removed by rotary evaporation. The residue was chromatographed (silica gel, 6.5 × 31 cm column, packed in hexanes and eluted with a CH_2Cl_2/hexanes gradient). The solvent was removed from the product containing fractions (assayed by TLC, eluent 1:2 v/v CH_2Cl_2/hexanes) by rotary evaporation to give **2b** as a white crystalline solid (4.831 g, 9.934 mmol, 41%), mp 74 °C. Anal. calcd. (%) for $C_{22}H_{30}Br_2O_2$ (486.2870): C 54.34, H 6.22, Br 32.86; found C 54.29, H 6.11, Br 32.78.

NMR (δ/ppm, $CDCl_3$): **^{1}H** (500 MHz) 7.64 (d, $^3J_{HH}$ = 8.9 Hz, 2H, OCCHC<u>H</u>), 7.03 (d, $^4J_{HH}$ = 2.4 Hz, 2H, OCC<u>H</u>C), 6.98 (dd, $^3J_{HH}$ = 8.9 Hz, $^4J_{HH}$ = 2.4 Hz, 2H, OCC<u>H</u>CH), 4.06 (t, $^2J_{HH}$ = 6.4 Hz, 4H, OC<u>H</u>$_2$), 3.44 (t, $^2J_{HH}$ = 6.8 Hz, 4H, BrC<u>H</u>$_2$), 1.94-1.83 (2 overlapping m, 8H, OCH$_2$C<u>H</u>$_2$, BrCH$_2$C<u>H</u>$_2$), 1.58-1.51 (m, 8H, OCH$_2$CH$_2$C<u>H</u>$_2$, BrCH$_2$CH$_2$C<u>H</u>$_2$); **^{13}C{^{1}H}** (125 MHz) 157.7 (s, O<u>C</u>CH), 136.1, 129.2, 124.3, 116.4, 106.1 (5 × s, aryl), 67.8 (s, O<u>C</u>H$_2$), 34.0, 32.8, 29.2, 28.1, 25.5 (5 × s, OCH$_2$<u>C</u>H$_2$<u>C</u>H$_2$, Br<u>C</u>H$_2$<u>C</u>H$_2$<u>C</u>H$_2$).

MS (*m/z*, APCI$^+$):[25] 487 ([**2b** + 1]$^+$, 100%), 407 ([**2b** − Br]$^+$, 3%), 161 ([dihydroxynaphthalene + 1]$^+$, 20%).

1,3-bis(4-bromomethylbenzyloxy)benzene (2c). A round bottom flask was charged with a solution of resorcinol (1.016 g, 9.229 mmol) in acetone (15 mL) and fitted with a condenser. Then K_2CO_3 (3.189 g, 23.21 mmol) was added with stirring, followed by a solution of 1,4-bis (bromomethyl)benzene (7.309 g, 27.69 mmol) in acetone (25 mL). The mixture was refluxed in the dark. After 3.5 d, the solvent was removed by rotary evaporation. Water (200 mL) was added. The mixture was extracted with ethyl acetate (400 mL). The extract was washed with aqueous NaOH (10% w/v)

and dried ($MgSO_4$). The solvent was removed by rotary evaporation. The residue was chromatographed (silica gel, 4.5 × 23 cm, packed in hexanes and eluted with a CH_2Cl_2/hexanes gradient 10:90 → 20:80 → 30:70 → 40:60 → 50:50 v/v). The solvent was removed from the product containing fractions (assayed by TLC, eluent both 1:2 and 2:1 v/v CH_2Cl_2/hexanes) by rotary evaporation to give **2c** as a white powder (0.928 g, 1.95 mmol, 21%), mp 107.7-111.8 °C. Anal. calcd. (%) for $C_{22}H_{20}Br_2O_2$ (476.2076): C 55.49, H 4.23; found C 55.22, H 4.13.

NMR (δ/ppm, $CDCl_3$): **^{1}H** (500 MHz) 7.41 (br s, 8H, *p*-C_6H_4), 7.20 (t, $^3J_{HH}$ = 7.2 Hz, 1H, OCCHC<u>H</u>), 6.58-6.57 (m, 2H, OCC<u>H</u>CH), 6.60 (m, 1H, OCC<u>H</u>CO), 5.03 (s, 4H, OC<u>H_2</u>), 4.51 (s, 4H, BrC<u>H_2</u>); **^{13}C{^{1}H}** (125 MHz) 160.0 (s, O<u>C</u>CH), 137.6, 137.4, 130.1 (3 × s, aryl), 129.4, 128.0 (2 × s, <u>C</u>H of *p*-C_6H_4), 107.6, 102.4 (2 × s, aryl), 69.7 (s, O<u>C</u>H_2), 33.3 (s, Br<u>C</u>H_2).

MS (*m/z*, ESI^+):[25] 538 ([**2c** + 62]$^+$, 16%), 477 ([**2c** + 1]$^+$, 7%).

1,3-bis(3-bromomethylbenzyloxy)benzene (2d). A round bottom flask was charged with resorcinol (2.565 g, 23.30 mmol), 1,3-bis(bromomethyl)benzene (18.449 g, 69.896 mmol), and acetone (93 mL) and fitted with a condenser. Then K_2CO_3 (8.050 g, 58.25 mmol) was added with stirring. The mixture was refluxed in the dark. After 3 d, the solvent was removed by rotary evaporation. Water (200 mL) was added. The mixture was extracted with ethyl acetate (7 × 100 mL). The extract was washed with aqueous NaOH (100 mL, 10 % w/v) and brine (200 mL) and dried ($MgSO_4$). The solvent was removed by rotary evaporation. The residue was chromatographed (silica gel, 4.5 × 25 cm, packed in hexanes, eluted with a CH_2Cl_2/hexanes gradient 5:95 → 20:80 v/v). The solvent was removed from the product containing fractions (assayed by TLC, eluent 1:2 v/v CH_2Cl_2/hexanes) by rotary evaporation to give **2d** as a white solid (4.190 g, 8.799 mmol, 38%), mp 74.7-79.8 °C. Anal. calcd. (%) for $C_{22}H_{20}Br_2O_2$ (476.2076): C 55.49,

H 4.23; found C 54.83, H 4.07.

NMR (δ/ppm, $CDCl_3$): **^{1}H** (500 MHz) 7.47 (br s, 2H, $CH_2CC\underline{H}CCH_2$), 7.36 (br, 6H, $BrCH_2CC\underline{H}C\underline{H}C\underline{H}$) 7.21 (t, $^3J_{HH}$ = 8.2 Hz, 1H, $OCCHC\underline{H}$), 6.63 (t, $^4J_{HH}$ = 2.1 Hz, 1H, $OCC\underline{H}CO$), 6.61 (dd, $^3J_{HH}$ = 8.1 Hz, $^4J_{HH}$ = 2.2 Hz, 2H, $OCC\underline{H}CH$), 5.04 (s, 4H, $OC\underline{H}_2$), 4.52 (s, 4H, $BrC\underline{H}_2$); **^{13}C{^{1}H}** (125 MHz) 160.0 (s, $O\underline{C}CH$), 138.3, 137.8, 130.2, 129.2, 128.8, 128.2, 127.6, 107.6, 102.3 (9 × s, aryl), 69.8 (s, $O\underline{C}H_2$), 33.4 (s, $Br\underline{C}H_2$).

MS (*m/z*, ESI$^+$):[25] 477 ([**2d** + 1]$^+$, 1%).

(2,9-(1,10-phenanthrolinediyl))(4-$C_6H_4O(CH_2)_6O)_2$(2,7-naphthdiyl) (3b). A round bottom flask was charged with DMSO solutions (573 mL total) of **2b** (1.393 g, 2.865 mmol) and 2,9-bis(4-hydroxyphenyl)-1,10-phenanthroline (**1**;[9a,15] 1.044 g, 2.865 mmol) that had been neutralized as reported earlier.[9a] Then K_2CO_3 (5.544 g, 40.11 mmol) and water (5.7 mL) were added with stirring. The sample was kept at 65 °C. After 19 h, the solvent was removed by rotary evaporation. Water (100 mL) was added and the mixture was extracted with CH_2Cl_2 (400 mL). The extract was dried (Na_2SO_4). The solvent was removed by rotary evaporation. The residue was chromatographed (alumina, 4.5 × 25 cm column, packed and eluted with CH_2Cl_2). The solvent was removed from the product containing fractions (assayed by TLC, eluent 1:1 v/v CH_2Cl_2/ hexanes) by rotary evaporation to give **3b** as a moderately light sensitive white solid (1.242 g, 1.803 mmol, 63%) that was stored in the dark, mp 240 °C. Anal. calcd. (%) for $C_{46}H_{44}N_2O_4$ (688.8664): C 80.20, H 6.44, N 4.07; found C 79.70, H 6.26, N 4.12.

NMR (δ/ppm, $CDCl_3$):**^{1}H** (500 MHz) 8.43 (d, $^3J_{HH}$ = 8.8 Hz, 4H, H_o),[26] 8.25 (d, $^3J_{HH}$ = 8.4 Hz, 2H, H_4 or H_7),[26] 8.08 (d, $^3J_{HH}$ = 8.4 Hz, 2H, H_3 or H_8),[26] 7.73 (s, 2H, H_5 or H_6),[26] 7.65 (d, $^3J_{HH}$ = 8.9 Hz, 2H, $OCCHC\underline{H}$ of naphthyl), 7.12 (d, $^4J_{HH}$ = 2.4 Hz, 2H, $OCC\underline{H}CC$), 7.11-7.09 (dm, $^3J_{HH}$ = 8.8 Hz, 4H, H_m),[26] 7.00 (dd, $^3J_{HH}$ = 8.9 Hz,

$^4J_{HH}$ = 2.4 Hz, 2H, OCC<u>H</u>CH of naphthyl), 4.14 (t, $^3J_{HH}$ = 6.8 Hz, 4H, OC<u>H</u>$_2$), 4.08 (t, $^3J_{HH}$ = 6.4 Hz, 4H, O'C'<u>H</u>$_2$), 1.96 (overlapping p, $^3J_{HH}$ = 6.5 Hz, 4H, OCH$_2$C<u>H</u>$_2$), 1.90 (overlapping p, $^3J_{HH}$ = 6.7 Hz 4H, O'C'H$_2$C'<u>H</u>$_2$), 1.67-1.60 (m, 8H, OCH$_2$CH$_2$C<u>H</u>$_2$, O'C'H$_2$C'H$_2$C'<u>H</u>$_2$); **^{13}C{^{1}H}** (125 MHz) 160.6, 157.8, 156.5, 146.1, 136.9, 136.1, 132.1, 129.2, 129.1, 127.6, 125.7, 124.3, 119.3, 116.8, 114.8, 105.8 (16 × s, aryl), 68.3, 67.4 (2 × s, O<u>C</u>H$_2$, O'<u>C</u>'H$_2$), 29.5, 29.1 (2 × s, OCH$_2$<u>C</u>H$_2$, O'C'H$_2$<u>C</u>'H$_2$), 26.0, 25.7 (2 × s, OCH$_2$CH$_2$<u>C</u>H$_2$, O'C'H$_2$C'H$_2$<u>C</u>'H$_2$).

MS (*m/z*, ESI$^+$):[25] 689 ([**3b** + 1]$^+$, 100%).

(2,9-(1,10-phenanthrolinediyl))(4-C$_6$H$_4$OCH$_2$-4-C$_6$H$_4$CH$_2$O)$_2$(1,3-C$_6$H$_4$) (3c). A round bottom flask was charged with DMSO solutions (210 mL total) of **2c** (0.501 g, 1.05 mmol) and **1** (0.383 g, 1.05 mmol) that had been neutralized as reported earlier.[9a] Then K_2CO_3 (0.435 g, 3.15 mmol) and water (2.1 mL) were added with stirring. The sample was kept at 65 °C in the dark. After 4 h, the solvent was removed by rotary evaporation. Water (50 mL) was added and the mixture was extracted with CH_2Cl_2 (5 × 50 mL). The extract was washed with water (2 × 50 mL) and brine (50 mL) and dried ($MgSO_4$). The solvent was removed by rotary evaporation. The residue was chromatographed (silica gel, 3 × 26 cm, packed in CH_2Cl_2, eluted with MeOH/CH_2Cl_2 gradient 1:999 → 2:998 v/v). The solvent was removed from the product containing fractions (assayed by TLC, eluent 1:99 v/v MeOH/CH_2Cl_2) by rotary evaporation to give **3c** as a moderately light sensitive very pale yellow powder (0.278 g, 0.410 mmol, 39%) that was stored in the dark, and darkened slightly at 115 °C and melted at 165 °C. Anal. calcd. (%) for $C_{46}H_{34}N_2O_4$ (678.7870): C 81.40, H 5.05, N 4.13; calcd. (%) for $C_{46}H_{34}N_2O_4 \cdot H_2O$ (696.8022): C 79.29, H 5.21, N 4.02; found C 79.30, H 5.16, N 3.97.[27]

NMR (δ/ppm, $CDCl_3$): **^{1}H** (500 MHz) 8.33 (dm, $^3J_{HH}$ = 8.8 Hz, 4H, H$_o$),[26] 8.26

(d, $^3J_{HH}$ = 8.4 Hz, 2H, H_4 or H_7),[26] 8.07 (d, $^3J_{HH}$ = 8.4 Hz, 2H, H_3 or H_8),[26] 7.73 (s, 2H, H_5 or H_6),[26] 7.36 (br, 8H, *p*-$C_6\underline{H}_4CH_2O$), 7.17 (t, $^3J_{HH}$ = 8.2 Hz, 1H, OCCHC$\underline{H}$ of *m*-$C_6H_4O_2$), 7.11 (d, $^3J_{HH}$ = 8.8 Hz, 4H, H_m),[26] 6.59 (dd, $^3J_{HH}$ = 8.2 Hz, $^4J_{HH}$ = 2.3 Hz, 2H, OCC$\underline{H}$CH of *m*-$C_6H_4O_2$), 6.41 (t, $^4J_{HH}$ = 2.3 Hz, 1H, OCC$\underline{H}$CO), 5.32 (s, 4H, OC$\underline{H}_2$), 5.07 (s, 4H, O'C'$\underline{H}_2$); **^{13}C{^{1}H}** (125 MHz) 160.3, 159.8, 156.3, 145.8, 137.3, 136.9, 136.5, 129.9, 129.1, 127.5, 127.3, 126.6, 125.7, 119.5, 116.0, 107.9, 103.0 (17 × s, aryl), 70.2, 69.8 (2 × s, O$\underline{C}H_2$, O'C'H_2).

MS (*m/z*, ESI$^+$):[25] 679 ([**3c** + 1]$^+$, 100%).

(2,9-(1,10-phenanthrolinediyl))(4-$C_6H_4OCH_2$-3-$C_6H_4CH_2O)_2$(1,3-C_6H_4) (3d). A round bottom flask was charged with DMSO solutions (422 mL total) of **2d** (1.005 g, 2.109 mmol) and **1** (0.769 g, 2.110 mmol) that had been neutralized as reported earlier.[9a] Then K_2CO_3 (2.187 g, 15.82 mmol) and water (4.2 mL) were added with stirring. The sample was kept at 65 °C in the dark. After 5 h, the solvent was removed by rotary evaporation. Water (300 mL) was added and the mixture was extracted with CH_2Cl_2 (6 × 100 mL). The extract was washed with brine (100 mL) and water (100 mL) and dried (Na_2SO_4). The solvent was removed by rotary evaporation. The residue was chromatographed (silica gel, 4.5 × 25 cm, packed in CH_2Cl_2, eluted with a MeOH/CH_2Cl_2 gradient 1:999 → 2:998 → 3:997 v/v). The solvent was removed from the product containing fractions (assayed by TLC, eluent 1:99 v/v MeOH/CH_2Cl_2) by rotary evaporation to give **3d** as a moderately light sensitive white solid (0.308 g, 0.454 mmol, 22%) that was stored in the dark, and darkened slightly at 120 °C and melted at 161 °C. Anal. calcd. (%) for $C_{46}H_{34}N_2O_4$ (678.7870): C 81.40, H 5.05, N 4.13; calcd. (%) for $C_{46}H_{34}N_2O_4 \cdot 2H_2O$ (714.8175): C 77.29, H 5.36, N 3.92; found C 77.58, H 5.34, N 3.99.[27]

NMR (δ/ppm, $CDCl_3$): **^{1}H** (500 MHz) 8.37 (dm, $^3J_{HH}$ = 8.9 Hz, 4H, H_o),[26] 8.24

(d, $^3J_{HH}$ = 8.4 Hz, 2H, H_4 or H_7),[26] 8.05 (d, $^3J_{HH}$ = 8.4 Hz, 2H, H_3 or H_8),[26] 7.72 (s, 2H, H_5 or H_6),[26] 7.66 (br s, 2H, $CH_2CC\underline{H}C$), 7.40-7.34 (m, 6H, $CH_2CC\underline{H}C\underline{H}C\underline{H}C$), 7.23 (t, $^3J_{HH}$ = 8.2 Hz, 1H, OCCHC$\underline{H}$ of *m*-$C_6H_4O_2$), 7.16 (dm, $^3J_{HH}$ = 8.9 Hz, 4H, H_m),[26] 6.85 (t, $^4J_{HH}$ = 2.4 Hz, 1H, OCC$\underline{H}$CO), 6.65 (dd, $^3J_{HH}$ = 8.2 Hz, $^4J_{HH}$ = 2.4 Hz, 2H, OCC$\underline{H}$CH of *m*-$C_6H_4O_2$), 5.30 (s, 4H, OC$\underline{H}_2$), 5.13 (s, 4H, O'C'$\underline{H}_2$); **^{13}C{^{1}H}** (125 MHz) 160.2, 159.8, 156.5, 146.2, 137.9, 137.6, 136.8, 132.8, 130.1, 129.1, 128.9, 127.6, 126.6, 126.2, 125.7, 119.4, 115.7, 107.4, 102.9 (19 × s, aryl), 69.9, 69.7 (2 × s, O$\underline{C}H_2$, O'C'H_2).

MS (*m/z*, ESI$^+$):[25] 679 ([**3d** + 1]$^+$, 100%), 757 ([**3d** + 78]$^+$, 9%), 1358 ([2 × **3d** + 1]$^+$, 7%).

(3b)CuI (4b). A solution of CuI (0.140 g, 0.734 mmol) in CH_3CN (14 mL) was transferred via a Teflon cannula to a solution of **3b** (0.505 g, 0.734 mmol) in CH_2Cl_2 (33 mL) in a Schlenk flask. The mixture was stirred in the dark. After 1 h, the solvent was removed by rotary evaporation to give a pale orange solid. The residue was recrystallized from hot CH_2Cl_2 (refrigerator storage). The precipitate was isolated by filtration and dried by oil pump vacuum to give **4b** as a bright orange crystalline solid (0.508 g, 0.577 mmol, 79%), which darkened slightly (contraction) at 124 °C and melted at 226 °C. Anal. calcd. (%) for $C_{46}H_{44}CuIN_2O_4$ (879.3168): C 62.83, H 5.04, N 3.19; found C 63.38, H 5.34, N 3.13.

NMR (δ/ppm, $CDCl_3$): **^{1}H** (500 MHz) 8.42 (br s, $w_{1/2}$ = 27 Hz, 2H), 8.16 (overlapping br d, $^3J_{HH}$ = 7.9 Hz, 4H, *p*-C_6H_4), 8.12 (overlapping br s, $w_{1/2}$ = 23 Hz, 2H), 7.88 (br s, 2H), 7.63 (d, $^3J_{HH}$ = 8.8 Hz, 2H), 7.16 (br s, $w_{1/2}$ = 36 Hz, 2H), 7.13 (br d, $^3J_{HH}$ = 7.5 Hz, 4H, *p*-C_6H_4), 6.97 (br d, $^3J_{HH}$ = 8.8 Hz, 2H), 4.20-4.02 (overlapping br s and t, $^3J_{HH}$ = 6.7 Hz, 8H, OC$\underline{H}_2$, O'C'$\underline{H}_2$), 2.02-1.82 (br m, 8H, $OCH_2C\underline{H}_2$, $O'C'H_2C'\underline{H}_2$), 1.69-1.56 (br, 8H, $OCH_2CH_2C\underline{H}_2$, $O'C'H_2C'H_2C'\underline{H}_2$); **^{13}C{^{1}H}**[28] (125

MHz, cryoprobe) 161.4, 158.6, 157.8, 138.0, 136.3, 131.4, 129.1, 127.6, 126.0, 124.3, 116.8, 115.0, 106.2 (13 × s, aryl), 68.1, 67.5 (2 × s, $O\underline{C}H_2$, $O'\underline{C}'H_2$), 29.2, 28.9 (2 × s, $OCH_2\underline{C}H_2$, $O'C'H_2\underline{C}'H_2$), 25.6, 25.5 (2 × s, $OCH_2CH_2\underline{C}H_2$, $O'C'H_2C'H_2\underline{C}'H_2$).

MS (*m/z*, ESI^+):[25] 751 ($[(\mathbf{3b})Cu]^+$, 60%), 689 ($[\mathbf{3b} + 1]^+$, 100%).

(3c)CuI (4c). A solution of CuI (0.035 g, 0.18 mmol) in CH_3CN (3.5 mL) and a solution of **3c** (0.035 g, 0.18 mmol) in CH_2Cl_2 (8 mL) were combined in a procedure analogous to that for **4b** (3 h stirring). An identical workup gave **4c** as a pale orange solid (0.061 g, 0.073 mmol, 40%), mp 107.7-111.8 °C. Anal. calcd. (%) for $C_{46}H_{34}CuIN_2O_4$ (869.2374): C 63.56, H 3.94, N 3.22; calcd. (%) for $C_{46}H_{34}CuIN_2O_4 \cdot CH_2Cl_2$ (954.1643): C 59.16, H 3.80, N 2.94; found C 60.04, H 3.92, N 2.90.[29]

MS (*m/z*, ESI^+): 741 ($[(\mathbf{3c})Cu]^+$, 50%), 679 ($[\mathbf{3c} + 1]^+$, 100%); (*m/z*, ESI^-): 127 ($[I]^-$, 100%).

(3d)CuI (4d). A solution of CuI (0.019 g, 0.098 mmol) in CH_3CN (1 mL) and a solution of **3d** (0.067 g, 0.098 mmol) in CH_2Cl_2 (4 mL) were combined in a procedure analogous to that for **4b** (0.5 h stirring). The precipitate was isolated by filtration and dried by oil pump vacuum to give **4d** as a yellow solid (0.068 g, 0.078 mmol, 80%). mp 107.7-111.8 °C. Anal. calcd. (%) for $C_{46}H_{34}CuIN_2O_4$ (869.2374): C 63.56, H 3.94, N 3.22; calcd. (%) for $C_{46}H_{34}CuIN_2O_4 \cdot CH_2Cl_2 \cdot 0.75H_2O$ (967.6758): C 58.34, H 3.91, N 2.89; found C 58.59, H 4.01, N 2.92.[30]

Crystallography. A. A CH_2Cl_2 solution of **3a** was allowed to evaporate slowly at room temperature. After 3 d, the resulting colorless plates were analyzed as outlined in Table 1. Cell parameters were obtained from 1080 frames using a 0.5° scan[31] and refined with 24948 reflections. Integrated intensity information for each reflection was obtained by reduction of the data frames with APEX2.[32] The integration method

employed a three dimensional profiling algorithm. All data were corrected for Lorentz and polarization factors, as well as crystal decay effects. SADABS was used for absorption corrections.[33] The space group was determined from systematic reflection conditions and statistical tests. The structure was solved by direct methods using SHELXTL (SHELXS).[34] Non-hydrogen atoms were refined with anisotropic thermal parameters. Hydrogen atoms were placed in idealized positions, and were refined using a riding model. The structure was refined (weighted least squares refinement on F^2) to convergence.[34] The absence of additional symmetry or voids was confirmed using PLATON (ADDSYM).[35]

B. A $CHCl_3$ solution of **3b** was allowed to evaporate slowly at room temperature. After 3 d, the resulting colorless prisms were analyzed as outlined in Table 1. Cell parameters were obtained from 180 frames using a 0.5° scan.[31] Integrated intensity information for each reflection was obtained by reduction of the data frames with the program APEX2.[32] SADABS was used for absorption corrections.[33] The space group was determined from systematic reflection conditions and statistical tests. The structure was solved by direct methods using SHELXTL (SHELXS).[34] Two $CHCl_3$ molecules were found for each molecule of **3b**. One was successfully modeled (disordered over two positions). The other could not be modeled so the electron density contribution was extracted with the program PLATON/SQUEEZE.[35] Restraints were used to keep the bond distances and thermal ellipsoids chemically meaningful. Note that the formula and density reported in the CIF file reflects the results using SQUEEZE. Non-hydrogen atoms were refined with anisotropic thermal parameters. Hydrogen atoms were placed in idealized positions, and were refined using a riding model. The structure was refined (weighted least squares refinement on F^2) to convergence.[34] The absence of additional symmetry or voids was confirmed using PLATON (ADDSYM).[35]

C. A CH_2Cl_2 solution of **3c** was allowed to evaporate slowly at room temperature. After 4 d, the resulting colorless plates were analyzed as outlined in Table 1. Cell parameters were obtained from 60 frames using a 0.5° scan. Integrated intensity information for each reflection was obtained by reduction of the data frames with the program APEX2.[32] SADABS was used for absorption corrections.[33] The space group was determined from systematic reflection conditions and statistical tests. The structure was solved by direct methods using SHELXTL (SHELXS).[34] One molecule of CH_2Cl_2 was present, but were disordered and could not be successfully modeled. Thus, the electron density contribution was extracted with the program PLATON/SQUEEZE.[35] Restraints were used to keep the bond distances and thermal ellipsoids chemically meaningful. Non-hydrogen atoms were refined with anisotropic thermal parameters. Hydrogen atoms were placed in idealized positions, and were refined using a riding model. The structure was refined (weighted least squares refinement on F^2) to convergence.[34] The absence of additional symmetry or voids was confirmed using PLATON (ADDSYM).[35]

D. A CH_2Cl_2 solution of **4a** was allowed to evaporate slowly at room temperature. After 1 d, the resulting red plates were analyzed as outlined in Table 2. Cell parameters were obtained from 180 frames using a 0.5° scan.[31] Integrated intensity information for each reflection was obtained by reduction of the data frames with the program APEX2.[32] SADABS was used for absorption corrections.[33] The space group was determined from systematic reflection conditions and statistical tests. The structure was solved by direct methods using SHELXTL (SHELXS).[34] A CH_2Cl_2 molecule was found for nearly every molecule of **4a** (refined with an occupancy value close to 1). Nonhydrogen atoms were refined with anisotropic thermal parameters. Hydrogen atoms were placed in idealized positions, and were refined using a riding model. The structure

was refined (weighted least squares refinement on F^2) to convergence.[34] The absence of additional symmetry or voids was confirmed using PLATON (ADDSYM).[35]

E. A $CHCl_3$ solution of **4b** was allowed to evaporate slowly at room temperature. After 3 d, the resulting red prisms were analyzed as outlined in Table 2. Cell parameters were obtained from 60 frames using a 0.5° scan.[31] Integrated intensity information for each reflection was obtained by reduction of the data frames with the program APEX2.[32] SADABS was used for absorption corrections.[33] The space group was determined from systematic reflection conditions and statistical tests. The structure was solved by direct methods using SHELXTL (SHELXS).[34] Two $CHCl_3$ molecules were located and refined for each molecule of **4b**. Non-hydrogen atoms were refined with anisotropic thermal parameters. Hydrogen atoms were placed in idealized positions, and were refined using riding model. The structure was refined (weighted least squares refinement on F^2) to convergence.[34] The absence of additional symmetry or voids was confirmed using PLATON (ADDSYM).[35]

F. A CH_2Cl_2 solution of **4c** was allowed to evaporate slowly at room temperature. After 3 d, the resulting orange plates were analyzed as outlined in Table 2. Cell parameters were obtained from 60 frames using a 0.5° scan.[31] Integrated intensity information for each reflection was obtained by reduction of the data frames with the program APEX2.[32] SADABS was used for absorption corrections.[33] The space group was determined from systematic reflection conditions and statistical tests. The structure was solved by direct methods using SHELXTL (SHELXS).[34] A disordered CH_2Cl_2 molecule was found for each molecule of **4c**, and was successfully modeled by application of a restrained distance and displacement parameter refinement. Non-hydrogen atoms were refined with anisotropic thermal parameters. Hydrogen atoms were placed in idealized positions, and were refined using riding model. The structure was

refined (weighted least squares refinement on F^2) to convergence.[34] The absence of additional symmetry or voids was confirmed using PLATON (ADDSYM).[35]

DFT Calculations. Computations were performed using the Gaussian09 program package.[36] Full geometry optimizations and frequency calculations were carried out on macrocycles **3** and their CuI complexes **4** without any symmetry constraints. The B3LYP[37] functional was implemented with the D95V basis set for C, H, N, and O atoms whereas the LANL2DZDP ECP was used to include the appropriate polarization functions for I in **4a-f**. To account for the relativistic effects on Cu, SDD was employed.

2.5 References

(1) Bruns, C. J.; Stoddart, J. F.; *The Nature of the Mechanical Bond: From Molecules to Machines*; Wiley: Chichester, UK, 2016.

(2) (a) Lehn, J.-M.; *Supramolecular Chemistry: Concepts and Perspectives*; VCH: Weinheim, Germany, 1995. (b) Sauvage, J.-P.; Dietrich-Buchecker, C., Eds.; *Molecular Catenanes, Rotaxanes and Knots: A Journey Through the World of Molecular Topology*; Wiley-VCH: Weinheim, Germany, 1999.

(3) (a) Hubin, T. J.; Busch, D. H. *Coord. Chem. Rev.* **2000**, *200-202*, 5-52. (b) Forgan, R. S.; Sauvage, J.-P.; Stoddart, J. F. *Chem. Rev.* **2011**, *111*, 5434-5464. (c) Lindoy, L. F.; Park, K.-M.; Lee, S. S. *Chem. Soc. Rev.* **2013**, *42*, 1713-1727. (d) Evans, N. H.; Beer, P. D. *Chem. Soc. Rev.* **2014**, *43*, 4658-4683. (e) Gil-Ramírez, G.; Leigh, D. A.; Stephens, A. J. *Angew. Chem. Int. Ed.* **2015**, *54*, 6110-6150; *Angew. Chem.* **2015**, *127*, 6208-6249.

(4) (a) Pérez-Alvarez, M.; Raymo, F. M.; Rowan, S. J.; Schiraldi, D.; Stoddart, J. F.; Wang, Z.-H.; White, A. J. P.; Williams, D. J. *Tetrahedron* **2001**, *57*, 3799-3808. (b) Leigh, D. A.; Venturini, A.; Wilson, A. J.; Wong, J. K. Y.; Zerbetto, F. *Chem. Eur. J.* **2004**, *10*, 4960-4969. (c) Miljanić, O. Š.; Dichtel, W. R.; Khan, S. I.; Mortezaei, S.; Heath, J. R.; Stoddart, J. F. *J. Am. Chem. Soc.* **2007**, *129*, 8236-8246. (d) Aucagne, V.; Berná, J.; Crowley, J. D.; Goldup, S. M.; Hänni, K. D.; Leigh, D. A.; Lusby, P. J.; Ronaldson, V. E.; Slawin, A. M. Z.; Viterisi, A.; Walker, D. B. *J. Am. Chem. Soc.* **2007**, *129*, 11950-11963. (e) Berná, J.; Crowley, J. D.; Goldup, S. M.; Hänni, K. D.; Lee, A.-L.; Leigh, D. A. *Angew. Chem. Int. Ed.* **2007**, *46*, 5709-5713; *Angew. Chem.* **2007**, *119*, 5811-5815. (f) Meyer, C. D.; Forgan, R. S.; Chichak, K. S.; Peters, A. J.; Tangchaivang, N.; Cave, G. W. V.; Khan, S. I.; Cantrill, S. J.; Stoddart, J. F. *Chem. Eur. J.* **2010**, *16*,

12570-12581. (g) Crowley, J. D.; Hänni, K. D.; Leigh, D. A.; Slawin, A. M. Z. *J. Am. Chem. Soc.* **2010**, *132*, 5309-5314. (h) Spence, G. T.; White, N. G.; Beer, P. D. *Org. Biomol. Chem.* **2012**, *10*, 7282-7291. (i) Iwamoto, H.; Takizawa, W.; Itoh, K.; Hagiwara, T.; Tayama, E.; Hasegawa, E.; Haino, T. *J. Org. Chem.* **2013**, *78*, 5205-5217. (j) Ayme, J.-F.; Beves, J. E.; Campbell, C. J.; Leigh, D. A. *Chem. Soc. Rev.* **2013**, *42*, 1700-1712. (k) Frasconi, M.; Kikuchi, T.; Cao, D.; Wu, Y.; Liu, W.-G.; Dyar, S. M.; Barin, G.; Sarjeant, A. A.; Stern, C. L.; Carmieli, R.; Wang, C.; Wasielewski, M. R.; Goddard, W. A., III; Stoddart, J. F. *J. Am. Chem. Soc.* **2014**, *136*, 11011-11026.

(5) (a) Weisbach, N.; Baranová, Z.; Gauthier, S.; Reibenspies, J. H.; Gladysz, J. A. *Chem. Commun*. **2012**, *48*, 7562-7564. (b) Baranová, Z.; Amini, H.; Bhuvanesh, N.; Gladysz, J. A. *Organometallics*, **2014**, *33*, 6746-6749.

(6) Computational study: Sahnoune, H.; Baranová, Z.; Bhuvanesh, N.; Gladysz, J. A.; Halet, J.-F. *Organometallics* **2013**, *32*, 6360-6367.

(7) (a) Mohr, W.; Stahl, J.; Hampel, F.; Gladysz, J. A. *Chem. Eur. J.* **2003**, *9*, 3324-3340. (b) Zheng, Q.; Bohling, J. C.; Peters, T. B.; Frisch, A. C.; Hampel, F.; Gladysz, J. A. *Chem. Eur. J.* **2006**, *12*, 6486-6505. (c) Stahl, J.; Mohr, W.; de Quadras, L.; Peters, T. B.; Bohling, J. C.; Martín-Alvarez, J. M.; Owen, G. R.; Hampel, F.; Gladysz, J. A. *J. Am. Chem. Soc.* **2007**, *129*, 8282-8295. (d) de Quadras, L.; Bauer, E. B.; Mohr, W.; Bohling, J. C.; Peters, T. B.; Martín-Alvarez, J. M.; Hampel, F.; Gladysz, J. A. *J. Am. Chem. Soc.* **2007**, *129*, 8296-8309. (e) de Quadras, L.; Bauer, E. B.; Stahl, J.; Zhuravlev, F.; Hampel, F.; Gladysz, J. A. *New. J. Chem.* **2007**, *31*, 1594-1604. (f) Owen, G. R.; Stahl, J.; Hampel, F.; Gladysz, J. A. *Chem. Eur. J.* **2008**, *14*, 73-87. (g) Clough, M. C.; Fiedler, T.; Bhuvanesh, N.; Gladysz, J. A. *J. Organomet. Chem.* **2015**, *812*, 34-42.

(8) Hay, A. S. *J. Org. Chem.* **1962**, *27*, 3320-3321.

(9) (a) Dietrich-Buchecker, C.; Sauvage, J.-P. *Tetrahedron* **1990**, *46*, 503-512. (b) Chambron, J.-C.; Sauvage, J.-P.; Mislow, K.; De Cian, A.; Fischer, J. *Chem. Eur. J.* **2001**, *7*, 4085-4096. (c) Joosten, A.; Trolez, Y.; Collin, J.-P.; Heitz, V.; Sauvage, J.-P. *J. Am. Chem. Soc.* **2012**, *134*, 1802-1809.

(10) (a) Saito, S.; Takahashi, E.; Nakazono, K. *Org. Lett.* **2006**, *8,* 5133-5136. (b) Sato, Y.; Yamasaki, R.; Saito, S. *Angew. Chem., Int. Ed.* **2009***, 48,* 504-507 and 2630; *Angew. Chem.* **2009**, *121*, 512-515 and 2668. (c) Saito, S. *J. Incl. Phenom. Macrocycl. Chem.* **2015**, *82*, 437-451. (d) Hayashi, R.; Mutoh, Y.; Kasama, T.; Saito, S. *J. Org. Chem.* **2015**, *80*, 7536-7546. (e) Hayashi, R.; Slavík, Y.; Kasama, T.; Saito, S. *J. Org. Chem.* **2016**, *81*, 1175-1184.

(11) (a) Movsisyan, L. D.; Kondratuk, D. V.; Franz, M.; Thompson, A. L.; Tykwinski, R. R.; Anderson, H. L. *Org. Lett*. **2012**, *14*, 3424-3426. (b) Movsisyan, L. D.; Franz, M.; Hampel, F.; Thompson, A. L.; Tykwinski, R. R. *J. Am. Chem. Soc.* **2016**, *138*, 1366-1376.

(12) (a) Crowley, J. D.; Goldup, S. M.; Lee, A. L.; Leigh, D. A.; McBurney, R. T. *Chem. Soc. Rev.* **2009**, *38*, 1530-1541. (b) Beves, J. E.; Blight, B. A.; Campbell, C. J.; Leigh, D. A.; McBurney, R. T. *Angew. Chem., Int. Ed.* **2011**, *50*, 9260-9327; *Angew. Chem.* **2011**, *123*, 9428-9499. (c) Aucagne, V.; Hänni, K. D.; Leigh, D. A.; Lusby, P. J.; Walker, D. B. *J. Am. Chem. Soc.* **2006**, *128*, 2186-2187.

(13) Baranová, Z.; Amini, H.; Weisbach, N.; Gauthier, S.; Bhuvanesh, N.; Reibenspies, J. H.; Gladysz, J. A. manuscript in preparation.

(14) Saito, S.; Nakazono, K.; Takahashi, E. *J. Org. Chem.* **2006**, *71*, 7477-7480 (see also the supporting information therein).

(15) (a) Dietrich-Buchecker, C. O.; Sauvage, J. P. *Tetrahedron Letters* **1983**, *24*, 5091-5094. (b) Dietrich-Buchecker, C. O.; Sauvage, J.-P. *J. Am. Chem. Soc.* **1984**, *106*, 3043-3045.

(16) (a) Ogawa, T.; Kishimoto, T.; Kobayashi, K.; Ono, N. *J. Chem. Soc., Perkin Trans 1* **1998**, 529-538. (b) Watarai, N.; Kawasaki, H.; Azumaya, I.; Yamasaki, R.; Saito, S. *Heterocycles* **2009**, *79*, 531-548.

(17) A reviewer has questioned why the yield of **4c** is only 40%, as compared to 80% for the other CuI complexes. It is thought that the crystallization of this complex is not as efficient, as the mother liquor remains a pale orange.

(18) The atom labels for **3a** (Figure 2.2) correspond to those in the cif file for the crystal structure of **3a**. In the text, the atoms of **3b**,**c**, and **4a**-**c** have been renumbered to match (Figures 2.2 and 2.3 and Table 2.3). It should be kept in mind that due to the mirror plane in **3c**, there are fewer unique carbon, nitrogen, and oxygen atoms. Thus, atoms that are equivalent by symmetry bear different numbers. The crystal structure of **3a** has also been reported in an earlier paper.[6]

(19) (a) Healy, P. C. *J. Chem. Soc. Dalton Trans.* **1985**, 2531-2539. (b) Zhou, X.-P.; Li, D.; Ng, S. W. *Acta Cryst.* **2005**, *E61*, m654-m655.

(20) Yang, Y.; Chai, W.; Song, L.; Shu, K. *Acta Cryst.* **2010**, *E66*, m1486-m1486.

(21) Nitsch, J.; Kleeberg, C.; Fröhlich, R.; Steffen, A. *Dalton Trans.* **2015**, *44*, 6944-6960.

(22) Macrae, C. F.; Bruno, I. J.; Chisholm, J. A.; Edgington, P. R.; McCabe, P.; Pidcock, E.; Rodriguez-Monge, L.; Taylor, R.; van de Streek, J.; Wood, P. A. *J. Appl. Cryst.* **2008**, *41*, 466-470.

(23) The exact comparisons are as follows: **3a**, N1···C29 10.886 Å and N2···C25 11.054 Å; **3b**, N1···C301 12.696 Å and N2···C303 12.696 Å; **3c**, N1···C29 9.519 Å and N1···C28 8.487 Å; **4a**, N1···C29 11.618 Å and N2···C25 11.751 Å; **4b**, N1···C301 11.955 Å and N2···C303 12.119 Å; **4c**, N1···C29 11.953 Å and N2···C25 11.451 Å.

(24) Loos, M.; Gerber, C.; Corona, F.; Hollender, J.; Singer, H. *Anal. Chem.* **2015**, *87*, 5738-5744.; *enviPat* Web 2.1, http://www.envipat.eawag.ch/index.php (accessed September 2016).

(25) Each *m*/*z* value corresponds to the most intense peak of the isotope envelope, and the assignments have been verified by simulations.

(26) These ^{1}H NMR assignments are based upon those given in reference 9a. For the numbering or labeling of certain atoms, see Figure A.1.

(27) Traces of H_2O are apparent in the ^{1}H NMR spectrum.

(28) The ^{13}C NMR signals were assigned based upon data for a similar macrocycle.[10a] The solubility of this compound was very low in most NMR solvents (CD_2Cl_2, $CDCl_3$, C_6D_6, toluene-d_8, CD_3CN) at room temperature, and three signals could not be observed, even in spectra recorded using a cryoprobe.

(29) This compound is not sufficiently soluble for ^{1}H and ^{13}C NMR spectra. However, the crystal (Figure 2.3, bottom) is a CH_2Cl_2 monosolvate, and the microanalysis better fits this formula.

(30) This compound is not sufficiently soluble for ^{1}H and ^{13}C NMR spectra that would verify the solvation model that fits the data.

(31) Sheldrick, G. M. "Cell_Now (version 2008/1): Program for Obtaining Unit Cell Constants from Single Crystal Data" University of Göttingen, Germany.

(32) APEX2 "Program for Data Collection on Area Detectors" BRUKER AXS Inc., 5465 East Cheryl Parkway, Madison, WI 53711-5373 USA.

(33) SADABS, Sheldrick, G. M. "Program for Absorption Correction of Area Detector Frames", BRUKER AXS Inc., 5465 East Cheryl Parkway, Madison, WI 53711-5373 USA.

(34) Sheldrick, G. M. *Acta Cryst*. **2008**, *A64*, 112-122.

(35) Spek, A. L. *J. Appl. Cryst.* **2003**, *36*, 7-13.

(36) Frisch, M. J.; Trucks, G. W.; Schlegel, H. B.; Scuseria, G. E.; Robb, M. A.; Cheeseman, J. R.; Scalmani, G.; Barone, V.; Mennucci, B.; Petersson, G. A.; Nakatsuji, H.; Caricato, M.; Li, X.; Hratchian, H. P.; Izmaylov, A. F.; Bloino, J.; Zheng, G.; Sonnenberg, J. L.; Hada, M.; Ehara, M.; Toyota, K.; Fukuda, R.; Hasegawa, J.; Ishida, M.; Nakajima, T.; Honda, Y.; Kitao, O.; Nakai, H.; Vreven, T.; Montgomery, J. A., Jr.; Peralta, J. E.; Ogliaro, F.; Bearpark, M.; Heyd, J. J.; Brothers, E.; Kudin, K. N.; Staroverov, V. N.; Kobayashi, R.; Normand, J.; Raghavachari, K.; Rendell, A.; Burant, J. C.; Iyengar, S. S.; Tomasi, J.; Cossi, M.; Rega, N.; Millam, J. M.; Klene, M.; Knox, J. E.; Cross, J. B.; Bakken, V.; Adamo, C.; Jaramillo, J.; Gomperts, R.; Stratmann, R. E.; Yazyev, O.; Austin, A. J.; Cammi, R.; Pomelli, C.; Ochterski, J. W.; Martin, R. L.; Morokuma, K.; Zakrzewski, V. G.; Voth, G. A.; Salvador, P.; Dannenberg, J. J.; Dapprich, S.; Daniels, A. D.; Farkas, Ö.; Foresman, J. B.; Ortiz, J. V.; Cioslowski, J.; Fox, D. J. *Gaussian 09, Revision D.01*; Gaussian, Inc., Wallingford CT, 2009.

(37) (a) Becke, A. D. *J. Chem. Phys.* **1993**, *98*, 5648-5652. (b) Lee, C.; Yang, W.; Parr; R. G. *Phys. Rev. B.* **1989**, *37*, 785-789.

3. 1,10-PHENANTHROLINE-BASED MACROCYCLES THREADED BY PtC_8Pt, $PtC_{12}Pt$, AND $PtC_{16}Pt$ AXLES: METAL-CAPPED ROTAXANES AS INSULATED MOLECULAR WIRES

3.1 Introduction

There has been much interest in the synthesis and redox chemistry of complexes in which two metals are separated by an unsaturated linker, especially with respect to the electronic properties associated with each accessible redox state.[1,2] A related situation is found with break junctions in which a single unsaturated fragment spans two metallic electrodes.[3] Many types of phenomena involving electron delocalization or transfer between the termini have been documented, and such systems have often been referred to as molecular wires.[4]

However, there have been fewer studies directed at the "insulation" of the unsaturated linkers in these assemblies.[5,6] In one limit, this would have the potential of suppressing linker/solvent and linker/linker reactions, leading to longer-lived species, as well as diminishing the solvent or counter-ion reorganization energy associated with mixed valence states.[7] In the opposite limit, the insulation could respond to a redox or charge transfer event in a defined chemical or mechanical manner.[8]

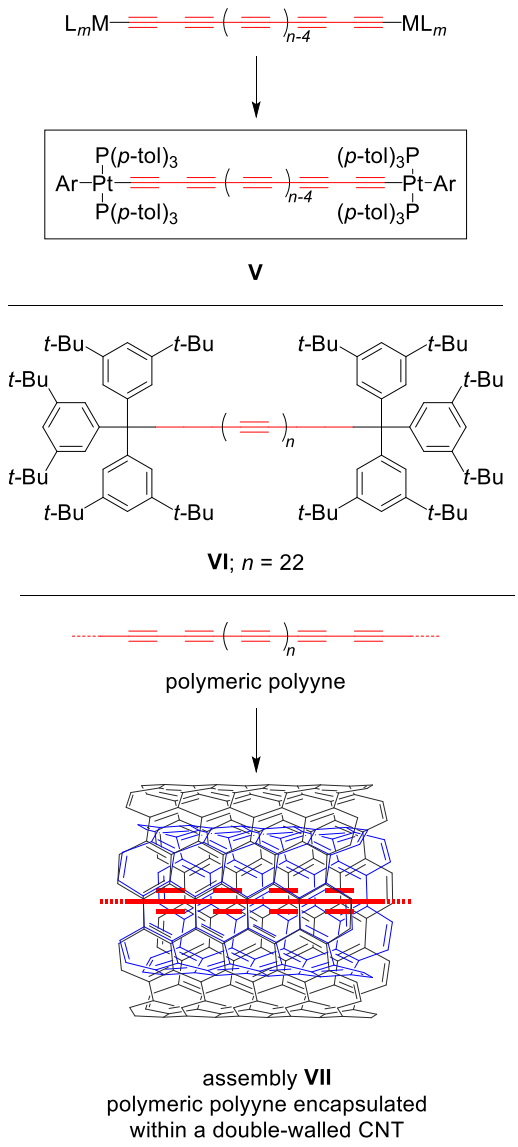

Scheme 3.1. Oligomeric and polymeric polyynes: a representative type of diplatinum complex (**V**); the polyyne with the longest sp carbon chain isolated to date (**VI**); the encapsulation of polymeric polyynes within double-walled carbon nanotubes (**VII**).

We[9] and others[2] have had an ongoing interest in dimetallic polyynediyl complexes, $L_mM(C{\equiv}C)_nML_m$, which feature the most fundamental unsaturated carbon linker. In previous efforts, we have synthesized a series of diplatinum adducts *trans,trans*-(Ar)(*p*-tol$_3$P)$_2$Pt(C≡C)$_n$Pt(P*p*-tol$_3$)$_2$(Ar) (**V**, Scheme 3.1) that have extended

to as many as 28 sp hybridized carbon atoms.[9c] However, in all studies of long chain polyynes, stability limits have always been reached.[9,10] The current "record" for length features a $(C{\equiv}C)_{22}$ or C_{44} bridge between two bulky organic triarylmethyl endgroups (**VI**, Scheme 3.1).[10] Although there appear to be few reports regarding polymeric sp carbon chains (**VII**, Scheme 3.1) that are not subject to dispute, a recent publication makes a credible claim of stabilization upon encapsulation in a carbon nanotube.[11]

In the course of our work with diplatinum polyynediyl complexes **V**, and dirhenium analogs,[9a,12] we have sought to sterically protect or insulate the sp carbon chains. Three distinct strategies have been employed. One features termini spanning diphosphine ligands of the formula $Ar_2P(CH_2)_zPAr_2$,[6a-d,12b] which can be introduced by substitution or metathesis reactions as illustrated in Scheme 3.2 for diplatinum complexes (**V** and **VIII**). When sufficiently long, the sp^3 chains adopt double helical conformations (**IX**). This chiral motif has been documented in a number of crystal structures. Oxidations to mixed valence Pt(II)/Pt(III) species become considerably more reversible. However, the two double helix enantiomers rapidly interconvert in solution, the mechanism of which involves the uncoiling of the protective helices.

The next approach involved phosphine ligands with long perfluoroalkyl containing chains such as $P((CH_2)_xR_{fy})_3$ (R_{fy} = $(CF_2)_{y-1}CF_3$; *x*/*y* = **a**, 2/8; **b**, 3/8; **c**, 3/10).[6e] The thinking here was that the perfluoroalkyl groups would segregate into fluorous domains, consistent with their established lipophobicity. It was thought that structural motifs of the type **X** (Scheme 3.3) might result. While the crystal structures of many precursors exhibited such phase segregation,[6e,13] suitable crystals of **X** could not be obtained. Furthermore, the reversibilities of electrochemical oxidations were not enhanced in solution.

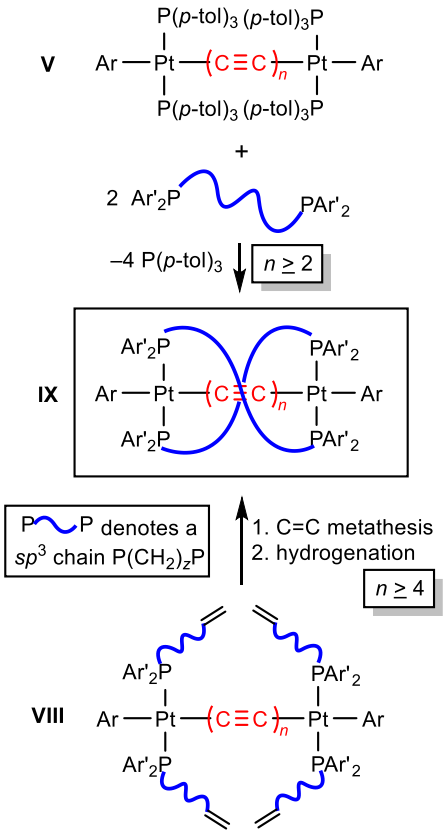

Scheme 3.2. First generation approach to sterically insulated diplatinum polyynediyl complexes (**IX**).

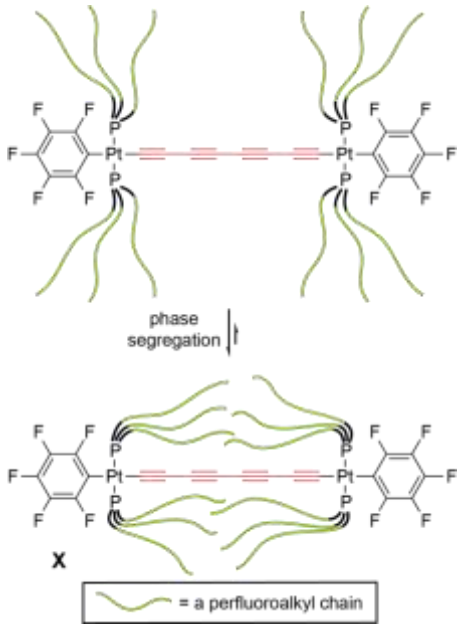

Scheme 3.3. Second generation approach to sterically insulated diplatinum polyynediyl complexes.

We have therefore sought to sterically protect the sp carbon chains in ways that would not be compromised by dynamic processes and definitively envelop the unsaturated moiety. Rotaxanes, which have garnered much attention in connection with the Nobel Prizes of the last year,[14,15,16] would present a particularly attractive strategy. Thus, we set out to synthesize diplatinum polyynediyl complexes that would be mechanically interlocked with macrocycles, as depicted in **XI** in Scheme 3.4.

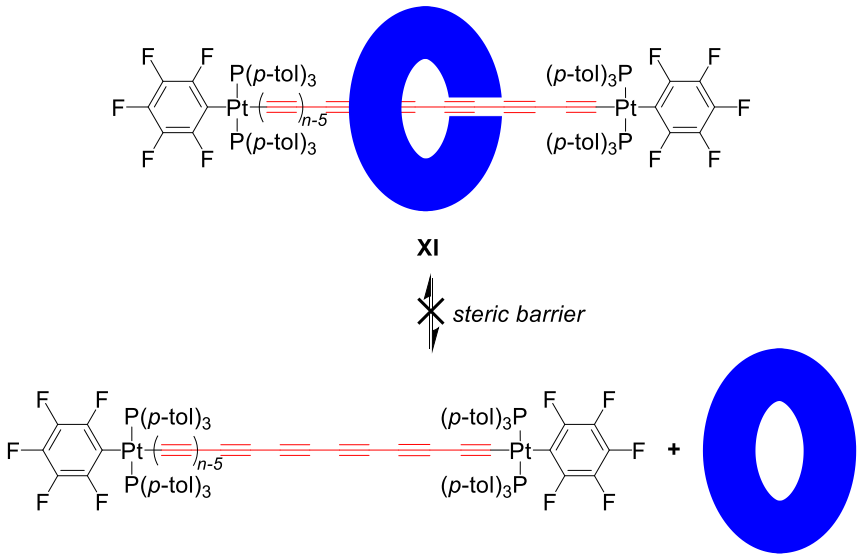

Scheme 3.4. Third generation approach to sterically insulated diplatinum polyynediyl complexes.

Some years back, our attention was drawn to a report from the Saito group of the oxidative homocoupling of an organic terminal alkyne with bulky endgroups, (*p*-$PhC_6H_4)_3C(CH_2)_6$-*p*-$OC_6H_4C{\equiv}CH$, by a copper complex of a 1,10-phenanthroline containing macrocycle.[17] As shown in Scheme 3.5, a rotaxane featuring a 1,3-butadiyne based axle was isolated in 72% yield. The copper was proposed to provide a vehicle for coupling two alkynyl units from opposite sides of the macrocycle.[17] Additional 1,3-butadiyne containing rotaxanes have been similarly prepared since,[18] or accessed by other routes.[19,20] The KCN workup was designed to detach the copper from the 1,10-phenanthroline moiety of the rotaxane, but does not always appear to be necessary (*vide infra*). This protocol has been termed an "active metal template" synthesis,[21] and many variants have been developed. An extension to catenane synthesis is shown in Scheme 3.5 (right).[22]

Given the many terminal polyynes with bulky organometallic endgroups that have been prepared in our laboratory ($L_mM(C{\equiv}C)_nH$),[9] we were naturally curious

whether this method could be extended to rotaxanes with dimetallic polyynediyl axles. In this full paper, we document a number of successful syntheses involving two related macrocycles and differing sp carbon chain lengths. Some of these have been described in preliminary communications;[23] complementary computational investigations, and independent studies of macrocycle properties, have also been reported.[24,25] The physical and chemical properties of these rotaxanes are carefully compared to those of their axle and macrocycle components. Approximately concurrently with our efforts, analogous approaches involving organic terminal polyynes were undertaken in the Tykwinski and Anderson laboratories.[26]

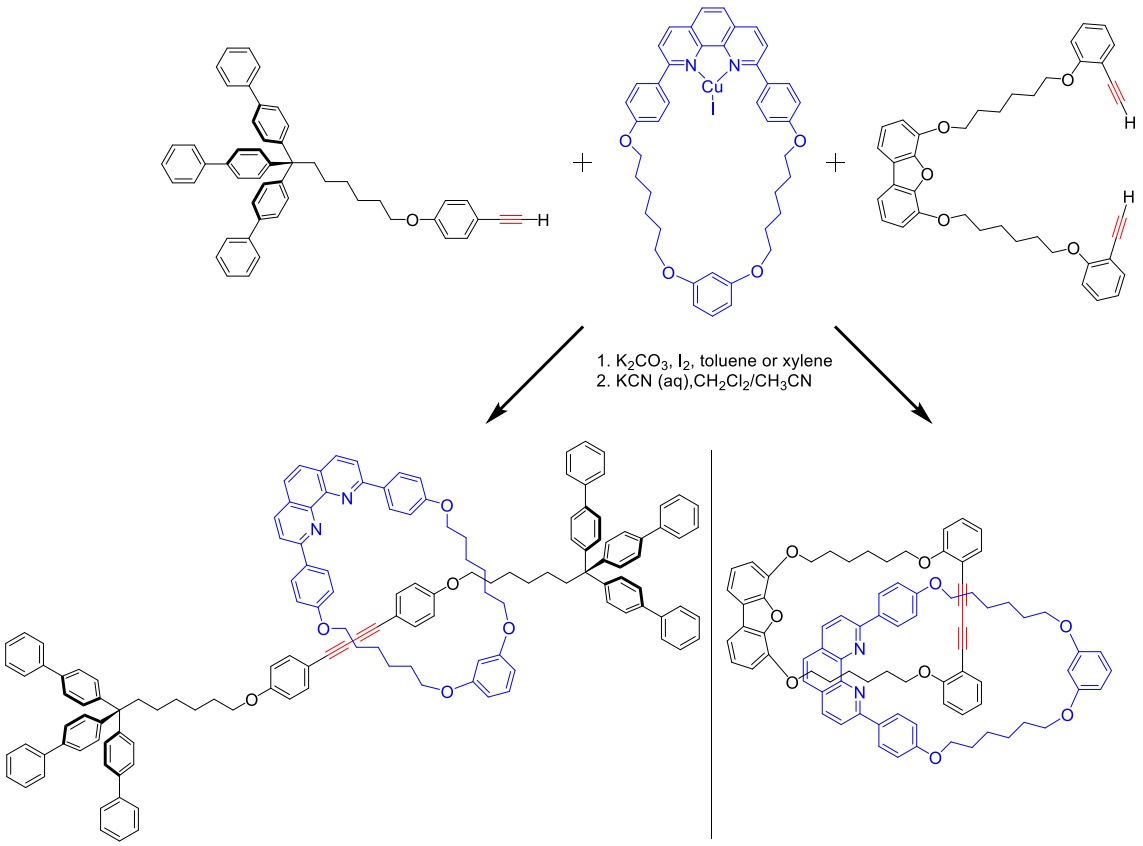

Scheme 3.5. Representative prior art: rotaxanes and catenanes formed via oxidative homocouplings of alkynes.

3.2 Results

3.2.1. Monoplatinum Complexes: Background and Syntheses. The easily accessed platinum butadiynyl complex *trans*-$(C_6F_5)(p\text{-}tol_3P)_2Pt(C{\equiv}C)_2H$ (**5**)[9b] has been shown to undergo ready oxidative homocoupling under the "Hay conditions" (O_2, CuCl/TMEDA) that have been applied to numerous organic terminal alkynes. As detailed earlier,[9b] workup gives the diplatinum octatetraynediyl complex *trans,trans*-$(C_6F_5)(p\text{-}tol_3P)_2Pt(C{\equiv}C)_4Pt(p\text{-}tol_3P)_2(C_6F_5)$ (**6**) in 97% yield.

The next higher homolog, hexatriynyl complex *trans*-$(C_6F_5)(p\text{-}tol_3P)_2Pt(C{\equiv}C)_3H$ (**7**), has been isolated in 85% yield via a low temperature deprotection of the triethylsilylhexatriynyl complex *trans*-$(C_6F_5)(p\text{-}tol_3P)_2Pt(C{\equiv}C)_3SiEt_3$ (**8a**). The latter was in turn isolated in 53% yield from the oxidative heterocoupling of **5** and the terminal alkyne $HC{\equiv}CSiEt_3$. Complex **7** undergoes an analogous oxidative homocoupling under slightly milder conditions to give the diplatinum dodecahexaynediyl complex *trans,trans*-$(C_6F_5)(p\text{-}tol_3P)_2Pt(C{\equiv}C)_6Pt(p\text{-}tol_3P)_2(C_6F_5)$ (**9**) in 92% yield.[9b]

The terminal polyynyl complexes *trans*-$(C_6F_5)(p\text{-}tol_3P)_2Pt(C{\equiv}C)_nH$ become dramatically less stable as the sp carbon chains are lengthened.[9b] In contrast to **5**, the next higher homolog **7** darkens after several minutes at room temperature. A need for the octatetraynyl complex *trans*-$(C_6F_5)(p\text{-}tol_3P)_2Pt(C{\equiv}C)_4H$ (**10**) was foreseen in this work. Although **10** has been generated in situ by deprotection of the triethylsilyloctatetraynyl complex *trans*-$(C_6F_5)(p\text{-}tol_3P)_2Pt(C{\equiv}C)_4SiEt_3$ (**11a**), and oxidatively homocoupled to give the hexadecaoctaynediyl complex $(C_6F_5)(p\text{-}tol_3P)_2Pt(C{\equiv}C)_8Pt(p\text{-}tol_3P)_2(C_6F_5)$ (**12**, 92% overall), spectroscopic monitoring indicates a species that is extremely sensitive to any manipulation.[9b] In order to maximize the availability of this critical building block,

a more labile silicon protecting group was sought. Hence, the analogous trimethylsilyloctatetraynyl complex *trans*-$(C_6F_5)(p\text{-}tol_3P)_2Pt(C{\equiv}C)_4SiMe_3$ (**11b**) was targeted.

As shown in Scheme 3.6, the butadiynyl complex **5** and commercial $HC{\equiv}CSiMe_3$ were reacted under conditions that had been used previously for $HC{\equiv}CSiEt_3$. Workup gave the new trimethylsilylhexatrienyl complex *trans*-$(C_6F_5)(p\text{-}tol_3P)_2Pt(C{\equiv}C)_3SiMe_3$ (**8b**) in 69% yield. Both **8a** and **8b** were combined with $HC{\equiv}CSiMe_3$ in a sequence that had been used previously for heterocouplings with $HC{\equiv}CSiEt_3$.[9b] As shown in Scheme 3.6, this entailed an initial $Pt(C{\equiv}C)_3SiR_3$ desilylation step that used a fluoride ion source. Workups gave **11b** in 26-14% yields. Alternatively, **11b** could be accessed in comparable overall yield by an analogous hetereocoupling of **5** and $H(C{\equiv}C)_2SiMe_3$.[27] However, this diyne is not commercially available.

Although several of the yields in Scheme 3.6 are disappointing, they could be tolerated in the penultimate step. In a control reaction described in the Appendix B, **8b** was converted to the dodecahexaynediyl complex **9** in 91% yield, using the same conditions as employed earlier with **8a**.[9b] The crystal structure of **8b** was also determined, and the rather routine data are provided in Appendix B (Tables 6.1 and 6.2, Figure B.1). All features, including the packing and unit cell dimensions, closely corresponded to those found earlier for **8a**.[28]

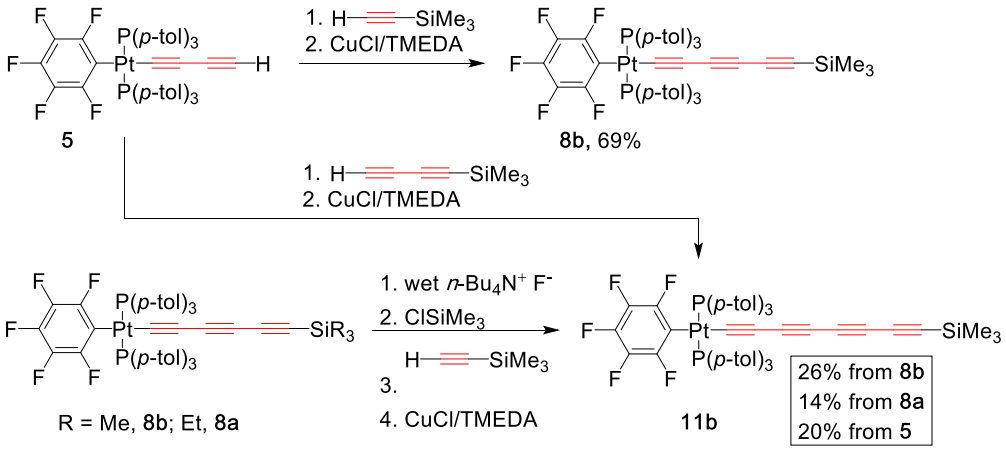

Scheme 3.6. Syntheses of monoplatinum trimethylsilylpolyynyl complexes **8b** and **11b**.

3.2.2. Syntheses of rotaxanes. Pt(C≡C)$_4$Pt axles. As noted above, the oxidative homocoupling of the butadiynyl complex **5** to octatetraynediyl complex **6** has been effected under Hay conditions (O_2, cat. CuCl/TMEDA, acetone).[9b] However, for this study the recipe used to access rotaxanes from the alkyne (p-PhC_6H_4)$_3$C(CH_2)$_6$-p-OC_6H_4C≡CH in Scheme 3.5 was applied. Thus, **5**, K_2CO_3, and the copper iodide complex of the 1,10-phenanthroline based 33-membered macrocycle **3a** shown in Scheme 3.7 (**4a**)[17a,24b] were combined in THF (2.5:4.0:1.0 mol ratio) at 55 °C (Conditions A). Then a THF solution of I_2 (1.9 equiv) was added dropwise. A silica gel column gave a mixture of the target rotaxane **6·3a** and unthreaded **3a**.

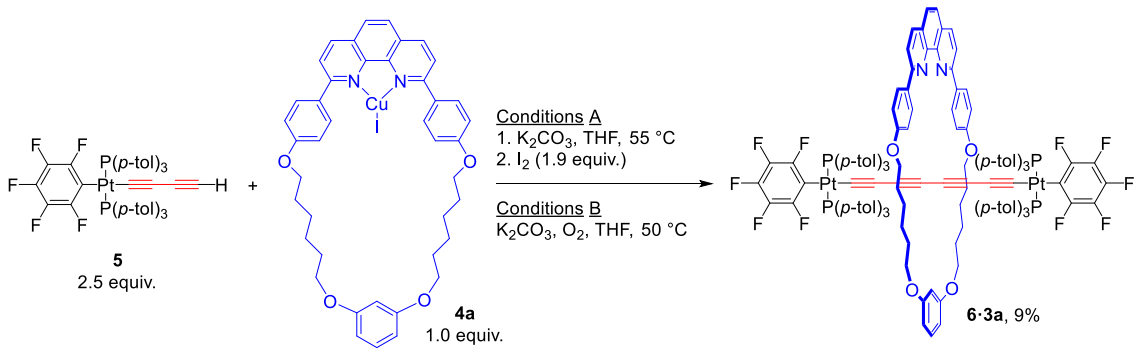

Scheme 3.7. Synthesis of a rotaxane derived from the diplatinum octatetraynediyl complex **6**.

The yields of **6·3a** in replicate reactions were low. Interestingly, data suggested the concurrent formation of an iodinated PtC≡CCI=CHI species, which could be independently generated from **5** and I_2 (mass spectrum (MALDI$^+$/DCTB matrix, *m/z*): 1346 (M+2K); ^{1}H NMR ($CDCl_3$, δ/ppm) 6.13 and 5.91 (2s, 86:14, tentatively assigned as E/Z CI=CHI)). Hence, an alternative procedure involving **4a**, O_2, and the base K_2CO_3 (50 °C) was investigated (Conditions B). Comparable quantities of **6·3a** were obtained. Alumina column chromatography afforded **6·3a** as an air stable light yellow solid in an average yield of 9%. The rotaxane structure was unequivocally established by NMR and crystallographic data described below. In some of the preceding reactions, variable amounts of the homocoupling product **6** were evident by TLC and NMR. In no case did yields improve when aqueous KCN was added as in Scheme 3.5 or other studies.[17,18c,19a,21c]

<u>Pt(C≡C)$_6$Pt axles</u>. Two series of experiments were conducted. The first involved the copper iodide macrocycle complex employed above, **4a**. The second involved a 35-membered homolog **4b** in which the *m*-C_6H_4 group was replaced by a sterically expanded 2,7-naphthdiyl moiety (see Scheme 3.8).[24b]

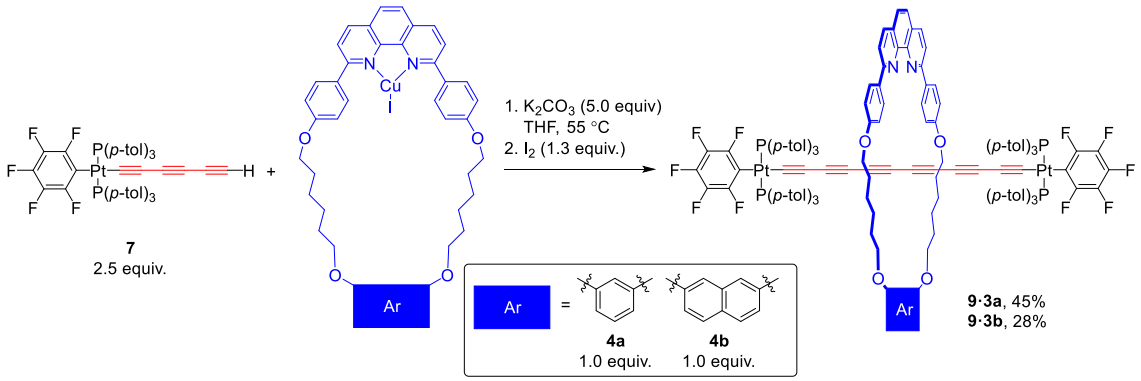

Scheme 3.8. Syntheses of rotaxanes derived from diplatinum dodecahexaynediyl complex **9**.

The isolated platinum hexatriynyl complex **7**[9b] was combined with **4a** or **4b** (2.5:1.0 mol ratio) and K_2CO_3 (5.0 equiv) in THF at 55 °C in the presence of I_2 (1.3 equiv). Chromatographic workups gave some of the previously characterized dodecahexaynediyl complex **9** (30% based upon **7** in the reaction with **4a**). However, the major products were the target rotaxanes **9·3a** (45% based upon limiting macrocycle) and **9·3b** (28%). These yields are much higher than those realized for **6·3a**, presumably for steric and/or electronic reasons (as noted above, oxidative homocouplings of $L_mM(C{\equiv}C)_nH$ species become faster with increased sp carbon chain lengths).

<u>$Pt(C{\equiv}C)_8Pt$ axles</u>. The newly synthesized platinum trimethylsilyloctatetraynyl complex **11b** was combined with **4a** and K_2CO_3 (2.5:1.0:10.0 mol ratio) in THF at room temperature °C in the presence of I_2 (1.3 equiv), as described for the other rotaxanes. During a workup step, aqueous KCN was added. This reagent was applied here but not in Schemes 3.7 and 8 as ^1H NMR spectra of the crude reaction mixtures often showed characteristic features of macrocycle/CuX adducts. Preparative TLC gave the hexadecaoctaynyl complex **12** (4% based upon **11b**) and the target rotaxane **12·3a** in 7% yield based upon **4a**. The lower yield as compared to **9·3a** and **9·3b** in Scheme 3.8 may reflect the diminished stability of the octatetraynyl complex precursor **10**, as noted above.

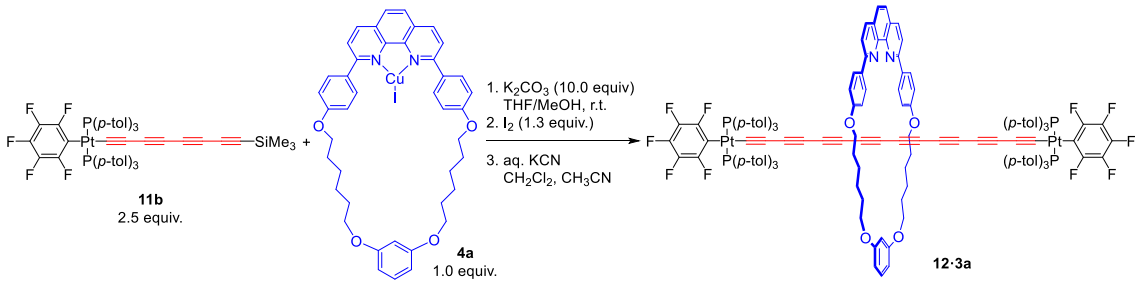

Scheme 3.9. Synthesis of a rotaxane derived from diplatinum hexadecaoctaynediyl complex **12**.

3.2.3. Spectroscopic Characterization. The structures of the rotaxanes were supported by a variety of data. In the case of the lowest homolog **6·3a**, the ^{1}H NMR spectrum showed distinctive changes in chemical shifts, as illustrated in Figures 3.1 and 3.2 and summarized in Table 3.1. For example, the $OC\underline{H}_2C\underline{H}_2C\underline{H}_2$ signals of the macrocycle **3a** shifted 0.65-0.82 ppm upfield (Figure 3.1), consistent with contemporary models for the magnetic shielding anisotropies of polyynes.[29] The signal for the *p*-C_6H_4 protons closest to the OCH_2 substituent also shifted upfield (0.21 ppm), as did that for the *m*-C_6H_4 proton *ortho* to the two OCH_2 groups (0.34 ppm; Figure 3.2). However, the other *m*-C_6H_4 protons, which are exo to the polyyne chain, shifted slightly downfield. The methyl signals of the *p*-tol_3P ligands also shifted upfield (0.24 ppm, Figure 3.1), consistent with shielding by the arene rings of the macrocycle, in accord with the crystal structure below.

Table 3.1. Changes in ^{1}H NMR chemical shifts of the macrocycle (**3a**, **3b**) or axle (**6**, **9**, **12**) components upon rotaxane formation (Δδ/ppm; negative = upfield shift, positive = downfield shift).

Rotaxane	**6·3a**	**9·3a**	**12·3a**	**9·3b**
OC<u>H</u>$_2$C<u>H</u>$_2$C<u>H</u>$_2$	–0.65 to –0.82	–0.31 to –0.40	–0.18 to –0.27	–0.28 to –0.41
p-C$_6$H$_4$				
OCC<u>H</u>CH	–0.21	–0.10	–0.09	–0.07
OCCHC<u>H</u>	0.00	–0.05	–0.05	–0.13
phenanthryl	+0.12 to +0.13	0.00 to +0.10	–0.01 to +0.07	–0.07 to 0.00
m-C$_6$H$_4$				
OCC<u>H</u>CCO	–0.34	–0.24	–0.21	-
OCC<u>H</u>CH	+0.04	–0.08	–0.09	-
OCCHC<u>H</u>	+0.04	–0.12	–0.04	-
2,7-naphthdiyl				
OCCHC<u>H</u>	-	-	-	–0.05
OCC<u>H</u>CC	-	-	-	–0.15
OCC<u>H</u>CH	-	-	-	–0.07
CH$_3$ of *p*-tol$_3$P	–0.24	–0.12	–0.07	–0.15
o to P	–0.11	–0.005	+0.08	–0.31
m to P	–0.20	–0.10	–0.05	–0.15

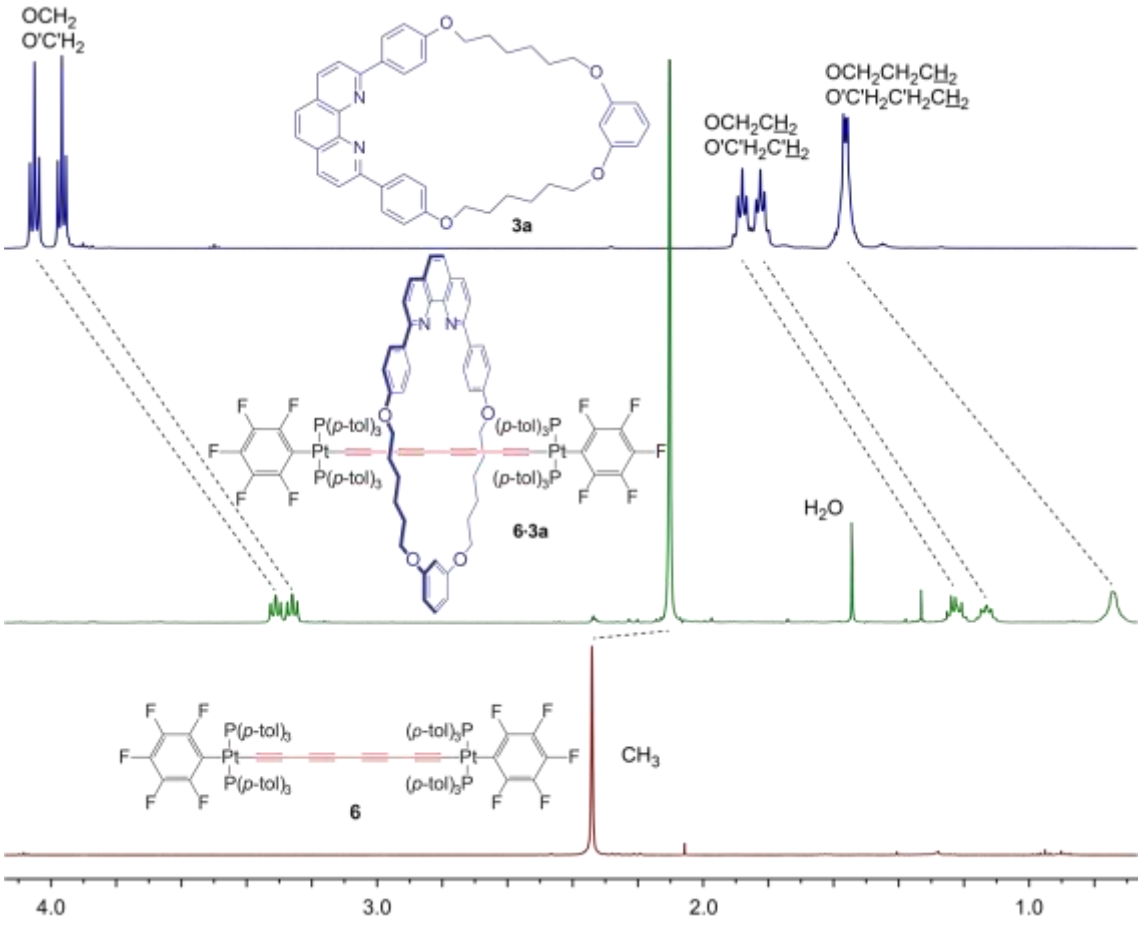

Figure 3.1. Shifts in ^{1}H NMR signals (aliphatic region, $CDCl_3$) for the rotaxane **6·3a** (middle) as compared to the macrocycle and axle components **3a** (top) and **6** (bottom).

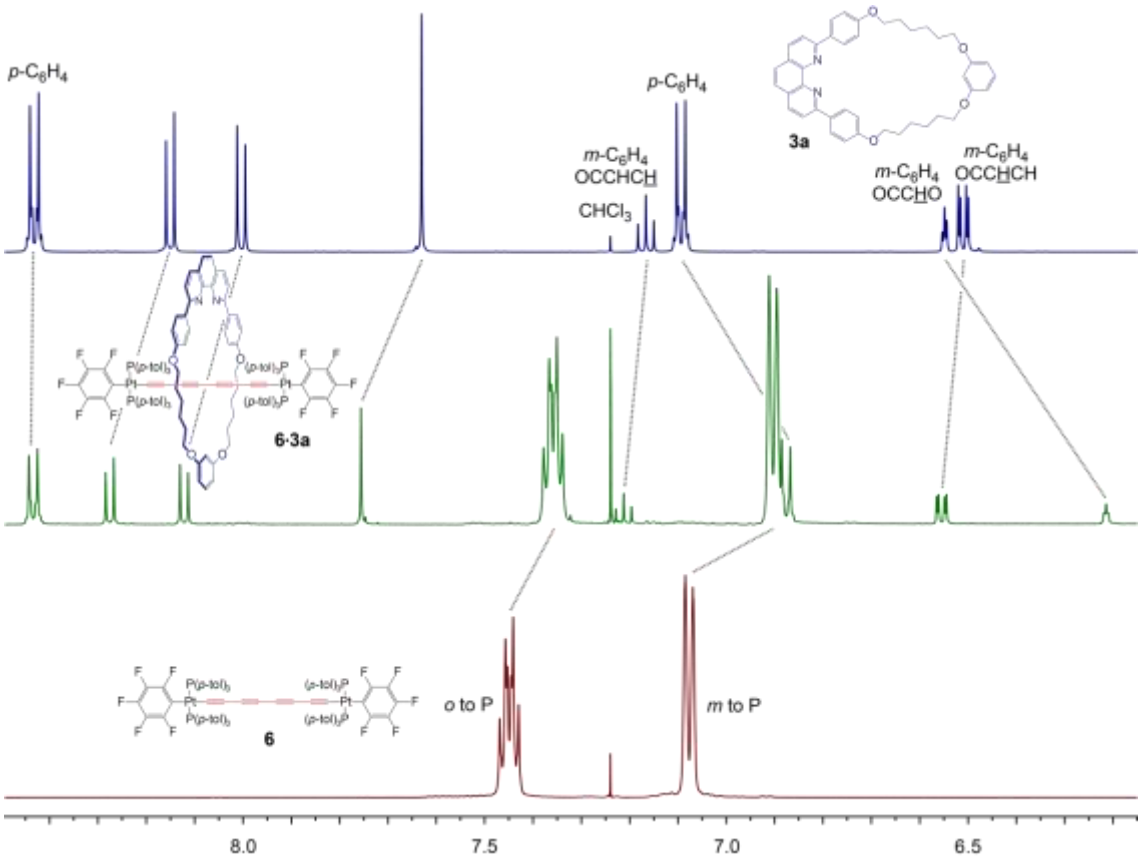

Figure 3.2. Shifts in ^{1}H NMR signals (aromatic region, $CDCl_3$) for the rotaxane **6·3a** (middle) as compared to the macrocycle and axle components **3a** (top) and **6** (bottom).

As illustrated in Figure 3.3, the $^{13}C\{^{1}H\}$ NMR spectrum of **6·3a** showed modest but unambiguously upfield shifts for the $O\underline{C}H_2\underline{C}H_2\underline{C}H_2$ signals (0.2-1.5 ppm). The CH group *ortho* to the two OCH_2 substituents of the *m*-C_6H_4 moiety gave a more pronounced upfield shift (4.4 ppm), as depicted in Figure 3.4. In contrast, the two CH groups *ortho* to a single OCH_2 substituent of the *m*-C_6H_4 moiety gave a slight downfield shift (1.6 ppm), as seen with the ^{1}H NMR signals. However, there were no conspicuous trends in the other signals. Analogous but often less pronounced upfield ^{1}H and ^{13}C NMR shifts can be observed with diyne-based rotaxanes and catenanes.[17,18,19]

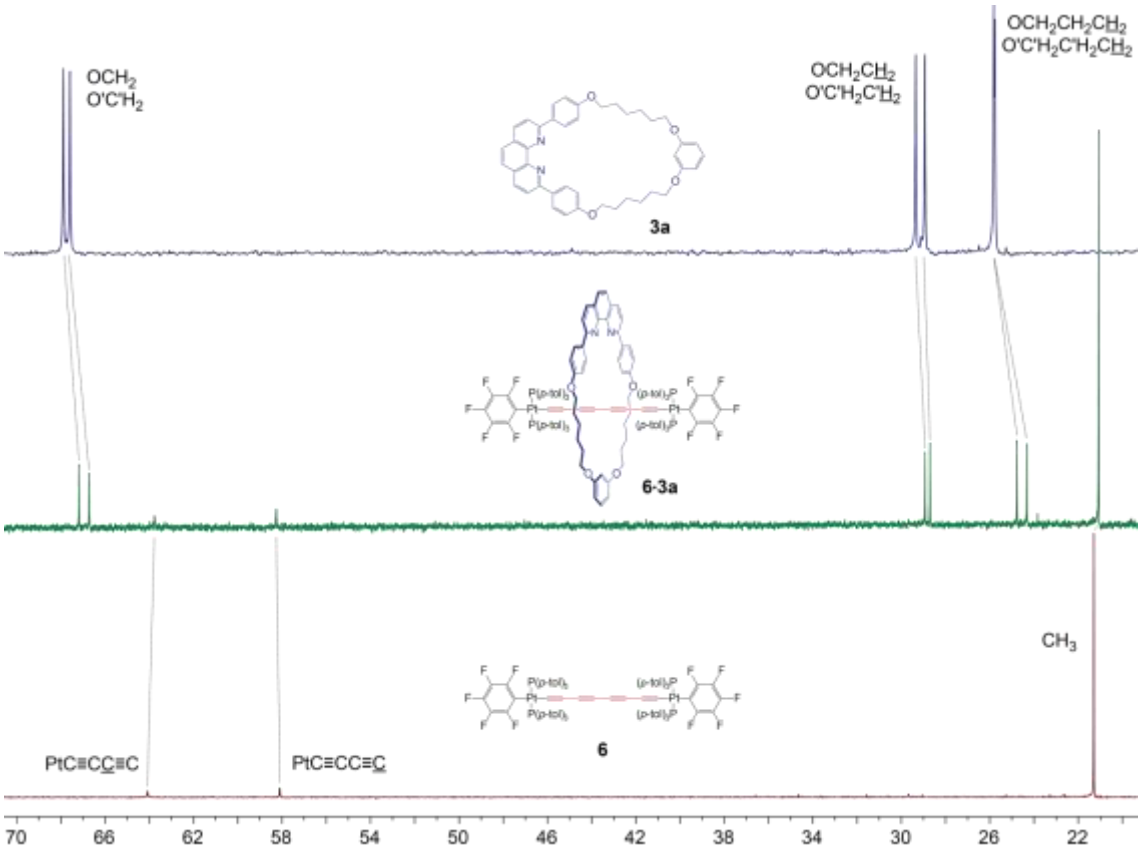

Figure 3.3. Shifts in $^{13}C\{^{1}H\}$ NMR signals (upfield region, $CDCl_3$) for the rotaxane **6·3a** (middle) as compared to the macrocycle and axle components **3a** (top) and **6** (bottom).

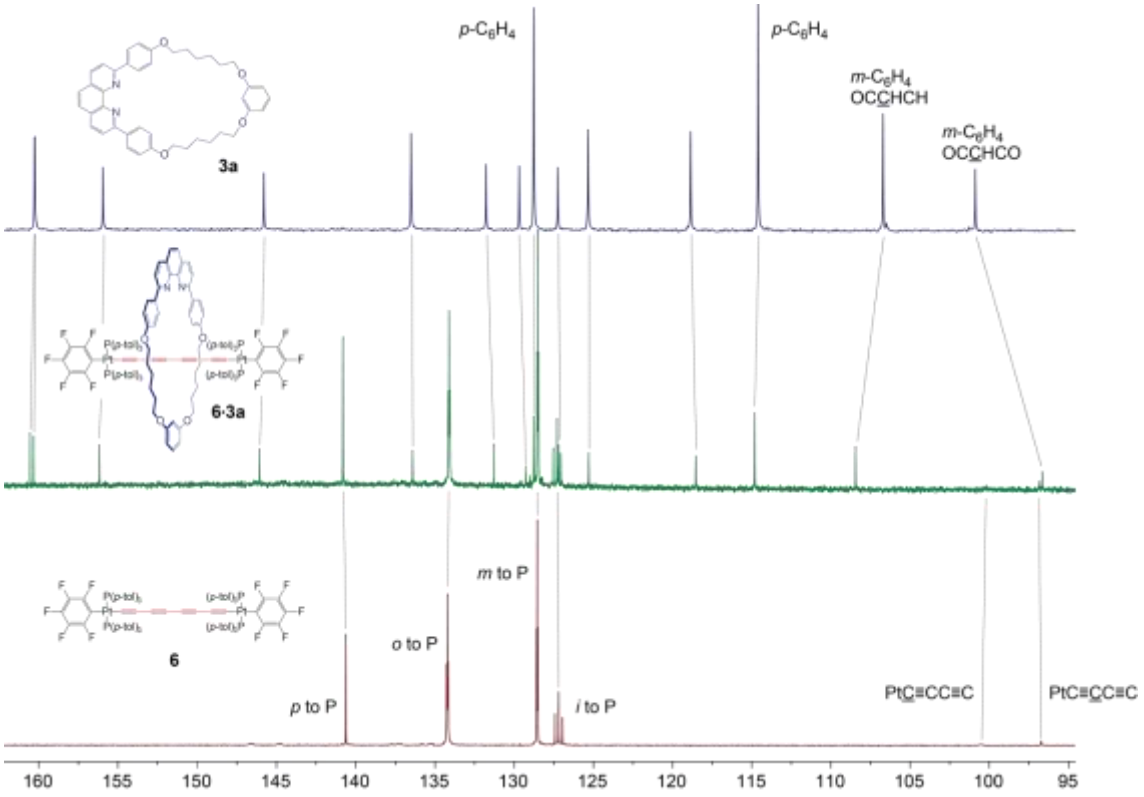

Figure 3.4. Shifts in $^{13}C\{^{1}H\}$ NMR signals (downfield region, $CDCl_3$) for the rotaxane **6·3a** (middle) as compared to the macrocycle and axle components **3a** (top) and **6** (bottom).

The rotaxanes with $Pt(C{\equiv}C)_6Pt$ axles, **9·3a** and **9·3b**, gave similar ^{1}H and $^{13}C\{^{1}H\}$ NMR chemical shift patterns. The ^{1}H NMR spectra are illustrated in Figures 3.5 and 3.6, and key trends are summarized in Table 3.1. The $OC\underline{H}_2C\underline{H}_2C\underline{H}_2$ signals shifted upfield from those of the macrocycles, but like most signals to a lesser degree than the lower homolog **6·3a** (0.32-0.41 vs. 0.65-0.82 ppm). The proton between the two *m*-C_6H_4 substituents in **9·3a** also shifted upfield (0.24 vs. 0.34 ppm), as did the *peri* 1,8-naphthyl protons between the 2,7 substituents in **9·3b** (0.15 ppm). The *p*-tol_3P methyl ^{1}H signals similarly moved upfield (0.12-0.15 vs. 0.24 ppm). The ^{13}C NMR spectrum showed an upfield shift for the CH group between the two *m*-C_6H_4 substituents in **9·3a** (2.4 vs. 4.2 ppm), but differences in the other CH_2 signals were less than 1.0 ppm. When

^{1}H NMR spectra of CD_2Cl_2 solutions of **9·3a** were recorded at –80 °C, no decoalescence phenomena were observed, although some peaks noticeably broadened.

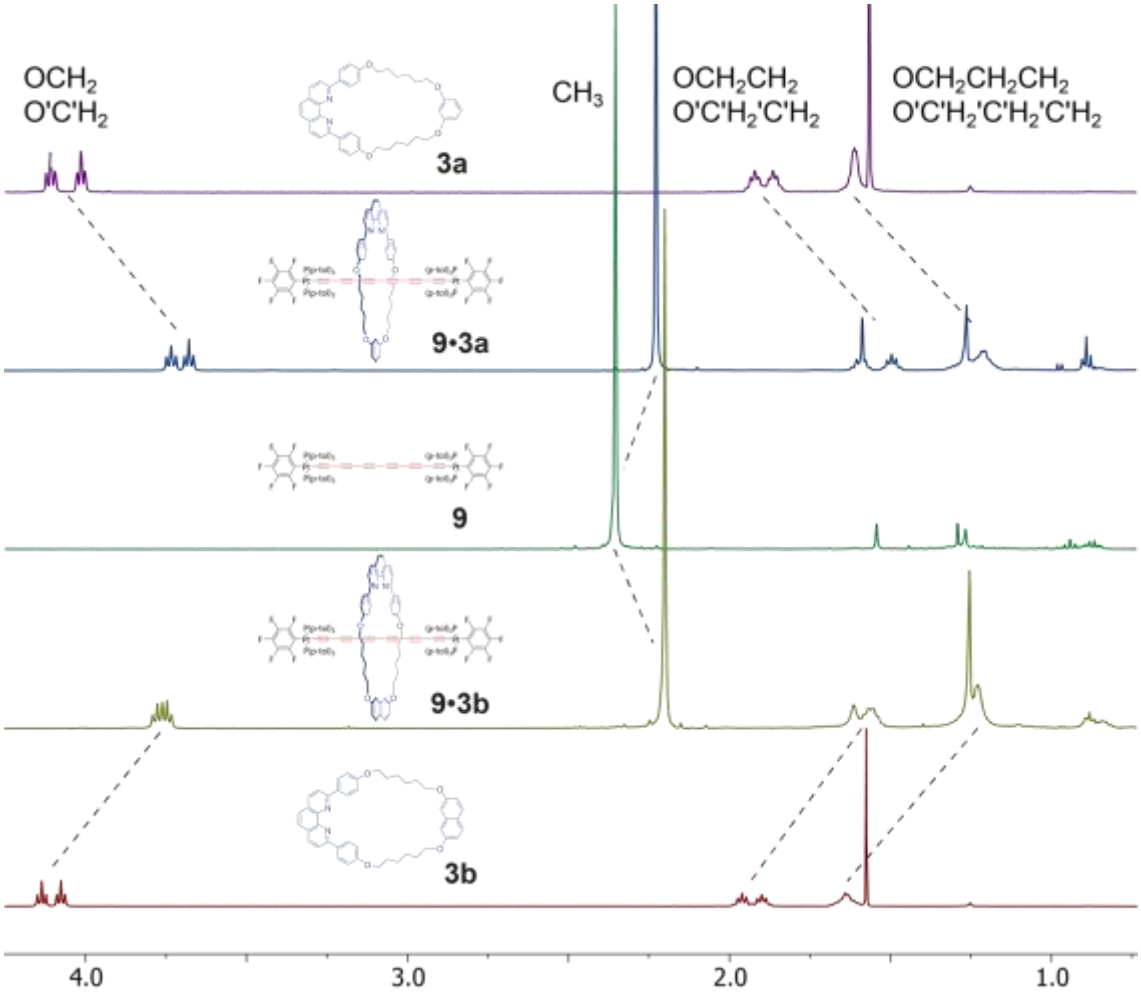

Figure 3.5. Shifts in ^{1}H NMR signals (aliphatic region, $CDCl_3$) for the rotaxanes **9·3a** and **9·3b** as compared to the macrocycle and axle components **3a** or **3b** (top, bottom) and **6** (middle).

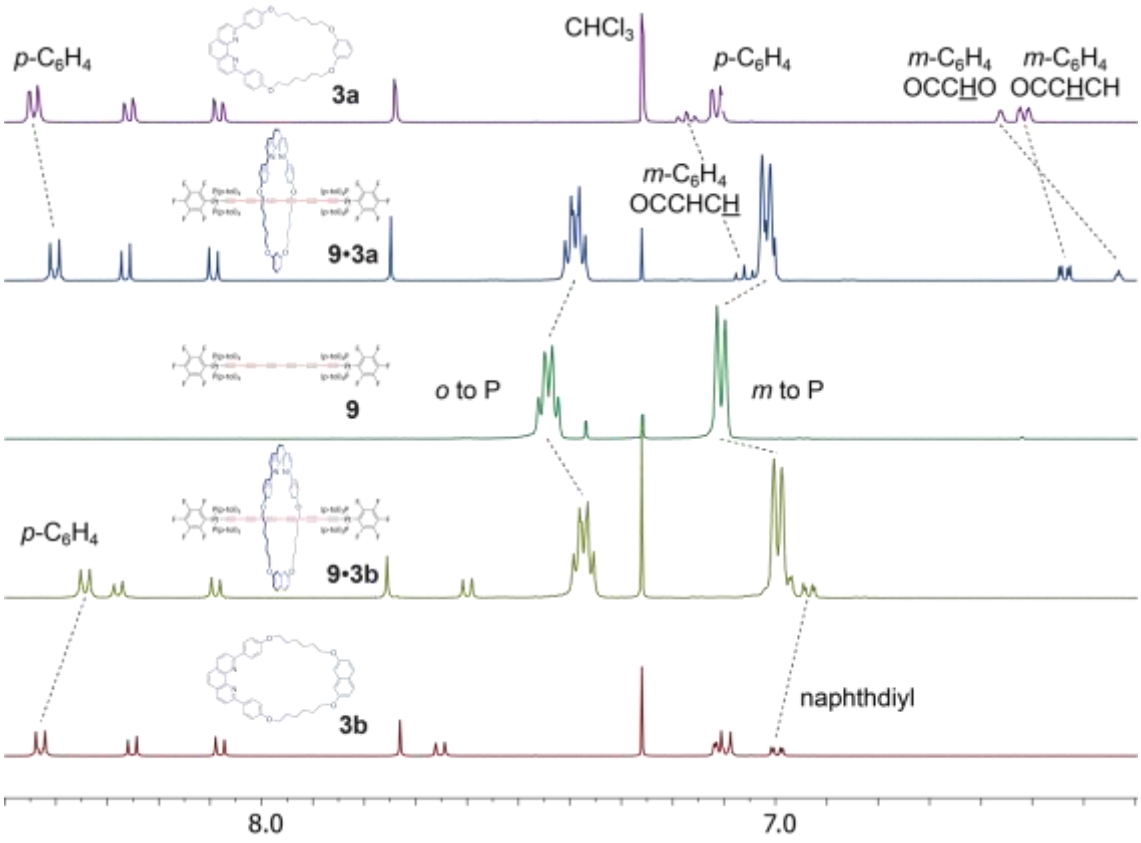

Figure 3.6. Shifts in ^{1}H NMR signals (aromatic region, $CDCl_3$) for the rotaxanes **9·3a** and **9·3b** as compared to the macrocycle and axle components **3a** or **3b** (top, bottom) and **2** (middle).

The rotaxane with a $Pt(C{\equiv}C)_8Pt$ axle, **12·3a**, usually exhibited ^{1}H and $^{13}C\{^{1}H\}$ NMR chemical shift trends analogous to those of the lower homologs **6·3a** and **9·3a**. The ^{1}H NMR spectra are depicted in Figures 3.7 and 3.8, and changes in chemical shifts are summarized in Table 3.1. In general, these are diminished relative to those of the lower homologs. Other NMR spectra that compare features of the rotaxanes are provided in Figure B.2 (Appendix B).

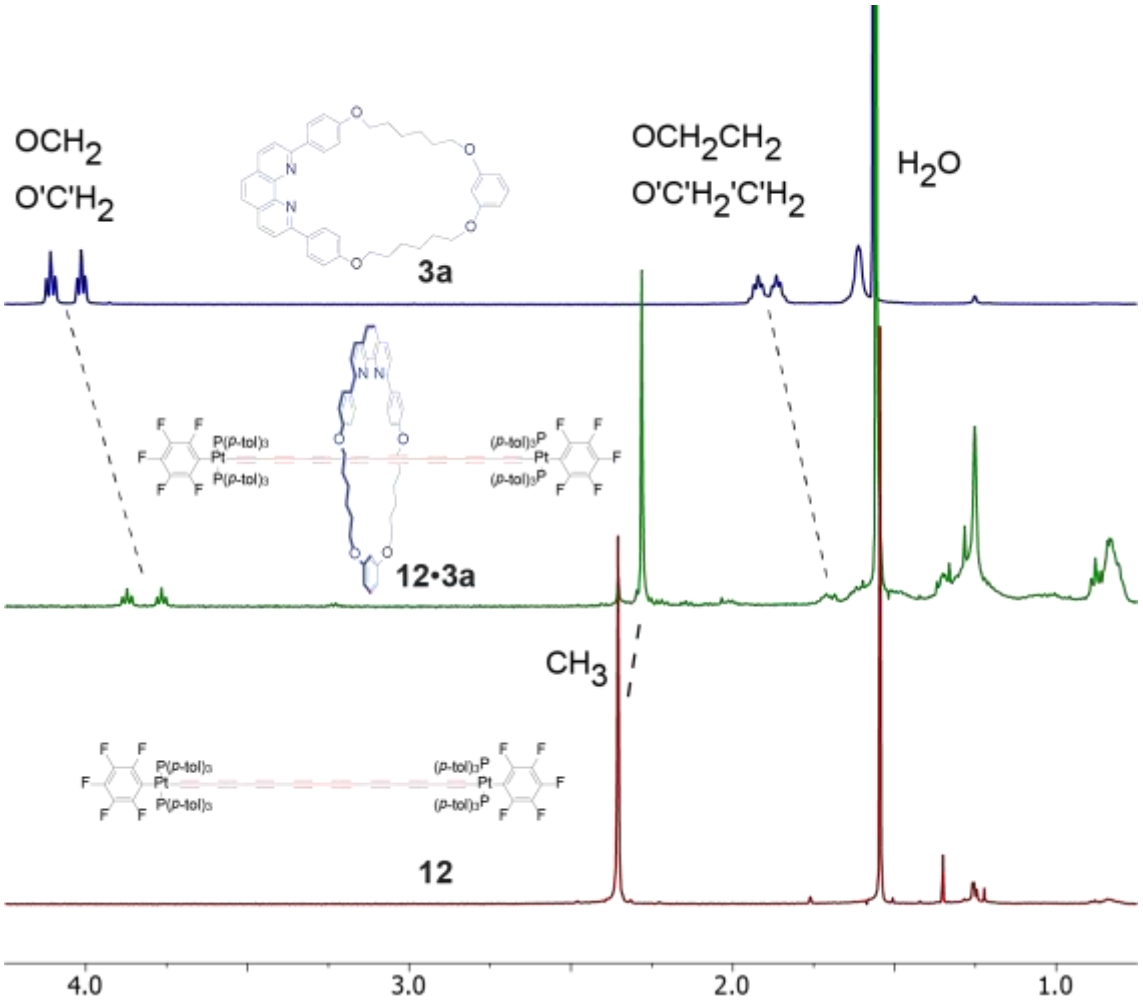

Figure 3.7. Shifts in ^{1}H NMR signals (aliphatic region, $CDCl_3$) for the rotaxane **12·3a** (middle) as compared to the macrocycle and axle components **3a** (top) and **12** (bottom).

The ^{31}P NMR spectra of the diplatinum polyynediyl complexes **6**, **9**, and **12** were essentially unaffected upon rotaxane formation. The IR $\nu_{C\equiv C}$ bands of **6·3a** were at slightly higher frequencies than those of **6** when recorded under side-by-side conditions (ATR/powder film, cm^{-1}: 2149 vs. 2139 (m/m); 2008 vs. 1996 (w/w)). However, no trends were apparent with **9·3a**, **9·3b**, and **9** (**9·3a** 2160/2090/1993 w/m/w; **9·3b**

2127/2088/1992 m/m/w; **9** 2131/2092/2015 m/m/m), or **12·3a** and **12** (**12·3a** 2161/2094/2056/1992 w/w/m/w; **12** 2154/2088/2054/1984 w/w/s/m).

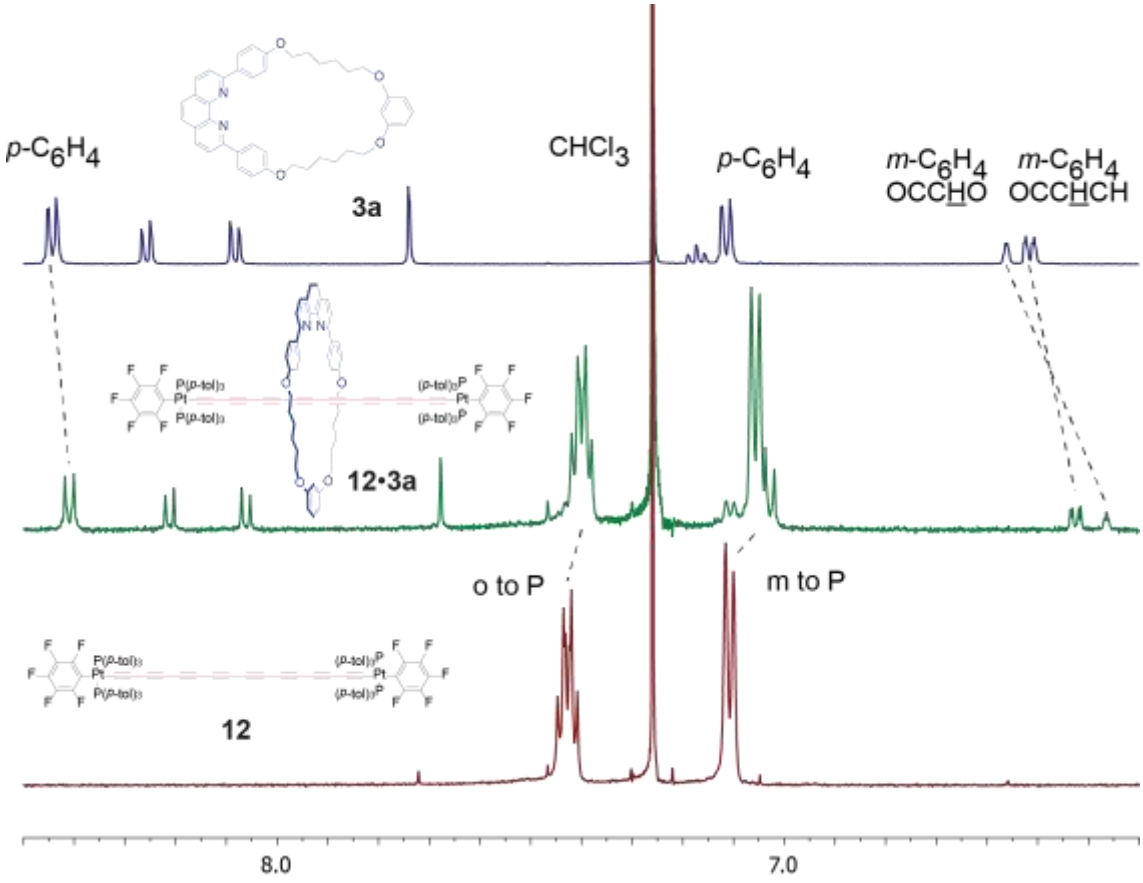

Figure 3.8. Shifts in ^{1}H NMR signals (aromatic region, $CDCl_3$) for the rotaxane **12·3a** (middle) as compared to the macrocycle and axle components **3a** (top) and **12** (bottom).

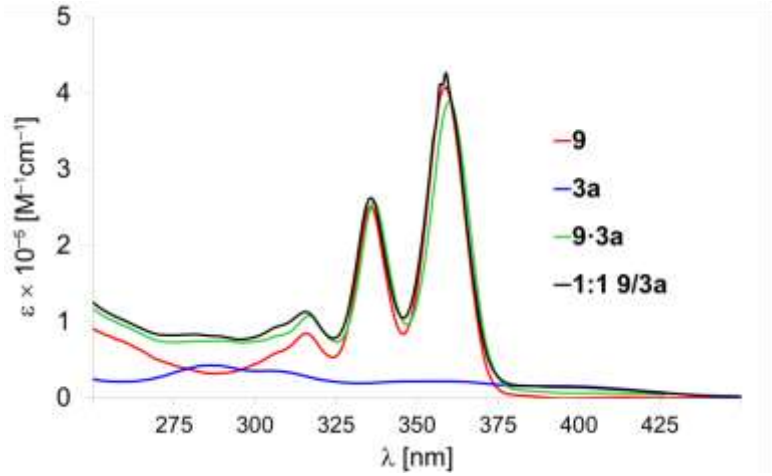

Figure 3.9. UV-visible spectra of rotaxane **9·3a**, its macrocycle (**3a**) and axle (**9**) components, and 1:1 mixture thereof (in CH_2Cl_2).

The UV-visible spectra of the rotaxanes did not show any evidence for significant electronic interaction between the diplatinum and macrocycle components. As summarized in Table 3.2, they were essentially identical to those of separately prepared 1:1 mixtures. Representative series of spectra are depicted in Figures 3.9 and 6.5 (Appendix B). Time dependent DFT calculations[24] also failed to identify any unique interactions of significant magnitudes.

Table 3.2. UV-visible data for rotaxanes **6·3a**, **9·3a**, **9·3b**, and **12·3a**, their macrocycle (**3a** or **3b**) and axle (**6**, **9**, and **12**) components, and 1:1 mixtures thereof (in CH_2Cl_2).

Substrate	Wavelength (nm) [ε, $M^{-1}cm^{-1}$]
6	267 (61000), 275 (87000), 295 (91000), 326 (126000), 355 (8100), 383 (6000), 414 (4000)
3a	238 (34000), 286 (50000), 326 (25000), 339 (24000)
6·3a	267 (69000), 293 (120000), 325 (129000), 355 (27000), 381 (9000), 414 (5000)
1:1 **6**/**3a**	267 (81000), 277 (103000), 292 (106000), 325 (123000), 355 (22000), 382 (6000), 415 (3000)
9	280 (172000), 307 (168000), 315 (181000), 335 (353000), 360 (497000), 412 (2460), 448 (1680), 490 (744)
9·3a	289 (75100), 317 (108000), 337 (257000), 360 (389000), 413 (6570)
1:1 **9**/**3a**	281 (83300), 288 (81200), 306 (93100), 316 (113000), 335 (264000), 359 (434000), 396 (14300)
3b	287 (52300), 311 (30900), 326 (29100), 341 (24700), 392 (7030)
9·3b	312 (69700), 320 (69800), 341 (80400), 367 (95100), 415 (20000), 451 (9460)
1:1 **9**/**3b**	315 (119000), 336 (256000), 358 (463000), 396 (29800)
12	290 (46000), 306 (42000), 326 (54000), 346 (151000), 369 (397000), 397 (602000)
12·3a	290 (40400), 306 (29400), 326 (31800), 347 (56900), 370 (115000), 399 (169000)
1:1 **12**/**3a**	281 (43300), 306 (93100), 316 (31100), 335 (26400), 359 (434000), 396 (143000)

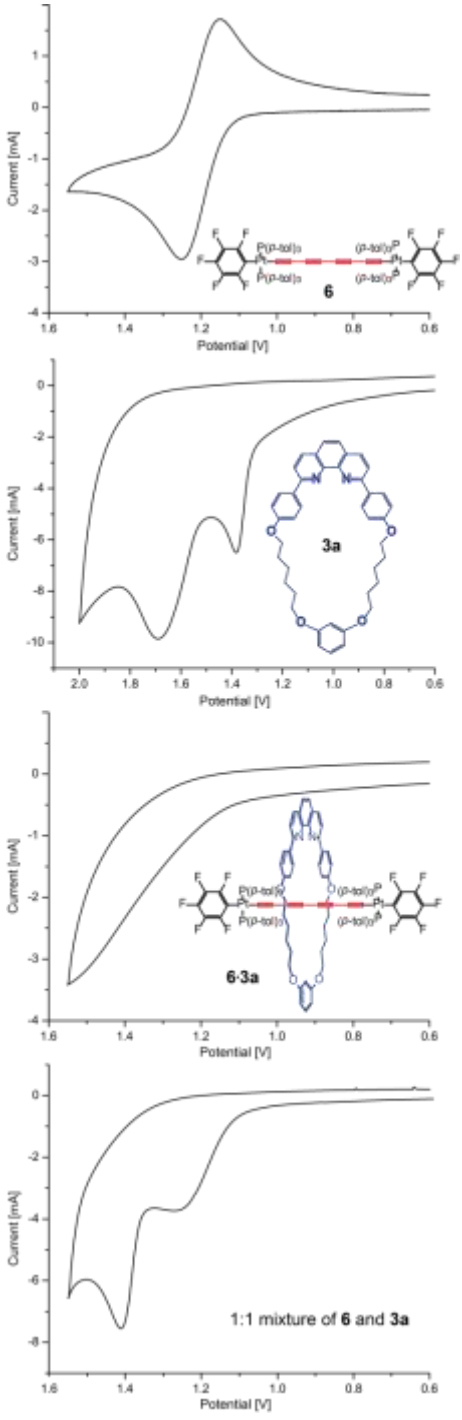

Figure 3.10. Representative cyclic voltammograms from Table 3.3.

Cyclic voltammograms of rotaxanes **6**·**3a**, **9**·**3a**, and **9**·**3b** and the macrocycles **3a** and **3b** were recorded in CH_2Cl_2 under conditions previously used for the axles **6**, **9**, and **12**, and higher homologs.[9b] Data are summarized in Table 3.3, and representative traces are provided in Figure 3.10. As noted earlier,[9b] diplatinum polyynediyl complexes become thermodynamically more difficult to oxidize as the sp carbon chain is extended, and the degree of reversibility markedly decreases. No significant cathodic current can be detected with **12**. No reductions of **6**, **9**, or **12** are observed in cathodic scans to the solvent imposed limit.

Table 3.3. Cyclic voltammetry data.

Substrate[a]	$E_{p,a}$ [V]	$E_{p,c}$ [V]	$E°$ [V]	ΔE [mV]	$i_{c/a}$
6	1.227	1.136	1.182	91	0.94
6[b,c]	1.261	1.143	1.202	118	0.48
9[b]	1.465	1.306	1.386	161	low
3a[d]	1.403, 1.710	-	-	-	0
3b	1.381, 2.000	-	-	-	0
1:1 **6**/**3a**[e]	1.266, 1.399	-	-	-	0
6·**3a**, **9**·**3a**, **9**·**3b**	-	-	-	-	0

[a] Conditions: 8×10^{-4} M in CH_2Cl_2, *n*-Bu_4N^+ PF_6^-, 23.0 °C ± 1 °C; Pt working and auxiliary electrodes, Ag/AgCl reference electrode; scan rate, 100 mV s^{-1}; ferrocene, $E°$ = 0.46 V. [b] These represent previously reported data obtained under essentially identical conditions but using the supporting electrolyte *n*-Bu_4N^+ BF_4^-; see reference 9b. [c] As the sample used in this study was repeatedly crystallized, the $i_{c/a}$ value progressively increased compared to that obtained in the earlier study. [d] The onset of another peak is apparent with further anodic scanning. [e] When the switching potential is shifted to 1.350 V (prior to reaching the second anodic peak), the first oxidation becomes partially reversible with an $i_{c/a}$ value of 0.66.

The macrocycles undergo irreversible oxidations at potentials comparable to that at which **9** undergoes a partially reversible oxidation. Thus, the cyclic voltammograms of **6**·**3a**, **9**·**3a**, and **9**·**3b** are essentially featureless, outside of gradually increasing anodic

current. The cyclic voltammogram of a 1:1 mixture of **6** and **3a** exhibits oxidations at potentials close to those of the axle and macrocycle components, but no cathodic current (unless the switching potential is shifted to after the first anodic peak). These data are further interpreted in the discussion section.

3.2.4. Crystallography. Crystals of solvates of the rotaxanes **6·3a**, **9·3a**, and **9·3b** could be grown as described in the experimental section. The structures were solved as summarized in Table 3.4 and the experimental section. Key metrical parameters are listed in Tables 3.5 and 3.6.[30] Thermal ellipsoid and space filling representations are provided in Figure 3.9. These illustrate the close proximity of the sp carbon chains to the macrocycle hydrogen and carbon atoms whose NMR chemical shifts are most affected (Table 3.1). Some contacts are slightly less than the sum of the van der Waals radii of sp and sp^3 hybridized carbon atoms (1.70 + 1.78 Å),[31] and a variety of nearest neighbor relationships and average distances are highlighted in Table 3.5. Only in the most sterically congested complex (**6·3a**) is the macrocycle locked into a narrow range of conformations by the bulky endgroups. These and related issues are further analyzed in the discussion section.

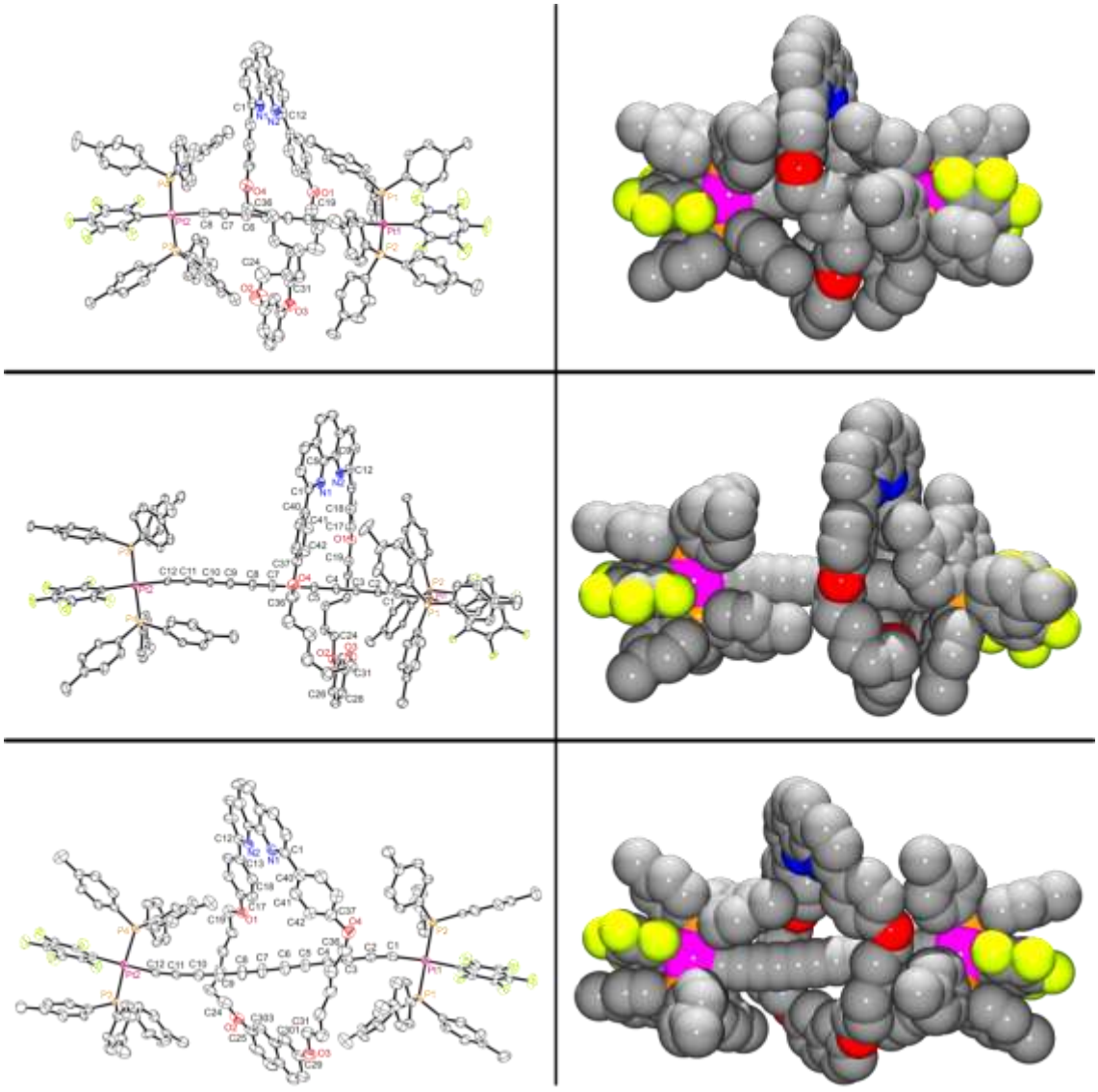

Figure 3.11. Thermal ellipsoid plots (50% probability; left) and space filling representations (right) of the molecular structures of **6·3a** (top), **9·3a** (middle), and **9·3b** (bottom); for comments on atom numbering see footnote 30.

Table 3.4. Crystallographic data for rotaxanes.

Complex	**6·3a**·$2CH_2Cl_2$	**9·3a**·$0.5CHCl_3$	**9·3b**·$2C_6H_6$
empirical formula	$C_{148}Cl_4H_{130}F_{10}N_2O_4P_4Pt_2$	$C_{150.5}H_{126.5}Cl_{1.5}F_{10}N_2O_4P_4Pt_2$	$C_{166}H_{140}F_{10}N_2O_4P_4Pt_2$
formula weight	2846.54	2784.26	2930.85
temperature [K]	100(2)	100.15	110(2)
diffractometer	Bruker D8 GADDS	ALS Beamline 11.3.1	Bruker APEX 2
wavelength [Å]	1.54178	0.6889	0.71073
crystal system	Triclinic	Triclinic	Triclinic
space group	*P-1*	*P-1*	*P-1*
unit cell dimensions			
a [Å]	18.5889(8)	12.601(3)	13.214(9)
b [Å]	20.1664(9)	26.978(5)	21.955(16)
c [Å]	21.3140(10)	20.408(4)	24.747(16)
α [°]	117.641(3)	92.508(3)	99.477(7)
β [°]	93.431(3)	96.172(3)	104.268(7)
γ [°]	103.009	107.174(3)	90.432(7)
volume [$Å^3$]	6770.4(5)	6569(2)	6854(8)
Z	2	2	2
ρ_{calcd} [Mg/m^3]	1.40	1.408	1.420
μ [mm^{-1}]	4.788	2.091	2.157
F(000)	2708	2814	2976
crystal size [mm^3]	0.27 × 0.22 × 0.03	0.08 × 0.08 × 0.02	0.41 × 0.33 × 0.01
range for data collection	2.38 to 60.00	2.591 to 27.362	1.592 to 22.500

Table 3.4 continued

Complex	**6·3a**·2CH_2Cl_2	**9·3a**·0.5$CHCl_3$	**9·3b**·2C_6H_6
index ranges	$-20 \le h \le 20$	$-16 \le h \le 16$	$-14 \le h \le 14$
	$-22 \le k \le 22$	$-27 \le k \le 27$	$-23 \le k \le 23$
	$-23 \le l \le 23$	$-35 \le l \le 35$	$-26 \le l \le 26$
reflections collected	126786	186612	39715
independent reflections	19677 [R(int) = 0.0524]	32484 [R(int) = 0.0462]	17699 [R(int) = 0.0662]
max. and min. transmission	0.8697 and 0.3580	0.7455 and 0.6444	0.7448 and 0.4425
data / restraints / parameters	19677 / 15 / 1512	32484 / 93 / 1634	17699 / 18 / 1681
goodness-of-fit on F^2	1.098	1.093	1.022
final R indices [$I>2\sigma(I)$]	R1 = 0.0339	R1 = 0.0275	R1 = 0.0476
	wR2 = 0.0844	wR2 = 0.0595	wR2 = 0.1018
R indices (all data)	R1 = 0.0449	R1 = 0.0337	R1 = 0.0908
	wR2 = 0.0880	wR2 = 0.0617	wR2 = 0.1242
largest diff. peak & hole [$eÅ^{-3}$]	0.994 and –0.650	1.302 and –1.370	1.943 and –1.917

Table 3.5. Key crystallographic distances [Å] and angles [°] for solvates of the axles **6**[9b] and **9**[9b] and the rotaxanes **6·3a**, **9·3a**, and **9·3b**.

Complex	**6**·(toluene)[9b]	**6·3a**·$2CH_2Cl_2$	**9**·$4C_6H_6$·EtOH[9b]	**9·3a**·$0.5CHCl_3$	**9·3b**·$2C_6H_6$
Pt1-C1	1.951(5)	1.993(3)	1.972(6)	1.996(2)	1.946(10)
C1≡C2	1.252(6)	1.207(5)	1.234(8)	1.221(3)	1.253(11)
C2-C3	1.365(6)	1.358(6)	1.361(8)	1.363(3)	1.371(13)
C3≡C4	1.209(6)	1.206(7)	1.209(8)	1.223(3)	1.196(12)
C4-C5	1.351(8)	1.359(7)	1.363(8)	1.356(4)	1.342(13)
C5≡C6	1.209(6)	1.213(6)	1.216(7)	1.221(4)	1.221(12)
C6-C7	1.365(6)	1.346(5)	1.358(8)	1.356(4)	1.350(14)
C7≡C8	1.252(6)	1.213(6)	1.210(7)	1.217(4)	1.202(12)
C8-C9		-	1.356(7)	1.357(4)	1.359(13)
C9≡C10		-	1.208(7)	1.221(4)	1.228(12)
C10-C11		-	1.374(7)	1.362(3)	1.357(12)
C11≡C12		-	1.223(7)	1.219(3)	1.233(10)
C8 or C12 -Pt2	1.951(5)	1.990(5)	1.983(5)	1.995(2)	1.946(8)
Pt1-C_{ipso}[a]	2.059(4)	2.071(3)	2.048(5)	2.062(2)	2.029(9)
Pt2-C_{ipso}[a]	2.059(4)	2.080(4)	2.058(5)	2.066(2)	2.025(9)
av. C_{sp}-C_{sp}	1.360	1.354	1.362	1.359	1.356
av. C_{sp}≡C_{sp}	1.231	1.210	1.217	1.221	1.222
Pt···Pt	12.895(3)	12.8395(7)	17.009(6)	18.015(3)	17.862(9)
sum, bond lengths Pt1 to Pt2	12.905	12.885	18.068	18.111	18.004

Table 3.5 continued

Complex	**6**·(toluene)[9b]	**6·3a**·2CH_2Cl_2	**9**·4C_6H_6·EtOH[9b]	**9·3a**·0.5$CHCl_3$	**9·3b**·2C_6H_6
P1-Pt1-P2	172.28(4)	170.18(4)	175.66(5)	173.23(2)	176.86(8)
P3-Pt2-P4	172.28(4)	174.39(4)	177.55(5)	177.35(2)	174.51(8)
C_{ipso}[a]-Pt1-C1	177.9(2)	178.6(2)	176.8(2)	172.36(1)	175.0(3)
C8 or C12 -Pt2-C_{ipso}[a]	177.9(2)	178.6(2)	176.3(2)	175.59(1)	178.7(3)
Pt1-C1-C2	177.6(4)	176.7(4)	172.9(5)	173.3(2)	170.7(7)
C1-C2-C3	179.2(5)	176.0(5)	173.2(7)	177.6(3)	175.6(9)
C2-C3-C4	177.1(5)	177.7(5)	178.3(7)	179.6(3)	178.6(5)
C3-C4-C5	178.5(6)	177.3(5)	175.6(7)	177.8(3)	178.4(11)
C4-C5-C6	178.5(6)	178.4(5)	175.3(6)	178.8(3)	179.4(11)
C5-C6-C7	177.1(5)	178.9(5)	175.7(6)	179.3(3)	178.5(11)
C6-C7-C8	179.2(5)	177.8(5)	175.7(6)	179.6(3)	177.5(11)
C7-C8-C9		-	175.3(6)	179.7(4)	178.6(11)
C8-C9-C10		-	173.4(6)	179.0(4)	176.4(11)
C9-C10-C11		-	176.2(6)	179.1(3)	177.3(10)
C10-C11-C12		-	171.8(6)	175.2(3)	175.8(9)
C7-C8 or C11-C12 -Pt2	177.6(4)	175.7(4)	171.6(5)	169.8(2)	171.9(7)
average Pt-C_{sp}-C_{sp}	177.9	176.2	172.3	171.6	171.3
average C_{sp}-C_{sp}-C_{sp}	178.2	177.7	175.1	178.6	177.6
average π stacking[b]	3.688	3.847	3.756	3.993	3.744
angle stacking[c]	147.5	154.3	159.5	150.9	158.8

Table 3.5 continued

Complex	**6**·(toluene)[9b]	**6**·**3a**·2CH_2Cl_2	**9**·4C_6H_6·EtOH[9b]	**9**·**3a**·0.5$CHCl_3$	**9**·**3b**·2C_6H_6
average sp···sp^3 distance[d]		4.242	-	4.603	4.350
average sp···sp^2 distance[e]	-	5.785	-	5.741	6.041
average sp···O distance[f]	-	5.311	-	4.787	4.821
average sp···N distance[g]	-	6.792	-	7.108	7.890
average sp···macrocycle distance[h]		5.533	-	5.560	5.776
shortest sp/sp^3 distance		3.734 (C138···C5)	-	3.535 (C36···C6)[i]	3.420 (C24···C9)[i]
shortest sp/sp^2 distance		3.832 (C146···C6)	-	4.096 (C42···C6)[i]	3.984 (C30···C8)[i]
shortest sp/O distance		4.929 (O4···C6)	-	4.722 (O1···C3)[i]	4.483 (O1···C8)[i]
shortest sp/N distance		6.685 (N2···C6)	-	7.105 (N1···C5)[i]	7.729 (N2···C7)[i]
(P1-Pt1-P2)Pt2 vs. (P3-Pt2-P4)Pt1[j]	0	46.4	18.4	84.6	5.01
(C_{ipso}-P1-Pt1-P2) vs. (P3-Pt2-P4-C_{ipso})[j]	0	46.8	68.3	76.9	6.12
C_{sp}···C_{sp}[k]	11.936	9.629 (C6···C8)	7.536 (C1···C7)	11.404 (C5···C9)	9.431(C4···C11)

[a] C_{ipso} is the ligating C_6F_5 carbon atom. [b] Average distance between centroids of the C_6F_5 and C_6H_4R rings (see Figure B.2). [c] Angle of centroids of the three rings in *c* (see Figure B.2). [d] Average distance from every CH_2 group to the nearest sp carbon atom (see Figure B.2). [e] Average distance from every sp2 carbon atom of the 35-37 membered rings to the nearest sp carbon atom (see Figure B.2). [f] Average distance from every oxygen atom to the nearest sp carbon atom (see Figure B.2). [g] Average distance from every nitrogen atom to the nearest sp carbon atom (see Figure B.2). [h] Average distance from all of the atoms in *d-g* to the nearest sp carbon atom. [i] For comments on the atom numbering, see footnote [30]. [j] Angle between planes defined by these atoms (see Figure B.2). [k] The shortest carbon-carbon distance between parallel sp chains in the crystal lattice.

Table 3.6. Key crystallographic distances [Å] and angles [°] for the macrocycles **3a**[24,25] and **3b**,[25] the corresponding CuI complexes **4a**[25] and **4b**,[25] and the rotaxanes **6·3a**, **9·3a**, and **9·3b**, or solvates thereof.

Complex	**3a**[24,25]	**4a**·CH_2Cl_2[25]	**6·3a**·$2CH_2Cl_2$	**9·3a**·$0.5CHCl_3$	**3b**·$CHCl_3$[25]	**4b**·$2CHCl_3$[25]	**9·3b**·$2C_6H_6$
C1-N1[a]	1.330(3)	1.346(6)	1.357(5)	1.331(4)	1.332(3)	1.346(6)	1.317(11)
N1-C5	1.357(3)	1.373(6)	1.327(5)	1.350(4)	1.358(3)	1.373(6)	1.329(11)
C5-C9	1.448(4)	1.437(6)	1.457(6)	1.453(4)	1.457(4)	1.437(6)	1.449(12)
C9-N2	1.356(3)	1.370(5)	1.330(5)	1.354(3)	1.364(3)	1.370(5)	1.352(11)
N2-C12	1.338(3)	1.349(5)	1.353(6)	1.330(4)	1.336(3)	1.349(5)	1.334(11)
C12-C13	1.481(4)	1.478(6)	1.479(6)	1.486(4)	1.483(4)	1.473(5)	1.467(12)
C16-O1	1.373(3)	1.364(5)	1.376(5)	1.371(3)	1.365(3)	1.361(4)	1.373(10)
O1-C19	1.438(3)	1.443(5)	1.437(5)	1.438(3)	1.442(3)	1.433(4)	1.436(10)
C19-C20	1.501(4)	1.494(6)	1.514(6)	1.513(4)	1.505(4)	1.493(5)	1.507(12)
C20-C21	1.511(4)	1.530(6)	1.504(6)	1.529(4)	1.529(4)	1.521(5)	1.501(11)
C21-C22	1.508(4)	1.528(6)	1.520(6)	1.530(4)	1.533(4)	1.515(5)	1.520(12)
C22-C23	1.533(4)	1.528(6)	1.525(6)	1.543(4)	1.528(4)	1.522(4)	1.514(12)
C23-C24	1.503(4)	1.501(6)	1.482(6)	1.508(4)	1.505(4)	1.509(4)	1.496(13)
C24-O2	1.435(3)	1.439(5)	1.434(5)	1.444(3)	1.445(3)	1.431(4)	1.438(11)
O2-C25	1.385(3)	1.376(5)	1.360(5)	1.379(3)	1.367(3)	1.367(4)	1.368(12)
C29-O3	1.376(3)	1.374(5)	1.357(6)	1.372(3)	1.372(3)	1.365(4)	1.360(13)
O3-C31	1.440(3)	1.445(5)	1.437(7)	1.436(3)	1.431(3)	1.427(4)	1.422(11)
C31-C32	1.505(4)	1.513(6)	1.539(8)	1.528(5)	1.507(4)	1.516(5)	1.492(13)
C32-C33	1.521(3)	1.516(6)	1.495(10)	1.496(5)	1.534(4)	1.517(4)	1.519(13)
C33-C34	1.528(4)	1.528(6)	1.604(8)	1.531(6)	1.516(4)	1.528(4)	1.506(12)

Table 3.6 continued

Complex	**3a**[24,25]	**4a**·CH_2Cl_2[25]	**6**·**3a**·$2CH_2Cl_2$	**9**·**3a**·$0.5CHCl_3$	**3b**·$CHCl_3$[25]	**4b**·$2CHCl_3$[25]	**9**·**3b**·$2C_6H_6$
C34-C35	1.524(3)	1.526(6)	1.500(7)	1.513(6)	1.521(4)	1.502(4)	1.495(12)
C35-C36	1.500(4)	1.524(6)	1.476(7)	1.481(6)	1.501(4)	1.520(4)	1.501(12)
C36-O4	1.437(3)	1.437(5)	1.443(5)	1.455(4)	1.439(3)	1.451(3)	1.441(11)
O4-C37	1.375(3)	1.369(5)	1.353(5)	1.375(4)	1.364(3)	1.363(3)	1.376(11)
C1-C40	1.485(4)	1.478(6)	1.483(6)	1.477(4)	1.485(4)	1.484(4)	1.470(12)
C1-N1-C5	118.8(2)	119.1(4)	118.6(4)	119.3(2)	118.7(2)	118.3(3)	119.0(8)
C9-N2-C12	118.9(2)	118.6(4)	118.9(4)	118.6(3)	118.6(2)	118.5(3)	118.7(8)
C16-O1-C19	118.8(2)	118.1(3)	117.7(3)	117.7(2)	119.55(19)	118.7(3)	117.3(7)
C24-O2-C25	117.1(2)	117.7(3)	119.5(5)	117.5(2)	117.10(19)	116.7(2)	116.7(8)
C29-O3-C31	117.5(2)	116.6(3)	117.4(4)	119.4(2)	116.59(19)	118.7(2)	119.0(9)
C36-O4-C37	117.4(2)	118.7(3)	120.1(3)	114.8(3)	117.89(19)	116.7(2)	117.8(8)
N1-C1-C40-C41	–29.24	26.05	–21.66	–19.82	–19.32	37.92	–16.50
N2-C12-C13-C18	–18.75	–26.01	1.91	–18.99	10.67	–32.40	–10.80
arene A vs. phen[b]	19.04	23.09	8.15	24.86	9.59	32.67	6.10
arene B vs. phen[b]	59.62	33.50	43.57	39.25	25.29	2.28	6.56
arene C vs. phen[b]	30.43	22.78	21.08	18.98	19.59	36.02	26.41
O1···O4	10.365	10.747	10.196	9.676	11.136	10.850	10.136
O2···O3	4.768	4.758	4.838	4.769	7.316	7.350	7.277
N1···O3	10.746	10.670	12.126	10.434	13.105	12.619	12.198
N2···O2	10.642	11.534	11.846	11.823	12.714	12.201	12.044
N1···C_{distal}[c]	10.886	11.618	12.569	11.344	12.696	11.955	11.928

Table 3.6 continued

Complex	**3a**[24,25]	**4a**·CH_2Cl_2[25]	**6**·**3a**·$2CH_2Cl_2$	**9**·**3a**·$0.5CHCl_3$	**3b**·$CHCl_3$[25]	**4b**·$2CHCl_3$[25]	**9**·**3b**·$2C_6H_6$
N2···C_{distal}[c]	11.054	11.751	12.394	12.075	12.634	12.119	11.645
O1···O3	10.331	7.835	9.447	9.553	12.644	12.998	10.216
O2···O4	8.426	11.834	10.175	8.597	11.574	10.230	12.341
C17···C42	6.630	6.808	6.231	5.924	6.935	7.110	6.333

[a] For comments on the atom numbering, see footnote 30. [b] These represent the absolute values of the angles between the $C_{12}N_2$ least-squares plane of the phenanthroline and those of the arene ring containing C13-C16 (plane A), the dioxygenated arene (plane B), and the arene ring containing C37-C40 (plane C). [c] The carbon atoms distal to N1 and N2 are taken as C29 and C25 (**3a**) and C301 and C303 (**3b**); see Figure 3.11.

3.3 Discussion

3.3.1. Synthetic strategy. The chemistry in Schemes 3.7-3.9 shows that the "active metal template" method, which was initially conceptualized by Leigh[21c] and extensively exploited by him,[21] Saito,[17] and others,[18] can be applied to a variety of rotaxanes with diplatinum polyynediyl axles. The low yields of the rotaxane with the shortest sp chain, **6**·**3a**, can be rationalized on steric grounds. The low yields of that with the longest sp chain, **12**·**3a**, may reflect the challenge associated with producing more than milligram quantities of the precursor **4b**, rendering optimization experiments difficult.

Anderson has carried out "active metal template" rotaxane syntheses with different types of metal containing alkynes, namely zinc porphyrins with ethynyl groups in the meso positions.[18a] He has also tethered zinc porphyrins to the macrocyclic components.[18d] Leigh and Saito have extended this protocol to other templating metals (Pd,[19a] Ni[19b]) and types of carbon-carbon bond forming reactions such as click[21c] and Sonogashira[19c] cross couplings. Saito has furthermore established the viability of carbon-sulfur bond forming reactions.[17a] These represent possible future means of constructing rotaxanes in which the axles terminate in metal fragments. More recently, these protocols have been extended to a variety of additional architectures such as [3]rotaxanes and rotacatenanes.[18c,26b,32]

After the submission of our original communication,[23a] Tykwinski and Anderson reported the use of Saito's protocol to synthesize rotaxanes with still longer polyynes.[26a] Their initial efforts involved the adducts shown in Scheme 3.10, with hydrocarbon axles ranging from $Ar_3C(C{\equiv}C)_4CAr_3$ (C_8) to $Ar_3C(C{\equiv}C)_{12}CAr_3$ (C_{24}). These purely organic systems could subsequently be derivatized with metals, but using the phenanthroline moiety of the macrocycle, as shown for **14**·**3a** (n = 6). Crystal structures of the rotaxanes

with $Ar_3C(C{\equiv}C)_6CAr_3$ and $Ar_3C(C{\equiv}C)_8CAr_3$ axles have been reported and extensively analyzed, together with rotaxanes involving related macrocycles.[26b] Tykwinski and Anderson also synthesized hexayne based rotaxanes that could be applied in break junction experiments.[5g]

3.3.2. Structural Analysis. There are abundant structural features of interest in rotaxanes. One entails geometric perturbations relative to the axle and macrocycle components. As summarized in Table 3.5, there are no significant differences in any of the bond lengths or angles associated with the $Pt(C{\equiv}C)_nPt$ units of **6**·**3a**, **9**·**3a**, and **9**·**3b**. However, some conformational changes are evident. Complex **9** crystallizes with marked bow-shaped curvature along the $Pt(C{\equiv}C)_6Pt$ linkage,[9b] greater than that observed in any other polyyne to date.[33] However, this is damped out in **9**·**3a** and **9**·**3b**, with the result that the platinum/platinum separations increase by about a full angstrom (18.015(3)-17.862(9) vs. 17.009(6) Å). Although some sp chain curvature is evident in the rotaxanes in Figure 3.11, these represent typical distortions that are commonly attributed to crystal packing forces.[34]

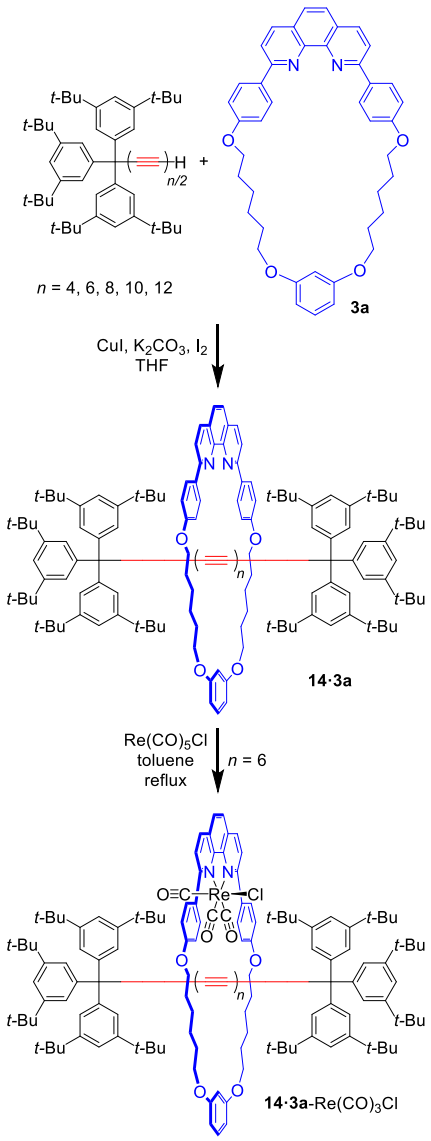

Scheme 3.10. Some polyynediyl containing rotaxanes reported by Tykwinski and Anderson.

Interestingly, the coordination planes of the endgroups are coplanar or nearly so in almost all crystal structures of diplatinum polyynediyl complexes, even those with the double helical motif **IX** in Scheme 3.2.[6a-d] One measure that has been used is the angle between the two four-atom planes defined by the P-Pt-P unit on one endgroup and the Pt atom on the other (Figure B.2 (Appendix B)). As shown in Table 3.5, the values range

from 0° to 18.4° in **6** and **9**, but are much larger in two of the rotaxanes (46.4°-84.6°). Alternatively, planes defined solely by atoms from each platinum coordination sphere can be compared. However, this becomes less useful when the Pt(C≡C)$_n$Pt linkages are markedly bow shaped, as evidenced by the high angle with **9** in Table 3.5 (68.3° vs. 18.4° for C$_{ipso}$-P-Pt-P vs. P-Pt-P/Pt plane angles).

The crystal structures of nearly all complexes with endgroups *trans*-(C$_6$F$_5$)(*p*-tol$_3$P)$_2$Pt exhibit π stacked *p*-tol/C$_6$F$_5$/*p*-tol arene rings.[6a-d,9b,c] This motif is also evident in the rotaxanes (Figure 3.11), and is quantified in Table 3.5 by the average of the four *p*-tol/C$_6$F$_5$ centroid distances (two from each endgroup; 3.744-3.993 Å). The three centroids on each terminus furthermore define an angle (Figure B.2 (Appendix B)). These are somewhat less than the idealized value of 180° (150.9°-158.8°). The basis for these attractive π/π interactions has abundant precedent,[34] per numerous citations in previous papers.[6a-d,9b,c]

Another feature of interest involves contacts between the Pt(C≡C)$_n$Pt axles and macrocycles. As briefly noted above, each of the three structures exhibit interactions that are slightly less than the sum of the van der Waals radii of the constituent atoms. The shortest contacts involving various types of atoms are summarized in Table 3.5, together with the corresponding average distances. For simplicity, these always involve the nearest C$_{sp}$ atom as opposed to a vector or other approximation of the carbon chain. When all atoms of the inner perimeters of the macrocycles are considered, the average distances are comparable for **6·3a** and **9·3a** (5.533 vs. 5.560 Å), and increase slightly for **9·3b** (5.776 Å), consistent with a larger macrocycle size. The longer average C$_{sp}$-C$_{sp}$^{3} distances in **9·3a** and **9·3b** (4.603 Å, 4.350 Å) as compared to **6·3a** (4.242 Å) may be a factor in the NMR shielding trends (Table 3.1).

A number of transannular distances associated with the macrocycles are given in Table 3.6. Interestingly, these remain relatively constant in the free macrocycles, their CuI adducts, and the rotaxanes (maximum deviation 12-15%). Some torsion and arene plane/arene plane angles differ slightly, reflecting variations in conformations. The most pronounced differences involve the angles of the phenanthroline and opposing dioxygenated arene planes (59.62° for **3a** vs. 39.25-43.57° for **9·3a** and **6·3a**). In all three rotaxanes, the arene rings remain remote from the sp carbon chains. With the phenanthroline unit, this is reflected by the long average nitrogen atom-C_{sp} distances (6.792-7.890 Å). The phenanthroline moieties are also remote from the sp carbon chains in the systems structurally characterized by Tykwinski and Anderson.[26] They further used calculated hydrogen atom positions to characterize CH/π_{sp} interactions, and in a broader literature survey noted the relative scarcity of π_{arene}/π_{sp} interactions.[26b]

The space filling representations of the rotaxanes in Figures 3.11 and 6.5 (Appendix B) clearly show that the platinum diphosphine endgroups are sufficiently bulky to block dethreading of the sp chain through the macrocycles. The endgroup/macrocycle interactions have been investigated by Halet and Sahnoune using DFT calculations in an earlier joint publication.[24] In the case of **6·3a**, the computed structure was very similar to that in the crystal. Obviously the close contacts between the *p*-tol_3P moieties of the endgroups and macrocycle mean that the macrocycle has very little if any translational freedom to "slip" along the sp carbon chain.

In crystalline **9·3a** and **9·3b**, the macrocycles are no longer firmly wedged between the endgroups. With **9·3a**, the macrocycle is approximately perpendicular to the axle and abuts one endgroup. Figure B.7 (Appendix B) shows how this motif is reinforced by neighboring molecules in the lattice. In contrast, the macrocycle in **9·3b** tilts so as to realize van der Waals contacts with both endgroups. Interestingly, the

structure computed for **9·3a**,[24] carried out in advance of experiment, exhibited the tilted macrocycle motif found in **9·3b**.

Rotaxanes derived from **3a** and analogous $Pt(C{\equiv}C)_5Pt$ and $Pt(C{\equiv}C)_7Pt$ units were also examined computationally.[24] In this series of four compounds (with **6·3a** and **9·3a**), the noncovalent macrocycle/axle binding energies were found to derive not only from van der Waals interactions enforced by the close proximities of the sp carbon chains and macrocycles, but also weak hydrogen bonding between the *p*-tol_3P protons and nitrogen and oxygen atoms of the macrocycles. Close inspection of the crystal structures suggests additional attractive C-H/π_{arene} interactions.

The total computed binding energies drop from 13.27 kcal/mol for **6·3a** to 11.41 kcal/mol for the corresponding decapentaynediyl ($Pt(C{\equiv}C)_5Pt$) adduct to a plateau of 7.71-8.15 kcal/mol for **9·3a** and the tetradecaheptaynediyl ($Pt(C{\equiv}C)_7Pt$) adduct.[24] At the same time, the computed macrocycle geometries vary from perpendicular to the sp chain and equally abutting both endgroups (**6·3a** and $Pt(C{\equiv}C)_5Pt$ analog) to tilted and partially interacting with both endgroups (**9·3a**; as seen in **9·3b**) to perpendicular and abutting one endgroup ($Pt(C{\equiv}C)_7Pt$ analog; as seen in **9·3a**). Of course, these gas phase calculations do not take into account lattice packing forces that influence the results in Figure 3.11. Nonetheless, the degree to which the limiting geometries are delineated is impressive. Interestingly, the binding energies calculated for an analogous series of *organic* polyynes (tris(3,5-di-*t*-butylphenyl)methyl endgroups as in **VI**, Scheme 3.1) were close to zero and varied only slightly with sp chain length. Hence, the organo-metallic polyynes should have stronger mechanical bonds and higher barriers for dethreading.

3.3.3. Spectroscopic and other data. Although the UV-visible data (Table 3.2) do not point to any significant electronic interactions between the diplatinum axles and

macrocycles in the rotaxanes, a very tiny charge transfer from the macrocycle to the axle (0.015 e according to a Hirshfield charge analysis) occurs upon threading.[24] Also, the NMR data (Table 3.1 and Figures 3.1-3.6) show a variety of shielding and deshielding phenomena resulting from electronic macrocycle/axle interactions triggered by applied magnetic fields. These are generally more pronounced at shorter sp carbon chain lengths. It may be possible to attribute some of these trends to differences in the magnetic anisotropies of the polyyne axles as a function of sp carbon chain lengths. However, to the authors' knowledge no computational data are yet available. The diminution of the upfield shifts of the methyl ^{1}H NMR signals of the *p*-tolyl groups with chain length (Table 3.1) may simply reflect a greater average distance of the methyl groups from the shielding arene moieties of the macrocycles.

The cyclic voltammetry data (Table 3.3 and Figure 3.10) are suggestive of axle/macrocycle interactions, but only after an initial one electron oxidation of one component. Thus, while the sp chains in the rotaxanes can be viewed as sterically shielded, the macrocycles provide loci for new redox chemistry that would have no counterpart in systems where the insulation is saturated, such as **IX** (Scheme 3.2). This problem can potentially be eliminated in second generation rotaxanes. One approach would involve saturated macrocycles, with the lone pairs of any nitrogen or phosphorus heteroatoms "quenched" with suitable Lewis acids in postsynthetic modifications. For example, Tykwinski and Anderson have shown (Scheme 3.11)[26a] that nitrogen lone pairs of the macrocycle in **14·3a** can be derivatized with a transition metal Lewis acid (albeit one known to be redox active).[35]

3.3.4. Prospective. Of the three methods for insulating the sp carbon chains of diplatinum polyynediyl complexes outlined in the introduction, Schemes 3.2 and 3.4 provide arguably the most sterically encumbered systems. The double helical complexes

of the type **IX** appear highly insulated by visual criteria, but undergo dynamic processes that expose the sp carbon chain.[6a-d] For the octatetraynediyl rotaxane **6·3a**, the crystal structure also shows a highly insulated sp chain by visual criteria. Furthermore, here there are no dynamic processes that expose the polyyne moiety. For the rotaxanes with longer dodecahexaynediyl axles, more of the sp chain becomes accessible. However, the "thickness" of the macrocycle belt can potentially be expanded by replacing methylene or *p*-C_6H_4 segments with 9,10-anthracenyl units, or better yet redox inactive aliphatic analogs with similar wingspans.

Every study directed at insulated molecular wires[5] provides new insights as to how to optimize steric and electronic shielding. This work has defined both advantages and disadvantages associated with the types of macrocycles that have been utilized to date in "active metal template" approaches to rotaxanes. The generation of mechanically interlocked systems involving polyynediyl complexes and other types of macrocycles will be investigated in future research.

3.4 Experimental

General Data. All reactions were conducted under nitrogen atmospheres using Schlenk techniques. Chemicals were treated as follows: THF and benzene, dried using a Glass Contour solvent purification system; acetone, distilled from anhydrous $CaSO_4$;[36] CH_2Cl_2 (EMD), CH_3CN, hexanes, ethyl acetate (3 × BDH), K_2CO_3 (BDH, anhydrous), I_2 (EM Science, 99.8%), KCN (Lancaster, 98+%), CuCl (Alfa Aesar, 99.998%), TMEDA (Strem, 99%), *n*-Bu_4N^+ F^- (Aldrich, 1.0 M in THF/5 wt% H_2O), $ClSiMe_3$ (Alfa Aesar, 98+%), HC_2SiMe_3 (Alfa Aesar, 98%), $CDCl_3$ (Cambridge Isotope Laboratories), silica (Silicycle, 40-63 μm, 230-400 mesh), and alumina (Al_2O_3, neutral, Brockmann I, for chromatography, 50-200 μm, Acros), used as received. Analytical thin-

layer chromatography (TLC) was carried out using EMD Silica Gel 60 F254 or EMD Aluminum Oxide 60 F254 (neutral) plates; preparative TLC was carried out using EMD Aluminum Oxide 60 F254 (neutral, 1.5 mm thickness) plates. These were visualized with 254 nm or 365 nm UV light.

NMR spectra (Varian NMRS 500 MHz unless noted) were recorded at ambient probe temperatures and referenced as follows (δ, ppm): ^{1}H, residual internal $CHCl_3$ (7.26); $^{13}C\{^{1}H\}$, internal $CDCl_3$ (77.16); ^{19}F, external C_6F_6 (–164.9); $^{31}P\{^{1}H\}$, external H_3PO_4 (0.00). IR spectra were recorded using a Shimadzu IRAffinity-1 spectrometer with a Pike MIRacle ATR system (diamond/ZnSe crystal). UV-visible spectra were recorded on a Shimadzu UV-1800 spectrometer. Melting points were determined on a Stanford Research Systems (SRS) MPA100 (Opti-Melt) automated device. Microanalyses were conducted by Atlantic Microlab.

CuCl/TMEDA adduct. A Schlenk flask was charged with CuCl (0.724 g, 7.32 mmol) and acetone (18 mL). Then TMEDA (1.2 mL, 8.0 mmol) was added with stirring. After 30 min, the colorless solution (0.40 M based upon CuCl) was stored in the dark under nitrogen. Samples were discarded if not used within several days.

***trans*-(C_6F_5)(*p*-$tol_3P)_2Pt(C{\equiv}C)_3SiMe_3$ (8b).** A three necked round bottom flask was charged with *trans*-(C_6F_5)(*p*-$tol_3P)_2Pt(C{\equiv}C)_2H$ (**1**;[9b] 1.001 g, 0.9812 mmol) and acetone (195 mL) and fitted with a dry ice condenser. Then $HC{\equiv}CSiMe_3$ (2.7 mL, 20 mmol) was added with stirring. The flask was placed in a 40 °C oil bath. Then O_2 was aspirated through the mixture, and the CuCl/TMEDA adduct (0.40 M in acetone; 5.5 mL, 2.2 mmol) was added in five portions over 3 h. After an additional 2 h, hexanes (200 mL) were added. The mixture was passed through a silica plug (3 × 11 cm, packed in 1:1 v/v acetone/hexanes). The plug was eluted with additional 1:1 v/v acetone/hexanes (100 mL) until the eluate became colorless (monitored by TLC for **8b**). The solvent was

removed from the pale yellow eluate by rotary evaporation under reduced pressure. The residue was chromatographed on a silica gel column (4.5 × 28 cm, packed in hexanes, eluted with a CH_2Cl_2/hexanes gradient). Complex **8b** eluted with 15:85 v/v CH_2Cl_2/hexanes, and a second yellow band containing **6** eluted with 30:70 v/v CH_2Cl_2/hexanes. The solvent was removed from the first band by rotary evaporation and oil pump vacuum to give **8b** as an off white solid (0.741 g, 0.681 mmol, 69%) that darkened slightly at 183 °C and turned black at 221 °C. Anal. calcd. (%) for $C_{57}H_{51}F_5P_2Pt{\cdot}0.5(C_6H_{14})$ (1159.2291): C 62.17, H 5.04; found: C 62.24, H 5.06.

NMR (δ/ppm, $CDCl_3$): **^{1}H** (500 MHz) 7.49-7.45 (m, 12H, *o* to P), 7.11 (d, $^3J_{HH}$ = 7.8 Hz, 12H, *m* to P), 2.37 (s, 18H, $C_6H_4C\underline{H}_3$), 1.28, 0.89 (2 × m, $(C_6H_{14})_{0.5}$), 0.09 (s, 9H, $SiC\underline{H}_3$); **^{13}C{^{1}H}** (125 MHz) 145.9 (dd, $^1J_{CF}$ = 226 Hz, $^2J_{CF}$ = 23 Hz, *o* to Pt), 141.0 (s, *p* to P), 137.0 (dm, $^1J_{CF}$ = 240 Hz, *p* to Pt), 136.6 (dm, $^1J_{CF}$ = 247 Hz, *m* to Pt), 134.4 (t, $^2J_{CP}$ = 6.4 Hz, *o* to P), 128.8 (t, $^3J_{CP}$ = 5.6 Hz, *m* to P), 127.2 (t, $^1J_{CP}$ = 30.3 Hz, *i* to P), 104.4 (s, Pt$\underline{C}$≡C),[37] 95.4 (s, $^1J_{PPt}$ = 268 Hz,[38] PtC≡$\underline{C}$),[37] 90.4 (s, C≡$\underline{C}$Si),[37] 82.4 (s, $\underline{C}$≡CSi),[37] 67.1 (s, $^1J_{PPt}$ = 5.2 Hz,[38] PtC≡C$\underline{C}$),[37] 55.7 (s, PtC≡CC≡$\underline{C}$),[37] 21.5 (s, $C_6H_4\underline{C}H_3$), 31.6, 22.7, 14.1 (3 × s, C_6H_{14}), –0.1 (s, $^1J_{SiC}$ = 56.5 Hz, $\underline{C}H_3$); **^{19}F** (470 MHz) –115.73 to –116.54 (m, $^3J_{FPt}$ = 292.4 Hz,[38] 2F, *o* to Pt), –163.48 to –163.89 (m, 2F, *m* to Pt), –164.17 (t, $^3J_{FF}$ = 19.4 Hz, 1F, *p* to Pt); **^{31}P{^{1}H}** (202 MHz) 18.02 (s, $^1J_{PPt}$ = 2633 Hz).[38]

***trans*-$(C_6F_5)(p\text{-}tol_3P)_2Pt(C{\equiv}C)_4SiMe_3$ (7b). A.** A two necked Schlenk flask was charged with **8b** (0.145 g, 0.130 mmol) and acetone (19 mL), and fitted with a dry ice condenser. Then *n*-Bu_4N^+ F^- (1.0 M in THF/5 wt% H_2O, 0.030 mL, 0.033 mmol) was added to the pale yellow solution with stirring. After 10 min, $ClSiMe_3$ (0.020 mL, 0.16 mmol) and $HC{\equiv}CSiMe_3$ (0.36 mL, 2.6 mmol) were added. Then O_2 was aspirated through the mixture, and the CuCl/TMEDA adduct (0.40 M in acetone; 0.84 mL, 0.33

mmol) was added in four portions over 1 h. The reaction was monitored by TLC (silica, eluted with 1:9 v/v ethyl acetate/hexanes). Hexanes (26 mL) were then added. The mixture was passed through an alumina plug (4.5 × 10 cm, packed with 1:1 v/v acetone/hexanes). The plug was eluted with 1:1 v/v acetone/hexanes until the eluate was colorless (monitored by TLC for **7b**). The solvent was removed from the yellow eluate by rotary evaporation. The residue was chromatographed on a silica gel column (4.5 × 25 cm, packed in hexanes, eluted with a CH_2Cl_2/hexanes gradient). Complex **7b** eluted with 15:85 v/v CH_2Cl_2/hexanes, and a second yellow band containing **9** eluted with 30:70 v/v CH_2Cl_2/hexanes. The solvent was removed from the first band by rotary evaporation and oil pump vacuum to give **7b** as a yellow solid (0.039 g, 0.033 mmol, 26%) that darkened slightly at 183 °C and turned black at 221 °C. Anal. calcd. (%) for $C_{59}H_{51}F_5P_2PtSi$ (1140.16): C 62.15, H 4.51; found: C 62.02, H 4.64. **B.** A two necked Schlenk flask was charged with **1**[9b] (0.1017 g, 0.09971 mmol) and acetone (50 mL), fitted with a dry ice condenser, and placed in an ice bath. Then $H(C{\equiv}C)_2SiMe_3$[27] (0.2438 g, 1.994 mmol) was added to the pale yellow solution with stirring, and O_2 was aspirated through the mixture. The CuCl/TMEDA adduct (0.40 M in acetone; 0.62 mL, 0.25 mmol) was added in portions over 40 min. The ice bath was removed. The reaction was monitored by TLC (silica, eluted with 1:9 v/v EtOAc/hexanes). After 2 h, hexanes (50 mL) was added. The sample was passed through an alumina plug (4.5 × 12 cm, packed with 1:1 v/v acetone/hexanes), which was eluted with 1:1 v/v acetone/hexanes until the eluate was colorless (monitored by TLC for **7b**). The solvent was removed from the yellow eluate by rotary evaporation. The residue was chromatographed on a silica gel column (4.5 × 20 cm, packed in hexanes, eluted with a CH_2Cl_2/ hexanes gradient). The solvent was removed from the product containing fractions by rotary evaporation and oil pump vacuum to give **7b** as a yellow solid (0.023 g, 0.020 mmol, 20%).

NMR (δ/ppm, $CDCl_3$): **^{1}H** (500 MHz) 7.43-7.47 (m, 12H, *o* to P), 7.11 (d, $^3J_{HH}$ = 7.8 Hz, 12H, *m* to P), 2.36 (s, 18H, $C_6H_4C\underline{H}_3$), 0.15 (s, 9H, $SiC\underline{H}_3$); **^{13}C{^{1}H}** (125 MHz)[39] 141.1 (s, *p* to P), 134.4 (t, $^2J_{CP}$ = 6.4 Hz, *o* to P), 128.9 (t, $^3J_{CP}$ = 5.6 Hz, *m* to P), 127.1 (t, $^1J_{CP}$ = 30.4 Hz, *i* to P), 95.3 (s, PtC≡$\underline{C}$),[37,40] 89.4 (s, C≡$\underline{C}$Si),[37] 84.7 (s, $\underline{C}$≡CSi),[37] 67.0, 65.0, 59.2, 56.4 (4 × s, PtC≡C$\underline{C}$≡$\underline{C}$C≡$\underline{C}$),[37] 21.5 (s, $C_6H_4\underline{C}H_3$), –0.24 (s, $\underline{C}H_3$); **^{19}F** (470 MHz) –115.81 to –116.50 (m, $^3J_{FPt}$ = 294.2 Hz,[38] 2F, *o* to Pt), –163.53 to –163.66 (m, 2F, *m* to Pt), –163.96 (t, $^3J_{FF}$ = 19.4 Hz, 1F, *p* to Pt); **^{31}P{^{1}H}** (202 MHz) 17.97 (s, $^1J_{PPt}$ = 2621 Hz).[38]

***trans,trans*-(C_6F_5)(*p*-tol_3P)$_2$Pt(C≡C)$_4$Pt(P*p*-tol_3)$_2$(C_6F_5)·(2,9-(1,10-phenanthrolinedi-yl))(*p*-$C_6H_4O(CH_2)_6O$)$_2$(1,3-C_6H_4) (6·3a).**[23a] **A.** A Schlenk flask was charged with **1**[9b] (0.051 g, 0.050 mmol), **4a**[24] (0.017 g, 0.021 mmol), K_2CO_3 (0.011 g, 0.083 mmol), and THF (5 mL). The flask was placed in a 55 °C oil bath, giving an orange solution. A THF solution of I_2 (0.0077 M; 5.0 mL, 0.039 mmol) was added dropwise with stirring over 6 h. The flask was removed from the bath, and the solvent was removed by rotary evaporation. The procedure was repeated using **1** (0.054 g, 0.053 mmol), **4a** (0.018 g, 0.022 mmol), K_2CO_3 (0.012 g, 0.087 mmol), THF (5 mL), and I_2 (0.0077 M in THF, 5.0 mL, 0.039 mmol). The combined residues were chromatographed on a silica gel column (2.5 × 30 cm, packed in hexanes, eluted with hexanes and then an ethyl acetate/hexanes gradient reaching 1:2 v/v) to give **6·3a** accompanied by macrocycle **3a**. **B.** A round bottom flask was charged with **1** (0.099 g, 0.097 mmol), **4a** (0.041 g, 0.049 mmol), K_2CO_3 (0.026 g, 0.19 mmol), and THF (20 mL). The flask was placed in a 50 °C oil bath, and oxygen was aspirated through the solution. The reaction was monitored via TLC (silica, 1:2 v/v ethyl acetate/hexanes). After 6 h and 14 h, additional **4a** was added (0.042 g, 0.051 mmol; 0.020 g, 0.024 mmol). After 22 h (TLC showed no remaining educt), the solvent was removed by rotary evaporation. The

residue was chromatographed on a silica gel column (2.5 × 30 cm, packed in hexanes, eluted with hexanes and then an ethyl acetate/hexane gradient reaching 1:2 v/v) to give **6·3a** accompanied by macrocycle **3a**. **C.** The samples from A and B were chromatographed on an alumina column (2.5 × 30 cm, packed in hexanes, eluted with hexanes and then a CH_2Cl_2/hexanes gradient reaching 10:1 v/v). The solvent was removed from the product containing fractions by rotary evaporation and oil pump vacuum. This gave **6·3a** as a light yellow solid (0.025 g, 0.0093 mmol, average yield 9%) that slightly darkened at 163 °C, turned black at 277 °C, and liquefied at 281 °C. Anal. calcd. (%) for $C_{146}H_{126}F_{10}N_2O_4P_4Pt_2$ (2676.66): C, 65.51; H, 4.74; N, 1.05. Found: C, 66.35; H, 5.32; N, 1.06.[41] Subsequent fractions from the column gave **3a** (0.053 g, 0.083 mmol).

NMR (δ/ppm, $CDCl_3$): **^{1}H** (500 MHz) 8.46 (d, $^3J_{HH}$ = 8.7 Hz, 4H, *p*-C_6H_4), 8.30 (d, $^3J_{HH}$ = 8.4 Hz, 2H, phenanthryl), 8.14 (d, $^3J_{HH}$ = 8.4 Hz, 2H, phenanthryl), 7.78 (s, 2H, phenanthryl), 7.40-7.36 (m, 24H, *o* to P), 7.23 (t, $^3J_{HH}$ = 8.0 Hz, 1H, OCCHC<u>H</u> of *m*-C_6H_4), 6.92 (overlapping d, $^3J_{HH}$ = 7.9 Hz, 24H, *m* to P), 6.90 (overlapping d, $^3J_{HH}$ = 8.8 Hz, 4H, *p*-C_6H_4), 6.58 (dd, $^3J_{HH}$ = 8.1 Hz, $^4J_{HH}$ = 2.1 Hz, 2H, OCC<u>H</u>CH of *m*-C_6H_4), 6.24 (distorted t, 1H, OCC<u>H</u>CO of *m*-C_6H_4), 3.33 (br t, $^3J_{HH}$ = 7.7 Hz, 4H, OCH_2), 3.28 (br t, $^3J_{HH}$ = 7.6 Hz, 4H, O'C'H_2), 2.12 (s, 36H, CH_3), 1.25-1.21 (m, 4H, $OCH_2C\underline{H}_2$), 1.18-1.12 (m, 4H, O'C'H_2C'$\underline{H}_2$), 0.76 (br s, 8H, $OCH_2CH_2C\underline{H}_2$, O'C'$H_2C'H_2C'\underline{H}_2$); **^{13}C{^{1}H}** (125 MHz)[39] 160.7, 160.5, 156.3, 146.2 (4 × s, macrocycle), 141.0 (s, *p* to P), 136.6 (s, macrocycle), 134.3 (virtual t,[42] $^2J_{CP}$ = 6.4 Hz, *o* to P), 131.4, 129.4 (2 × s, macrocycle), 128.9 (s, CH of *p*-C_6H_4),[43] 128.7 (virtual t,[42] $^3J_{CP}$ = 5.6 Hz, *m* to P), 127.5 (virtual t,[42] $^1J_{CP}$ = 30.2 Hz, *i* to P), 127.4, 125.5, 118.7 (3 × s, macrocycle), 115.0 (s, C'H of *p*-C_6H_4),[43] 108.6 (s, macrocycle), 100.2 (br s, Pt<u>C</u>≡C), 97.0 (s, PtC≡<u>C</u>), 96.8 (s, OC<u>C</u>HCO),[44] 67.3, 66.9 (2 × s, OCH_2,O'C'H_2), 63.9

(s, PtC≡C<u>C</u>≡C), 58.4 (s, PtC≡CC≡<u>C</u>), 29.1, 28.9 (2 × s, $OCH_2\underline{C}H_2$, $O'C'H_2\underline{C}'H_2$), 24.9, 24.5 (2 × s, $OCH_2CH_2\underline{C}H_2$, $O'C'H_2C'H_2\underline{C}'H_2$), 21.2 (s, CH_3); **^{19}F** (470 MHz) –116.10 (m, $^3J_{FPt}$ = 291 Hz,[38] 2F, *o* to Pt), –163.84 (m, 2F, *m* to Pt), –164.68 (t, $^3J_{FF}$ = 19.5 Hz, 1F, *p* to Pt); **^{31}P{^{1}H}** (202 MHz) 17.76 (s, $^1J_{PPt}$ = 2660 Hz).[38]

IR (ATR/powder film, cm^{-1}) 2149 m ($\nu_{C\equiv C}$), 2008 w ($\nu_{C\equiv C}$). **UV-vis** (nm, 4.37 × 10^{-6} M in CH_2Cl_2 (ε, $M^{-1}cm^{-1}$)) 267 (69000), 293 (120000), 325 (129000), 355 (27000), 381 (9000), 414 (5000). **MS** (MALDI$^+$, matrix: sinapic acid with CF_3COOK) 2714 ([**6·3a** + K]$^+$, 2%), 2676 ([**6·3a** + 1]$^+$, 2%), 1304 ([(tol$_3$P)(C$_6$F$_5$)Pt·**3a**]$^+$, 75%), 1137 ([(tol$_3$P)Pt·**3a**]$^+$, 100%), 803 ([(tol$_3$P)$_2$Pt]$^+$, 95%).

***trans,trans*-(C$_6$F$_5$)(*p*-tol$_3$P)$_2$Pt(C≡C)$_6$Pt(P*p*-tol$_3$)$_2$(C$_6$F$_5$)·(2,9-(1,10-phenanthrolinediyl))(*p*-C$_6$H$_4$O(CH$_2$)$_6$O)$_2$(1,3-C$_6$H$_4$) (9·3a).**[23b] A Schlenk flask wrapped with aluminum foil was charged with *trans*-(C$_6$F$_5$)(*p*-tol$_3$P)$_2$Pt(C≡C)$_3$H (**7**;[9b] 0.100 g, 0.0953 mmol), K_2CO_3 (0.026 g, 0.19 mmol), and **4a**[25] (0.032 g, 0.038 mmol). Then THF (5 mL) was added with stirring. The flask was placed in a 55 °C oil bath. A THF solution of I_2 (0.0078 M; 6.1 mL, 0.049 mmol) was added dropwise with stirring over 7 h. The flask was removed from the oil bath. After 12 h, the solvent was removed by rotary evaporation. The residue was chromatographed (alumina, 3 × 25 cm column, packed in hexanes and eluted with a CH_2Cl_2/hexanes gradient). The fractions were monitored by TLC (1:1 v/v CH_2Cl_2/hexanes). Complex **9** eluted first; the solvent was removed from the combined fractions by rotary evaporation to give **9** as a pale yellow solid (0.029 g, 0.014 mmol, 30% based upon **3**). The rotaxane **9·3a** eluted next (60:40 v/v CH_2Cl_2/hexanes); the solvent was removed from the combined fractions by rotary evaporation and then oil pump vacuum to give **9·3a** as a pale yellow solid (0.046 g, 0.017 mmol, 45% based on **4a**) that darkened at 190 °C and decomposed at 255 °C.

Anal. calcd. (%) for $C_{150}H_{126}F_{10}N_2O_4P_4Pt_2 \cdot 1.25C_6H_{14}$ (2832.43): C 66.79, H 5.11, N 0.99; found: C 66.85, H 5.28, N 1.03.

NMR (δ/ppm, $CDCl_3$) **^{1}H** (500 MHz, cryoprobe)[45] 8.40 (dm, $^3J_{HH}$ = 8.9 Hz, 4H, *p*-C_6H_4), 8.26 (d, $^3J_{HH}$ = 8.4 Hz, 2H, phenanthryl), 8.09 (d, $^3J_{HH}$ = 8.4 Hz, 2H, phenanthryl), 7.75 (s, 2H, phenanthryl), 7.41-7.37 (m, 24H, *o* to P), 7.06 (t, $^3J_{HH}$ = 8.1 Hz, 1H, OCCHC<u>H</u> of *m*-C_6H_4), 7.02, 7.01 (2 overlapping d, $^3J_{HH}$ = 7.8 Hz, 24H, *m* to P; $^3J_{HH}$ = 8.9 Hz, 4H, *p*-C_6H_4), 6.44 (dd, $^3J_{HH}$ = 8.1 Hz, $^4J_{HH}$ = 2.3 Hz, 2H, OCC<u>H</u>CH of *m*-C_6H_4), 6.33 (distorted t, $^4J_{HH}$ = 2.2 Hz, 1H, OCC<u>H</u>CO of *m*-C_6H_4), 3.73 (t, $^3J_{HH}$ = 7.5 Hz, 4H, OCH_2), 3.68 (t, $^3J_{HH}$ = 6.9 Hz, 4H, O'C'H_2), 2.23 (s, 36H, CH_3), 1.61-1.56 (m, 4H, $OCH_2C\underline{H}_2$), 1.52-1.47 (m, 4H, O'C'H_2C'$\underline{H}_2$), 1.23-1.19 (m, 8H, $OCH_2CH_2C\underline{H}_2$, O'C'$H_2C'H_2C'\underline{H}_2$), 1.26, 0.89 (2 × m, $(C_6H_{14})_{1.25}$); **^{13}C{^{1}H}** (125 MHz, cryoprobe)[45] 160.5, 160.4, 156.4, 146.0 (4 × s, macrocycle sp^2), 145.6 (m, $^1J_{CF}$ = 225 Hz, *o* to Pt), 140.9 (s, *p* to P), 136.8 (dm, $^1J_{CF}$ = 235 Hz, *p* to Pt), 137.8 (dm, $^1J_{CF}$ = 235 Hz, *m* to Pt), 136.5 (s, macrocycle sp^2), 134.1 (virtual t,[42] $^2J_{CP}$ = 6.4 Hz, *o* to P), 131.5, 129.4 (2 × s, macrocycle sp^2), 128.9 (s, CH of *p*-C_6H_4), 128.6 (virtual t,[42] $^3J_{CP}$ = 5.6 Hz, *m* to P), 127.2 (s, macrocycle sp^2), 126.8 (virtual t,[42] $^1J_{CP}$ = 30.4 Hz, *i* to P), 125.3, 118.8 (2 × s, macrocycle sp^2), 114.8 (s, C'H of *p*-C_6H_4), 107.9 (s, macrocycle sp^2), 106.2 (s, Pt<u>C</u>≡C), 98.5 (s, OC<u>C</u>HCO), 95.4 (s, PtC≡<u>C</u>), 67.6, 67.4 (2 × s, OCH_2, O'C'H_2), 65.8 (s, PtC≡C<u>C</u>), 63.3 (s, PtC≡CC≡<u>C</u>), 60.8 (s, PtC≡CC≡CC≡<u>C</u>), 57.1 (s, PtC≡CC≡C<u>C</u>≡C), 29.2, 28.8 (2 × s, $OCH_2\underline{C}H_2$, O'C'$H_2\underline{C}$'H_2), 25.3, 25.1 (2 × s, $OCH_2CH_2\underline{C}H_2$, O'C'$H_2C'H_2\underline{C}$'$H_2$), 21.2 (s, CH_3), 32.0, 22.8, 14.3 (3 × s, C_6H_{14}); **^{19}F** (470 MHz) –116.17 (m, $^3J_{FPt}$ = 287 Hz,[38] 2F, *o* to Pt), –163.60 to –163.73 (m, 2F, *m* to Pt), –164.11 (t, $^3J_{FF}$ = 19.4 Hz, 1F, *p* to Pt); **^{31}P{^{1}H}** (202 MHz) 17.89 (s, $^1J_{PPt}$ = 2623 Hz).[38]

IR (ATR/powder film, cm^{-1}) 2160 w ($\nu_{C\equiv C}$), 2090 m ($\nu_{C\equiv C}$), 1993 w ($\nu_{C\equiv C}$). **UV-vis** (nm, 4.63 × 10^{-6} M in CH_2Cl_2 (ε, $M^{-1}cm^{-1}$)) 289 (75100), 317 (108000), 337

(257000), 360 (389000), 413 (6570). **MS** (m/z, MALDI$^+$, DCTB/CF_3COOK matrix) 1138 ([$(tol_3P)Pt\cdot$**3a**+1]$^+$, 5%), 805 ([$(tol_3P)_2Pt$+2]$^+$, 93%), 641 (**3a**+3, 100%).

***trans,trans*-(C_6F_5)(*p*-tol_3P)$_2$Pt(C≡C)$_6$Pt(P*p*-tol_3)$_2$(C_6F_5)·(2,9-(1,10-phenanthrolinedi-yl))(*p*-$C_6H_4O(CH_2)_6O)_2$(2,7-naphthdiyl) (9·3b).**[23b] A Schlenk flask wrapped with aluminum foil was charged with **3**[9b] (0.050 g, 0.048 mmol), K_2CO_3 (0.013 g, 0.096 mmol), and **4b**[25] (0.017 g, 0.019 mmol). Then THF (2.5 mL) was added with stirring, and the flask was placed in a 55 °C oil bath. A THF solution of I_2 (0.0113 M; 2.1 mL, 0.024 mmol) was added dropwise with stirring over 8.5 h. The flask was removed from the oil bath. After 15 h, the solvent was removed by rotary evaporation. The residue was chromatographed (alumina, 1 × 24 cm column, packed in hexanes and eluted with a CH_2Cl_2/hexanes gradient). The fractions were monitored by TLC (1:1 v/v CH_2Cl_2/hexanes). Those containing **9·3b** eluted with 40:60 v/v CH_2Cl_2/hexanes and were combined. The solvent was removed by rotary evaporation and oil pump vacuum to give **9·3b** as a pale yellow solid (0.015 g, 0.0054 mmol, 28% based upon **4b**) that showed slight shrinkage above 100 °C and turned black at 150 °C. Anal. calcd. (%) for $C_{154}H_{128}F_{10}N_2O_4P_4Pt_2$ (2774.77): C 66.66, H 4.65, N 1.01; found: C 66.19, H 4.91, N 1.03.

NMR (δ/ppm, $CDCl_3$): **^{1}H** (500 MHz) 8.36 (dm, $^3J_{HH}$ = 8.4 Hz, 4H, *p*-C_6H_4), 8.27 (d, $^3J_{HH}$ = 8.4 Hz, 2H, phenanthryl), 8.08 (d, $^3J_{HH}$ = 8.4 Hz, 2H, phenanthryl), 7.75 (s, 2H, phenanthryl), 7.60 (d, $^3J_{HH}$ = 8.8 Hz, 2H, 2,7-naphthdiyl), 7.39-7.36 (m, 24H, *o* to P), 7.00-6.99 (2 overlapping d, $^3J_{HH}$ = 7.9 Hz, 24H, *m* to P and 4H, *p*-C_6H_4), 6.97 (d, $^3J_{HH}$ = 2.3 Hz, 2H, OCC<u>H</u>CC of 2,7-naphthdiyl), 6.94-6.92 (distorted dd, $^3J_{HH}$ = 8.7 Hz, $^4J_{HH}$ = 2.4 Hz, 2H, OCC<u>H</u>CH of 2,7-naphthdiyl), 3.80-3.74 (2 overlapping t, $^3J_{HH}$ = 7.3 Hz, 4H, OCH_2; $^3J_{HH}$ = 6.9 Hz, 4H, O'C'H_2),[46] 2.20 (s, 36H, CH_3), 1.59-1.54 (m, 8H, $OCH_2C\underline{H}_2$, O'C'H_2C'$\underline{H}_2$), 1.23 (m, 8H, $OCH_2CH_2C\underline{H}_2$, O'C'$H_2C'H_2C'\underline{H}_2$);

$^{13}C\{^1H\}$[47] (125 MHz, cryoprobe)[45] 160.9, 157.5, 156.7 (3 × s, macrocycle sp^2), 141.1 (s, *p* to P), 136.5 (s, macrocycle sp^2), 134.2 (virtual t,[42] $^2J_{CP}$ = 6.3 Hz, *o* to P), 131.3 (br s, macrocycle sp^2), 129.2 (s, macrocycle sp^2), 128.8 (virtual t,[42] $^3J_{CP}$ = 5.5 Hz, *m* to P), 127.5 (s, macrocycle sp^2), 127.0 (virtual t,[42] $^1J_{CP}$ = 30.2 Hz, *i* to P), 125.7, 124.0 (2 × s, macrocycle sp^2), 119.6 (br s, macrocycle sp^2), 116.8, 114.9, 106.0 (3 × s, macrocycle sp^2), 106.7 (br s, PtC≡C, tentative), 95.5 (s, PtC≡C), 67.8, 67.3 (2 × s, OCH_2, O'C'H_2) 66.0 (s, PtC≡CC), 63.3, 61.0, 57.2 (3 × s, PtC≡CC≡CC≡C), 29.9, 29.2, 28.8, 25.2 (4 × s, $OCH_2CH_2CH_2$, O'C'H_2'C'H_2'C'H_2), 21.4 (s, CH_3); **^{19}F** (470 MHz) –116.14 to –116.22 (m, $^3J_{FF}$ = 22.6 Hz, $^3J_{FPt}$ = 275.6 Hz,[38] 2F, *o* to Pt), –163.56 to –163.68 (m, 2F, *m* to Pt), –164.06 (t, $^3J_{FF}$ = 19.4 Hz, 1F, *p* to Pt); **$^{31}P\{^1H\}$** (202 MHz) 17.93 (s, $^1J_{PPt}$ = 2622 Hz).[38]

IR (ATR/powder film, cm^{-1}) 2127 m ($\nu_{C\equiv C}$), 2088 m ($\nu_{C\equiv C}$), 1992 w ($\nu_{C\equiv C}$). **UV-vis** (nm, 1.07 × 10^{-5} M in CH_2Cl_2 (ε, $M^{-1}cm^{-1}$)) 312 (69700), 320 (69800), 341 (80400), 367 (95100), 415 (20000), 451 (9460). **MS** (m/z, MALDI$^+$, DCTB matrix) 2774 ([**9·3b**+1]$^+$, 45%), 1187 ([(tol$_3$P)Pt·**3b**]$^+$, 100%).

***trans,trans*-(C$_6$F$_5$)(*p*-tol$_3$P)$_2$Pt(C≡C)$_8$Pt(P*p*-tol$_3$)$_2$(C$_6$F$_5$)·(2,9-(1,10-phenanthrolinedi-yl))(*p*-C$_6$H$_4$O(CH$_2$)$_6$O)$_2$(1,3-C$_6$H$_4$) (12·3a)**. A Schlenk flask wrapped with aluminum foil was charged with **7b** (0.059 g, 0.051 mmol) and K_2CO_3 (0.028 g, 0.21 mmol). Then THF (10.0 mL) followed by MeOH (1.0 mL) were added with stirring. After ca. 15 min, the pale yellow suspension darkened slightly, and a spot attributed to *trans,trans*-(C$_6$F$_5$)(*p*-tol$_3$P)$_2$Pt(C≡C)$_4$H (**11**) was observed by TLC (silica, eluted with 1:2 v/v CH_2Cl_2/hexanes). Then **4a**[25] (0.017 g, 0.021 mmol) was added, and the mixture gently warmed to effect dissolution. Then a THF solution of I_2 (0.0080 M; 3.21 mL, 0.0.0257 mmol) was added dropwise with stirring over 7 h. The reaction was monitored by TLC (alumina, eluted with 1:2 v/v CH_2Cl_2/hexanes). After 12 h, CH_2Cl_2 (5.0 mL),

CH_3CN (3.0 mL), and a solution of KCN (0.013 g, 0.21 mmol) in H_2O (2 mL) were sequentially added. After 4 h, the organic layer was separated and washed with H_2O (3 × 2 mL). The solvent was removed by oil pump vacuum. Preparative TLC of the orange residue (alumina, eluted with 1:2 v/v CH_2Cl_2/hexanes) gave several bands. Two were scraped from the plate and extracted with CH_2Cl_2. The solvents were removed by oil pump vacuum. The higher R_f band gave **12** as an orange solid (0.0019 g, 0.00089 mmol, 4% based on **7b**). The lower R_f band gave **12·3a** as a yellow solid (0.0042 g, 0.0015 mmol, 7% based on **4a**). Anal. calcd. (%) for $C_{154}H_{126}F_{10}N_2O_4P_4Pt_2$ (2772.75): C 66.71, H 4.58, N 1.01; found: C 63.14, H 6.09, N 1.56.[41].[41]

NMR (δ/ppm, $CDCl_3$): **^{1}H** (500 MHz) 8.41 (d, $^3J_{HH}$ = 8.78 Hz, 4H, *p*-C_6H_4), 8.21 (d, $^3J_{HH}$ = 8.3 Hz, 2H, phenanthryl), 8.08 (d, $^3J_{HH}$ = 8.5 Hz , 2H, phenanthryl), 7.67 (s, 2H, phenanthryl), 7.55-7.48 (m, 24H, *o* to P), 7.12-7.10 (overlapping m, 1H, OCCHC<u>H</u> of *m*-C_6H_4), 7.06 (overlapping d, $^3J_{HH}$ = 8.2 Hz, 24H, *m* to P) 7.03 (overlapping d, $^3J_{HH}$ = 8.7 Hz, 4H, *p*-C_6H_4), 6.43 (dd, $^3J_{HH}$ = 8.1 Hz, $^3J_{HH}$ = 2.3 Hz, 2H, OCC<u>H</u>CH of *m*-C_6H_4), 6.36 (distorted t, $^4J_{HH}$ = 2.2 Hz, 1H, OCC<u>H</u>CO of *m*-C_6H_4), 3.87 (t, ^3J = 7.1 Hz, 4H, OCH_2), 3.77 (t, ^3J = 6.8 Hz, 4H, O'C'H_2), 2.28 (s, 36H, CH_3), 1.71 (m, 4H, $OCH_2C\underline{H}_2$), 1.62 (overlapping m, 4H, O'C'H_2C'$\underline{H}_2$), 1.35 (overlapping m, 8H, $OCH_2CH_2C\underline{H}_2$, O'C'$H_2C'H_2C'\underline{H}_2$); **^{13}C{^{1}H}** (125 MHz)[39,40] 141.2 (s, *p* to P), 134.3 (virtual t,[42] $^2J_{CP}$ = 6.1 Hz, *o* to P), 128.9 (virtual t,[42] $^2J_{CP}$ = 5.5 Hz, *m* to P), 127.0 (virtual t,[42] $^2J_{CP}$ = 30.2 Hz, *i* to P), 21.5 (s, CH_3); **^{19}F** (470 MHz) –116.16 to –116.25 (m, 2F, *o* to Pt), –163.45 to –163.58 (m, 2F, *m* to Pt), –163.84 (t, $^3J_{FF}$ = 20.5 Hz, 1F, *p* to Pt); **^{31}P{^{1}H}** (202 MHz) 17.95 (s, $^1J_{PPt}$ = 2609 Hz).[38]

IR (ATR/powder film, cm^{-1}) 2161 w ($\nu_{C\equiv C}$), 2094 w ($\nu_{C\equiv C}$), 2056 m ($\nu_{C\equiv C}$), 1992 w ($\nu_{C\equiv C}$). **UV-vis** (nm, 7.93 × 10^{-6} M in CH_2Cl_2 (ε, $M^{-1}cm^{-1}$)) 290 (40400), 306 (29400), 326 (31800), 347 (56900), 370 (115000), 399 (169000).

Reference spectra, macrocycles. NMR data that were recorded under the same conditions as the rotaxanes are given elsewhere.[25] **UV-vis** (nm, 2.52 × 10^{-5} M in CH_2Cl_2 (ε, $M^{-1}cm^{-1}$)), 2,9-(1,10-phenanthrolinediyl))(*p*-$C_6H_4O(CH_2)_6O)_2$(1,3-C_6H_4) (**3a**): 238 (34000), 286 (50000), 326 (25000), 339 (24000). **UV-vis** (nm, 1.74 × 10^{-5} M in CH_2Cl_2 (ε, $M^{-1}cm^{-1}$)), (2,9-(1,10-phenanthrolinediyl))(*p*-$C_6H_4O(CH_2)_6O)_2$(2,7-naphthdiyl) (**3b**): 287 (52300), 311 (30900), 326 (29100), 341 (24700), 392 (7030).

Reference spectra, diplatinum axles. Spectra of these previously reported compounds were recorded under the same conditions as used for the rotaxanes. **A**. *trans,trans*-(C_6F_5)(*p*-$tol_3P)_2Pt(C{\equiv}C)_4Pt(P$*p*-$tol_3)_2(C_6F_5)$ (**6**).[9b,48] NMR (δ/ppm, $CDCl_3$): **^{1}H** (500 MHz) 7.49-7.45 (m, 24H, *o* to P), 7.10 (d, $^3J_{HH}$ = 7.8 Hz, 24H, *m* to P), 2.36 (s, 36H, CH_3); **^{13}C{^{1}H}** (125 MHz)[39] 140.8 (s, *p* to P), 134.4 (virtual t,[42] $^2J_{CP}$ = 6.4 Hz, *o* to P), 128.7 (virtual t,[42] $^3J_{CP}$ = 5.6 Hz, *m* to P), 127.3 (virtual t,[42] $^1J_{CP}$ = 30.2 Hz, *i* to P), 100.7 (br s, Pt$\underline{C}{\equiv}C$), 96.9 (s, PtC$\equiv\underline{C}$), 64.2 (s, PtC$\equiv C\underline{C}{\equiv}C$), 58.3 (s, PtC$\equiv$CC$\equiv\underline{C}$), 21.5 (s, CH_3); **^{31}P{^{1}H}** (202 MHz): 17.84 (s, $^1J_{PPt}$ = 2648 Hz).[38] **IR** (ATR/powder film, cm^{-1}) 2139 m ($\nu_{C\equiv C}$), 1996 w ($\nu_{C\equiv C}$). **UV-vis** (nm, 4.12 × 10^{-6} M in CH_2Cl_2 (ε, $M^{-1}cm^{-1}$)) 267 (61000), 275 (87000), 295 (91000), 326 (126000), 355 (8100), 383 (6000), 414 (4000). **B.** *trans,trans*-(C_6F_5)(*p*-$tol_3P)_2Pt(C{\equiv}C)_6Pt(P$*p*-$tol_3)_2(C_6F_5)$ (**9**).[9b,48] NMR (δ/ppm, $CDCl_3$): **^{1}H** (500 MHz) 7.44 (m, 24H, *o* to P), 7.11 (d, $^3J_{HH}$ = 7.9 Hz, 24H, *m* to P), 2.35 (s, 36H, CH_3); **^{13}C{^{1}H}** (125 MHz, cryoprobe)[45] 145.9 (m, *o* to Pt), 140.9 (s, *p* to P), 137.1 (dm, $^1J_{CF}$ = 240.6 Hz, *p* to Pt), 136.6 (dm, $^1J_{CF}$ = 241.5 Hz, *m* to Pt), 134.3 (virtual t,[42] $^2J_{CP}$ = 6.3 Hz, *o* to P), 128.8 (virtual t,[42] $^3J_{CP}$ = 5.6 Hz, *m* to P), 127.0 (virtual t,[42] $^1J_{CP}$ = 30.4 Hz, *i* to P), 106.6 (s, Pt$\underline{C}{\equiv}C$), 95.6 (s, PtC$\equiv\underline{C}$), 65.9 (s, PtC$\equiv C\underline{C}$), 63.2, 61.1, and 57.3 (3 × s, PtC$\equiv$CC$\equiv\underline{C}\underline{C}{\equiv}\underline{C}$), 21.5 (s, CH_3); **^{31}P{^{1}H}** (202 MHz) 17.96 (s, $^1J_{PPt}$ = 2623 Hz).[38] **IR** (ATR/powder film, cm^{-1}) 2131 m ($\nu_{C\equiv C}$), 2092 m ($\nu_{C\equiv C}$), 2015 m ($\nu_{C\equiv C}$). **UV-vis** (nm, 8.05 × 10^{-6} M in CH_2Cl_2

(ε, $M^{-1}cm^{-1}$)) 280 (172000), 307 (168000), 315 (181000), 335 (353000), 360 (497000), 412 (2460),[49] 448 (1680),[49] 490 (744).[49] **MS** (m/z, MALDI$^+$) ([**9**]+1$^+$) 2085, 80%). **C.** *trans,trans*-(C_6F_5)(*p*-tol_3P)$_2$Pt(C≡C)$_8$Pt(P*p*-tol_3)$_2$(C_6F_5) (**12**).[9b,48] NMR (δ/ppm, $CDCl_3$): **^{1}H** (500 MHz) 7.44 (m, 24H, *o* to P), 7.11 (d, $^3J_{HH}$ = 7.9 Hz, 24H, *m* to P), 2.35 (s, 36H, CH_3); **^{13}C{^{1}H}** (125 MHz) 145.7 (m, *o* to Pt), 141.0 (s, *p* to P), 137.0 (dm, $^1J_{CF}$ = 240.6 Hz, *p* to Pt), 136.5 (dm, $^1J_{CF}$ = 241.5 Hz, *m* to Pt), 134.2 (virtual t,[42] $^2J_{CP}$ = 6.3 Hz, *o* to P), 128.7 (virtual t,[42] $^3J_{CP}$ = 5.6 Hz, *m* to P), 126.8 (virtual t,[42] $^1J_{CP}$ = 30.4 Hz, *i* to P), 109.1 (s, Pt<u>C</u>≡C), 95.0 (s, PtC≡<u>C</u>), 66.7 (s, PtC≡C<u>C</u>), 64.9, 63.1, 61.5, 60.1, 56.8 (5 × s, PtC≡CC≡<u>CC</u>≡<u>CC</u>≡<u>C</u>), 21.3 (s, CH_3); **^{31}P{^{1}H}** (202 MHz) 18.00 (s, $^1J_{PPt}$ = 2609 Hz).[38] **IR** (ATR/powder film, cm^{-1}) 2154 w ($\nu_{C\equiv C}$), 2088 w ($\nu_{C\equiv C}$), 2054 s ($\nu_{C\equiv C}$), 1984 m ($\nu_{C\equiv C}$). **UV-vis** (nm, 1.25 × 10^{-6} M in CH_2Cl_2 (ε, $M^{-1}cm^{-1}$)) 290 (46000), 306 (42000), 326 (54000), 346 (151000), 369 (397000), 397 (602000).

Reference spectra, 1:1 macrocycle/diplatinum axle mixtures. A. UV-vis (nm, **6** = 1.03 × 10^{-5} M, **3a** = 1.01 × 10^{-5} M (ε, $M^{-1}cm^{-1}$)) 267 (81000), 277 (103000), 292 (106000), 325 (123000), 355 (22000), 382 (6000), 415 (3000). **B. UV-vis** (nm, **9** = 8.05 × 10^{-6} M, **3a** = 8.20 × 10^{-6} M in CH_2Cl_2 (ε, $M^{-1}cm^{-1}$)) 281 (83300), 288 (81200), 306 (93100), 316 (113000), 335 (264000), 359 (434000), 396 (14300). **C. UV-vis** (nm, 8.05 × 10^{-6} M each in CH_2Cl_2 (ε, $M^{-1}cm^{-1}$)) 315 (119000), 336 (256000), 358 (463000), 396 (29800). **D. UV-vis** (nm, **12** = 8.05 × 10^{-6} M, **3a** = 8.20 × 10^{-6} M in CH_2Cl_2 (ε, $M^{-1}cm^{-1}$)) 281 (83300), 288 (81200), 306 (93100), 316 (113000), 335 (264000), 359 (434000), 396 (14300).

Crystallography. **A.** A CH_2Cl_2/hexanes solution of **8b** was allowed to slowly concentrate. After several days, a colorless plate was mounted for data collection. Cell parameters were obtained from 180 data frames taken at widths of 0.5° using Cell_Now.[50] Integrated intensity information for each reflection was obtained by

reduction of the data frames with APEX2.[51] The data were corrected for Lorentz and polarization factors (APEX2), as well as for crystal decay and absorption effects (SADABS).[52] The structure was solved by direct methods using XT/XS.[53] Hydrogen atoms were placed in idealized positions and were refined using riding model. All non-hydrogen atoms were refined with anisotropic thermal parameters. The structure was refined (weighted least squares refinement on F^2)[54] to convergence. The absence of additional symmetry or voids was confirmed using PLATON (ADDSYM).[55]

B. A CH_2Cl_2 solution of **6·3a** was layered with hexanes and kept at room temperature. After 3 d, one of the yellowish prisms was mounted for data collection. Cell parameters were obtained from 1080 frames using a 0.5° scan and refined with 9961 reflections. Integrated intensity information for each reflection was obtained by reduction of the data frames with the program SAINT.[56] The program SADABS was used for absorption corrections.[52] The space group was determined from systematic reflection conditions and statistical tests. The structure was solved by direct methods using SHELXTL (SHELXS).[53] Non-hydrogen atoms were refined with anisotropic thermal parameters. Hydrogen atoms were placed in idealized positions. The parameters were refined by weighted least squares refinement on F^2 to convergence.[53] Additional electron density was observed, and tentatively assigned to a disordered methylcyclopentane molecule (a major component of hexanes), although hexane or CH_2Cl_2 could not be excluded. Thus, the electron density contribution was extracted with the program PLATON/SQUEEZE.[55] Two methylene carbon atoms (C127 and C128) were disordered over two positions, and refined to 0.546:0.454 occupancy ratios. Restraints were used to keep the bond distances and thermal ellipsoids chemically meaningful. Only the dominant conformation was considered in all analyses.

C. A solution of **9·3a** in $CHCl_3$ was allowed to slowly evaporate. After several days, one of the yellow plates was mounted for data collection. Synchrotron radiation (Advanced Light Source (Lawrence Berkeley National Laboratory)) was employed for crystal screening, unit cell determination, and data collection on a D8 goniostat equipped with CCD detector at Beamline 11.3.1 (λ=0.68890 Å**)**. Cell parameters were obtained from 60 data frames taken at widths of 0.5°. Integrated intensity information for each reflection was obtained by reduction of the data frames with the program APEX2.[51] Data were corrected for Lorentz and polarization factors (APEX2), as well as for crystal decay effects, and the data were corrected for absorption effects (SADABS).[52] The structure was solved by direct methods using SHELXTL (SHELXS).[53] Half a molecule of $CHCl_3$ was found disordered over two positions, indicating the composition **9·3a**·0.5$CHCl_3$; this was successfully modeled. All non-hydrogen atoms were refined with anisotropic thermal parameters. Hydrogen atoms were placed in idealized positions, and refined using a riding model. All non-hydrogen atoms were refined with anisotropic thermal parameters. The structure was refined (weighted least squares refinement on F^2)[54] to convergence. The absence of additional symmetry or voids was confirmed using PLATON (ADDSYM).[55]

D. Pentane vapor was allowed to slowly diffuse into a benzene solution of **9·3b**. After 3 d, one of the thin yellow plates was mounted for data collection. Cell parameters were obtained from 60 data frames taken at widths of 0.5°. Integrated intensity information for each reflection was obtained by reduction of the data frames with the program APEX2.[51] Data were corrected for Lorentz and polarization factors (APEX2), and using SADABS[52] absorption and crystal decay effects. The structure was solved by direct methods using SHELXTL (SHELXS).[53] Two molecules of benzene were found in the unit cell, indicating the composition **9·3b**·2C_6H_6. All non-hydrogen atoms were

refined with anisotropic thermal parameters. The hydrogen atoms were placed in idealized positions, and refined using a riding model. All non-hydrogen atoms were refined with anisotropic thermal parameters. Atoms C1, C12, C13, and C19 showed unusual thermal ellipsoids and RIGU/EADP restraints/constraints were used to render them meaningful. PLATON[55] indicated a void (31 $Å^3$) with 2 $e^-/Å^3$. No efforts were made to account for the void electrons. The parameters were refined by weighted least squares refinement on F^2 to convergence.[54]

3.5 References

(1) Some lead reviews from an extensive literature: (a) Barlow, S.; O'Hare, D. *Chem. Rev.* **1997**, *97*, 637-669. (b) Astruc, D. *Acc. Chem. Res.* **1997**, *30*, 383-391. (c) Paul, F.; Lapinte, C. *Coord. Chem. Rev.* **1998**, *178-180*, 431-509. (d) McCleverty, J. A.; Ward, M. D. *Acc. Chem. Res.* **1998**, *31*, 842-851. (e) Akita, M.; Sakurai, A.; Chung, M.-C.; Moro-oka, Y. *J. Organomet. Chem.* **2003**, *670*, 2-10. (f) Aguirre-Etcheverry, P.; O'Hare, D. *Chem. Rev.* **2010**, *110*, 4839-4864. (g) Low, P. J. *Coord. Chem. Rev.* **2013**, *257*, 1507-1532. (h) Halet, J.-F.; Lapinte, C. *Coord. Chem. Rev.* **2013**, *257*, 1584-1613. (i) Tanaka, S.; Tsurugi, H.; Mashima, K. *Coord. Chem. Rev.* **2014**, *265*, 38-51. (j) Astruc, D.; Rapakousiou, A.; Wang, Y.; Djeda, R.; Diallo, A.; Ruiz, J.; Ornelas, C. *J. Coord. Chem.* **2014**, *67*, 3809-3821. (k) Cook, T. R.; Stang, P. J. *Chem. Rev.* **2015**, *115*, 7001-7045.

(2) Representative literature since 2013 involving polyynediyl complexes: (a) Burgun, A.; Gendron, F.; Sumby, C. J.; Roisnel, T.; Cador, O.; Costuas, K.; Halet, J.-F.; Bruce, M. I.; Lapinte, C. *Organometallics* **2014**, *33*, 2613-2627. (b) Lissel, F.; Schwarz, F.; Blacque, O.; Riel, H.; Lörtscher, E.; Venkatesan, K.; Berke, H. *J. Am. Chem. Soc.* **2014**, *136*, 14560-14569. (c) Hau, S. C. K.; Mak, T. C. W. *J. Am. Chem. Soc.* **2014**, *136*, 902-905. (d) Bruce, M. I.; Cole, M. L.; Ellis, B. G.; Gaudio, M.; Nicholson, B. K.; Parker, C. R.; Skelton, B. W.; White, A. H. *Polyhedron* **2015**, *86*, 43-56. (e) Oerthel, M.-C.; Yufit, D. S.; Fox, M. A.; Bryce, M. R.; Low, P. J. *Organometallics* **2015**, *34*, 2395-2405. (f) Cook, T. D.; Natoli, S. N.; Fanwick, P. E.; Ren, T. *Organometallics* **2016**, *35*, 1329-1338.

(3) (a) Haick, H.; Cahen, D. *Prog. Surf. Sci.* **2008**, *83*, 217-261. (b) Xing, Y.; Park, T.-H.; Venkatramani, R.; Keinan, S.; Beratan, D. N.; Therien, M. J.; Borguet, E. *J.*

Am. Chem. Soc. **2010**, *132*, 7946-7956. (c) Meisner, J. S.; Kamenetska, M.; Krikorian, M.; Steigerwald, M. L.; Venkataraman, L.; Nuckolls, C. *Nano Lett.* **2011**, *11*, 1575-1579. (d) Song, H.; Reed, M. A.; Lee, T. *Adv. Mater.* **2011**, *23*, 1583-1608. (e) Huang, C.; Yang, J. *Nano-Micro Lett.* **2011**, *3*, 1-5. (f) Hong, W.; Li, H.; Liu, S.-X.; Fu, Y.; Li, J.; Kaliginedi, V.; Decurtins, S.; Wandlowski, T. *J. Am. Chem. Soc.* **2012**, *134*, 19425-19431. (g) Aradhya, S. V.; Venkataraman, L. *Nat. Nanotechnol.* **2013**, *8*, 399-410. (h) Zhou, X.-Y.; Peng, Z.-L.; Sun, Y.-Y.; Wang, L.-N.; Niu, Z.-J.; Zhou, X.-S. *Nanotechnology* **2013**, *24*, 465204. (i) Moreno-García, P.; Gulcur, M.; Manrique, D. Z.; Pope, T.; Hong, W.; Kaliginedi, V.; Huang, C.; Batsanov, A. S.; Bryce, M. R.; Lambert, C.; Wandlowski, T. *J. Am. Chem. Soc.* **2013**, *135*, 12228-12240. (j) Zhou, X.-Y.; Wang, Y.-H.; Qi, H.-M.; Zheng, J.-F.; Niu, Z.-J.; Zhou, X.-S. *Nanoscale Res. Lett.* 2014, **9**:77. (k) Schwarz, F.; Kastlunger, G.; Lissel, F.; Riel, H.; Venkatesan, K.; Berke, H.; Stadler, R.; Lörtscher, E. *Nano Lett.* **2014**, *14*, 5932-5940. (l) Huang, C.; Rudnev, A. V.; Hong, W.; Wandlowski, T. *Chem. Soc. Rev.* **2015**, *44*, 889-901. (m) Su, T. A.; Li, H.; Klausen, R. S.; Widawsky, J. R.; Batra, A.; Steigerwald, M. L.; Venkataraman, L.; Nuckolls, C. *J. Am. Chem. Soc.* **2016**, *138*, 7791-7795. (n) Olavarria-Contreras, I. J.; Perrin, M. L.; Chen, Z.; Klyatskaya, S.; Ruben, M.; van der Zant, H. S. J. *J. Am. Chem. Soc.* **2016**, *138*, 8465-8469. (o) Milan, D. C; Al-Owaedi, O. A.; Oerthel, M.-C.; Marques-González, S.; Brooke, R. J.; Bryce, M. R.; Cea, P.; Ferrer, J.; Higgins, S. J.; Lambert, C. J.; Low, P. J.; Manrique, D. Z.; Martin, S.; Nichols, R. J.; Schwarzacher, W.; García-Suárez, V. M. *J. Phys. Chem. C* **2016**, *120*, 15666-15674.

(4) (a) *Molecular Wires: From Design to Properties;* de Cola, L., Ed.; Topics in Current Chemistry, Vol. 257; Springer: Berlin, 2005. (b) For a widely accepted

definition, see Lehn, J.-M. *Supramolecular Chemistry*; VCH: Weinheim, 1995; Chapter 8.3.2.

(5) One-two lead references from each of several active groups: (a) Schenning, A. P. H. J.; Arndt, J.-D.; Ito, M.; Stoddart, A.; Schreiber, M.; Siemsen, P.; Martin, R. E.; Boudon, C.; Gisselbrecht, J.-P.; Gross, M.; Gramlich, V.; Diederich, F. *Helv. Chim. Acta* **2001**, *84*, 296-334. (b) Frampton, M. J.; Anderson, H. L. *Angew. Chem. Int. Ed.* **2007**, *46*, 1028-1064; *Angew. Chem.* **2007**, *119*, 1046-1083. (c) Leroux, Y. R.; Fave, C.; Zigah, D.; Trippe-Allard, G.; Lacroix, J. C. *J. Am. Chem. Soc.* **2008**, *130*, 13465-13470. (d) Parthey, M.; Gluyas, J. B. G.; Schauer, P. A.; Yufit, D. S.; Howard, J. A. K.; Kaupp, M.; Low, P. J. *Chem. Eur. J.* **2013**, *19*, 9780-9784. (e) Pan, C.; Zhao, C.; Takeuchi, M.; Sugiyasu, K. *Chem. Asian J.* **2015**, *10*, 1820-1835. (f) Masai, H.; Terao, J.; Fujihara, T.; Tsuji, Y. *Chem. Eur. J.* **2016**, *22*, 6624-6630. (g) Milan, D. C.; Krempe, M.; Ismael, A. K.; Movsisyan, L. D.; Franz, M.; Grace, I.; Brooke, R. J.; Schwarzacher, W.; Higgins, S. J.; Anderson, H. L.; Lambert, C. J.; Tykwinski, R. R.; Nichols, R. J. *Nanoscale*, **2017**, *9*, 355-361.

(6) (a) Stahl, J.; Mohr, W.; de Quadras, L.; Peters, T. B.; Bohling, J. C.; Martín-Alvarez, J. M.; Owen, G. R.; Hampel, F.; Gladysz, J. A. *J. Am. Chem. Soc.* **2007**, *129*, 8282-8295. (b) de Quadras, L.; Bauer, E. B.; Mohr, W.; Bohling, J. C.; Peters, T. B.; Martín-Alvarez, J. M.; Hampel, F.; Gladysz, J. A. *J. Am. Chem. Soc.* **2007**, *129*, 8296-8309. (c) de Quadras, L.; Bauer, E. B.; Stahl, J.; Zhuravlev, F.; Hampel, F.; Gladysz, J. A. *New. J. Chem.* **2007**, *31*, 1594-1604. (d) Owen, G. R.; Stahl, J.; Hampel, F.; Gladysz, J. A. *Chem. Eur. J.* **2008**, *14*, 73-87. (e) Clough, M. C.; Fiedler, T.; Bhuvanesh, N.; Gladysz, J. A. *J. Organomet. Chem.* **2015**, *812*, 34-42.

(7) Demadis, K. D.; Hartshorn, C. M.; Meyer, T. J. *Chem. Rev.* **2001**, *101*, 2655-2685.

(8) Redox events involving the axle components of rotaxanes have been used to induce macrocycle motion. See (a) Sauvage, J.-P. *Acc. Chem. Res.* **1998**, *31*, 611-619. (b) Steuerman, D. W.; Tseng, H.-R.; Peters, A. J.; Flood, A. H.; Jeppesen, J. O.; Nielsen, K. A.; Stoddart, J. F.; Heath, J. R. *Angew. Chem., Int. Ed.* **2004**, *43*, 6486-6491; *Angew. Chem.* **2004**, *116*, 6648-6653. (c) McConnell, A. J.; Wood, C. S.; Neelakandan, P. P.; Nitschke, J. R. *Chem. Rev.* **2015**, *115*, 7729-7793 and the extensive earlier literature cited therein.

(9) (a) Dembinski, R.; Bartik, T.; Bartik, B.; Jaeger, M.; Gladysz, J. A. *J. Am. Chem. Soc*. **2000**, *122*, 810-822. (b) Mohr, W.; Stahl, J.; Hampel, F.; Gladysz, J. A. *Chem. Eur. J.* **2003**, *9*, 3324-3340. (c) Zheng, Q.; Bohling, J. C.; Peters, T. B.; Frisch, A. C.; Hampel, F.; Gladysz, J. A. *Chem. Eur. J.* **2006**, *12*, 6486-6505.

(10) Chalifoux, W. A.; Tykwinski, R. R. *Nature Chem.* **2010**, *2*, 967-971.

(11) Shi, L.; Rohringer, P.; Suenaga, K.; Niimi, Y.; Kotakoski, J.; Meyer, J. C.; Peterlik, H.; Wanko, M.; Cahangirov, S.; Rubio, A.; Lapin, Z. J.; Novotny, L.; Ayala, P.; Pichler, T. *Nature Mater.* **2016**, *15*, 634-640.

(12) (a) Meyer, W. E.; Amoroso, A. J.; Horn, C. R.; Jaeger, M.; Gladysz, J. A. *Organometallics* **2001**, *20*, 1115-1127. (b) Horn, C. R.; Martín-Alvarez, J. M.; Gladysz, J. A. *Organometallics* **2002**, *21*, 5386-5393. (c) Horn, C. R.; Gladysz, J. A. *Eur. J. Inorg. Chem.* **2003**, *9*, 2211-2218.

(13) da Costa, R. C.; Hampel, F.; Gladysz, J. A. *Polyhedron* **2007**, *26*, 581-588.

(14) Sauvage, J.-P. *Nobel Prize Lecture* **2016**, https://www.nobelprize.org/nobel_prizes/ chemistry/laureates/2016/sauvage-lecture.html

(15) Stoddart, Sir J. F. *Nobel Prize Lecture* **2016**, https://www.nobelprize.org/ nobel_prizes/chemistry/laureates/2016/stoddart-facts.html

(16) Feringa, B. *Nobel Prize Lecture* **2016**, https://www.nobelprize.org/nobel_prizes/ chemistry/laureates/2016/feringa-facts.html

(17) Saito, S.; Takahashi, E.; Nakazono, K. *Org. Lett.* **2006**, *8*, 5133-5136.

(18) (a) Langton, M. J.; Matichak, J. D.; Thompson, A. L.; Anderson, H. L. *Chem. Sci.* **2011**, *2*, 1897-1901. (b) Yamashita, Y.; Mutoh, Y.; Yamasaki, R.; Kasama, T.; Saito, S. *Chem. Eur. J.* **2015**, *21*, 2139-2145. (c) Hayashi, R.; Slavík, Y.; Kasama, T.; Saito, S. *J. Org. Chem.* **2016**, *81*, 1175-1184. (d) Kohn, D. R.; Movsisyan, L. D.; Thomson, A. L.; Anderson, H. L. *Org. Lett.* **2017**, *19*, 348-351.

(19) (a) Berná, J.; Crowley, J. D.; Goldup, S. M.; Hänni, K. D.; Lee, A.-L.; Leigh, D. A. *Angew. Chem., Int. Ed.* **2007**, *46*, 5709-5713; **2007**, *119*, 5811-5815. (b) Crowley, J. D.; Goldup, S. M.; Gowans, N. D.; Leigh, D. A.; Ronaldson, V. E.; Slawin, A. M. Z. *J. Am. Chem. Soc.* **2010**, *132*, 6243-6248. (c) Ugajin, K.; Takahashi, E.; Yamasaki, R.; Mutoh, Y.; Kasama, T.; Saito, S. *Org. Lett.* **2013**, *15*, 2684-2687.

(20) (a) Diederich, F.; Dietrich-Buchecker, C.; Nierengarten, J.-F.; Sauvage, J.-P. *J. Chem. Soc., Chem. Commun.* **1995**, 781-782. (b) Taylor, P. N.; Hagan, A. J.; Anderson, H. L. *Org. Biomol. Chem.* **2003**, *1*, 3851-3856. (c) Yoon, I.; Miljanić, O. S.; Benítez, D.; Khan, S. I.; Stoddart, J. F. *Chem. Commun.* **2008**, 4561-4563. (d) Shir, I. B.; Sasmal, S.; Mejuch, T.; Sinha, M. K.; Kapon, M.; Keinan, E. *J. Org. Chem.* **2008**, *73*, 8772-8779.

(21) (a) Crowley, J. D.; Goldup, S. M.; Lee, A. L.; Leigh, D. A.; McBurney, R. T. *Chem. Soc. Rev.* **2009**, *38*, 1530-1541. (b) Beves, J. E.; Blight, B. A.; Campbell, C. J.; Leigh, D. A.; McBurney, R. T. *Angew. Chem., Int. Ed.* **2011**, *50*, 9260-9327; *Angew.*

Chem. **2011**, *123*, 9428-9499. (c) Aucagne, V.; Hänni, K. D.; Leigh, D. A.; Lusby, P. J.; Walker, D. B. *J. Am. Chem. Soc.* **2006**, *128*, 2186-2187.

(22) Sato, Y.; Yamasaki, R.; Saito, S. *Angew. Chem., Int. Ed.* **2009**, *48*, 504-507 and 2630; *Angew. Chem.* **2009**, *121*, 512-515 and 2668.

(23) (a) Weisbach, N.; Baranová, Z.; Gauthier, S.; Reibenspies, J. H.; Gladysz, J. A. *Chem. Commun*. **2012**, *48*, 7562-7564. (b) Baranová, Z.; Amini, H.; Bhuvanesh, N.; Gladysz, J. A. *Organometallics* **2014**, *33*, 6746-6749.

(24) Sahnoune, H.; Baranová, Z.; Bhuvanesh, N.; Gladysz, J. A.; Halet, J.-F. *Organometallics* **2013**, *32*, 6360-6367.

(25) Baranová, Z.; Amini, H.; Neupane, M.; Garrett, S. C.; Ehnbom, A.; Bhuvanesh, N.; Reibenspies, J. H.; Gladysz, J. A. *Aust. J. Chem.* **2017**, *70*, 373-386.

(26) (a) Movsisyan, L. D.; Kondratuk, D. V.; Franz, M.; Thompson, A. L.; Tykwinski, R. R.; Anderson, H. L. *Org. Lett*. **2012**, *14*, 3424-3426. (b) Movsisyan, L. D.; Franz, M.; Hampel, F.; Thompson, A. L.; Tykwinski, R. R.; Anderson, H. L. *J. Am. Chem. Soc.* **2016**, *138*, 1366-1376.

(27) Bartik, B; Dembinski, R.; Bartik, T.; Arif, A. M.; Gladysz, J. A. *New J. Chem.* **1997**, *21*, 739-750.

(28) Mohr, W.; Peters, T. B.; Bohling, J. C.; Hampel, F.; Arif, A. M.; Gladysz, J. A. *C. R. Chimie* **2002**, *5*, 111-118.

(29) Wannere , C. S.; Schleyer, P. v. R. *Org. Lett.* **2003**, *5*, 605-608.

(30) (a) The atom labels for the macrocycles of **9·3a** and **9·3b** correspond to those in the cif files (except for additional designations M that have been deleted), and those for **6·3a** have been renumbered to match. Some of the atoms of the axles and macrocycles share the same number in the absence of the M designation, but metrical

parameters associated with these atoms are presented in separate tables. (b) The atom labels for macrocyle **3a** correspond to those in the cif file.[24] Those for **3b**, **4a**, and **4b** have been renumbered to match.

(31) Bondi, A. *J. Phys. Chem.* **1964**, *68*, 441-451.

(32) Hayashi, R.; Mutoh, Y.; Kasama, T.; Saito, S. *J. Org. Chem.* **2015**, *80*, 7536-7546.

(33) (a) Szafert, S.; Gladysz, J. A. *Chem. Rev.* **2003**, *103*, 4175-4206. (b) Szafert, S.; Gladysz, J. A. *Chem. Rev.* **2006**, *106*, PR1-PR33.

(34) Tillack, A. F.; Robinson, B. H. *J. Phys. Chem. B* **2017**, *121*, in press. DOI: 10.1021/acs.jpcb.7b02259.

(35) Kaim, W.; Kohlmann, S. *Inorg. Chem.* **1990**, *29*, 2909-2914.

(36) Coetzee, J. F.; Chang, T.-H. *Pure & Appl. Chem.* **1986**, *58*, 1535-1540.

(37) The sp carbon ^{13}C signals were assigned by analogy to those established for closely related structures.

(38) This coupling represents a satellite (d, ^{195}Pt = 33.8%), and is not reflected in the peak multiplicity given.

(39) The C_6F_5 signals were not observed.

(40) Some of the sp carbon ^{13}C signals were not observed.

(41) This sample cannot be represented as analytically pure, but the microanalytical data are provided to illustrate the best result obtained to date. The ^{1}H and ^{13}C NMR spectra confirm the high level of purity. See also Gabbaï, F. P.; Chirik, P. J.; Fogg, D. E.; Meyer, K.; Mindiola, D. J.; Schafer, L. L.; You, S.-L. *Organometallics* **2016**, *35*, 3255-3256.

(42) The *J* values given for the virtual triplets represent the *apparent* couplings between adjacent peaks, and not the mathematically rigorous coupling constants. See Hersh, W. H. *J. Chem. Educ.* **1997**, *74*, 1485-1488.

(43) This assignment was based upon peak intensity (ca. 2 × as compared to other macrocycle signals).

(44) This ^{13}C chemical shift is characteristic of the CH carbon atom of resorcinol or resorcinol ethers that is flanked by the CO carbon atoms: (a) Nakai, Y.; Yamada, F. *Org. Mag. Res.* **1978**, *11*, 607-611. (b) Makriyannis, A.; Fesik, S. *J. Am. Chem. Soc.* **1982**, *104*, 6462-6463.

(45) These data were obtained with a Bruker Avance III cryoprobe 500 MHz spectrometer.

(46) The overlapping triplets share one shoulder; the *J* values were measured between the two outer peaks.

(47) For the C_6F_5 and one of the sp carbon ^{13}C signals, the signal/noise ratio was too low to resolve all couplings.

(48) The spectroscopic data provided for this compound were obtained with instruments and solvents identical to those used for the other compounds in this paper; complementary data can be found in the original report.

(49) Data for these absorptions were obtained from a 1.61×10^{-4} M CH_2Cl_2 solution.

(50) Sheldrick, G. M. "Cell_Now (version 2008/1): Program for Obtaining Unit Cell Constants from Single Crystal Data": University of Göttingen, Germany.

(51) APEX2 "Program for Data Collection on Area Detectors" BRUKER AXS Inc., 5465 East Cheryl Parkway, Madison, WI 53711-5373 USA.

(52) SADABS, Sheldrick, G. M. "Program for Absorption Correction of Area Detector Frames", BRUKER AXS Inc., 5465 East Cheryl Parkway, Madison, WI 53711-5373 USA.

(53) Sheldrick, G. M. *Acta Cryst.* **2015**, *A71*, 3-8.

(54) Dolomanov, O. V.; Bourhis, L. J.; Gildea, R. J.; Howard, J. A. K.; Puschmann, H. *J. Appl. Cryst.* **2009**, *42*, 339-341.

(55) Spek, A. L. *J. Appl. Cryst.* **2003**, *36*, 7-13.

(56) SAINT, "Program for Data Reduction from Area Detectors", BRUKER AXS Inc., 5465 East Cheryl Parkway, Madison, WI 53711-5373 USA.

4. SUMMARY AND CONCLUSIONS

In conclusion, this study presented a brief overview of the origins of polyyne chemistry. The role of rotaxane assemblies, a class of MIMs, in the steric insulation of platinum-capped polyynediyl complexes was introduced in section 1.

Various new 1,10-phenanthroline-based macrocycles were prepared via Williamson ether syntheses from numerous α,ω-bis(bromoalkoxy)aryl precursors. The corresponding mononuclear 1:1 complexes of copper(I) iodide were isolated in good yields (40-80%). All new compounds were fully spectroscopically characterized as detailed in section 2. The crystal structures of the macrocyclic ligands and their corresponding copper(I) iodide complexes were determined. Further, structural models resulting from DFT calculations were analyzed parallel to the crystallographic data with the focus on the macrocycle dimensions, void volumes, etc. The relative position of the copper(I) iodide with respect to the macrocyclic cavity was considered in the context of the formation of rotaxanes by the treatment of the macrocycle complex with terminal alkynes.

The preparation of four rotaxanes consisting of 1,10-phenanthroline-based macrocycles and platinum-capped polyynediyl-containing axles was detailed in section 3. An active metal template strategy was applied to thread two terminal alkynes of the formula *trans*-$(C_6F_5)(p\text{-}tol_3P)_2Pt(C{\equiv}C)_{n/2}H$ (n = 4, 6, 8) through the previously described copper(I) iodide macrocycle complexes resulting in [2]rotaxanes featuring a $Pt(C{\equiv}C)_nPt$ unit. NMR spectroscopy revealed some interesting shielding effects of sterically hindered polyynes within MIMs resulting from the inescapable proximity of the encircling macrocycle. Crystallographic studies confirmed extensive steric insulation of the polyynediyl complexes by visual criteria. While the UV-visible spectra exhibited

negligible electronic interactions between the Pt(C≡C)$_n$Pt axles and macrocycles, the cyclic voltammetry data suggested rapid reactions following oxidation.

The studies in this dissertation have significantly contributed to the understanding of diplatinum polyynediyl complexes as model compounds for molecular wires. The application of rotaxane assemblies to the steric and dynamic insulation of molecular wires was explored. The synthesis of MIMS via the active metal template strategy, as applied in this work to the homocoupling of terminal alkynes, allows for a wide range of modifications of templating components and target compounds in addition to the extension towards other coupling reactions (e.g. azide-alkyne cycloadditions).

APPENDIX A

A.1 Experimental, Part 2 for Section 2

General Data. General procedures and instrumentation are as specified in the main text. Additional chemicals used were treated as follows: diethyl ether (BDH), dried using a Glass Contour solvent purification system; *n*-BuLi (Sigma Aldrich, 1.6 M in hexanes), lithium (J. T. Baker), and 4-bromoanisole (Alfa Aesar, 99%), used as received.

1,3-bis(6-bromohexyloxy)benzene (2a).[s1,s2] A round bottom flask was charged with acetone solutions (200 mL total) of resorcinol (5.008 g, 45.49 mmol) and 1,6-dibromohexane (33.291 g, 136.45 mmol) and fitted with a condenser. Then K_2CO_3 (15.716 g, 113.71 mmol) was added with stirring. The mixture was refluxed in the dark. After 3 d, the solvent was removed by rotary evaporation. Water was added. The residue was extracted with ethyl acetate. The extract was washed with water and aqueous NaOH (10% w/v) and dried ($MgSO_4$). The solvent was removed under reduced pressure. The residue was chromatographed (silica gel, packed in hexanes, eluted with a CH_2Cl_2/hexanes gradient 10:90 → 10:60 → 10:30 v/v). The solvent was removed from the product containing fractions (assayed by TLC, eluent 2:1 v/v CH_2Cl_2/hexane) by rotary evaporation to give **2a** as a colorless oil (9.284 g, 21.28 mmol, 47%) that solidified after a few days in air as a white solid, mp 38.4-39.6 °C.

NMR (δ/ppm, $CDCl_3$): **^{1}H** (500 MHz) 7.15 (t, $^3J_{HH}$ = 8.2 Hz, 1H, OCCHC<u>H</u>), 6.48 (dd, $^3J_{HH}$ = 8.2 Hz, $^4J_{HH}$ = 2.4 Hz, 2H, OCC<u>H</u>CH), 6.45 (t, $^4J_{HH}$ = 2.3 Hz, 1H, OCC<u>H</u>CO), 3.94 (t, $^3J_{HH}$ = 6.4 Hz, 4H, OC<u>H</u>$_2$), 3.42 (t, $^3J_{HH}$ = 6.8 Hz, 4H, BrC<u>H</u>$_2$), 1.90 (quint, $^3J_{HH}$ = 7.1 Hz, 4H, BrCH$_2$C<u>H</u>$_2$), 1.79 (quint, $^3J_{HH}$ = 6.8 Hz, 4H, OCH$_2$C<u>H</u>$_2$), 1.52-1.49 (m, 8H, OCH$_2$CH$_2$C<u>H</u>$_2$, BrCH$_2$CH$_2$C<u>H</u>$_2$); **^{13}C{^{1}H}** (125 MHz)

160.6 (s, O<u>C</u>CH), 130.0, 107.0, 101.7 (3 × s), 68.0 (s, O<u>C</u>H_2), 34.1, 33.0, 29.3, 28.2, 25.6 (5 × s, OCH$_2$<u>C</u>H$_2$<u>C</u>H$_2$, Br<u>C</u>H$_2$<u>C</u>H$_2$<u>C</u>H$_2$).

2,7-bis(4-bromomethylbenzyloxy)naphthalene (2e). A round bottom flask was charged with acetone solutions (80 mL total) of 2,7-dihydroxynaphthalene (2.000 g, 12.49 mmol) and 1,4-bis(bromomethyl)benzene (8.877 g, 37.06 mmol) and fitted with a condenser. Then K_2CO_3 (4.315 g, 31.22 mmol) was added with stirring. The mixture was refluxed in the dark. After 3 d, the solvent was removed by rotary evaporation. Water (200 mL) was added. The residue was extracted with CH_2Cl_2 (350 mL). The extract was washed with aqueous NaOH (2 × 100 mL, 10% w/v) and brine (2 × 100 mL) and dried ($MgSO_4$). The solvent was removed by rotary evaporation. The residue was chromatographed (silica gel, 4.5 × 29 cm, packed in hexanes, eluted with a CH_2Cl_2/hexanes gradient). The solvent was removed from the product containing fractions (assayed by TLC, eluent 1:2 v/v CH_2Cl_2/hexanes) by rotary evaporation to give **2e** as an off-white solid (0.723 g, 1.37 mmol, 11%), mp 146-148 °C. Anal. calcd. (%) for $C_{26}H_{22}Br_2O_2$ (526.27): C 59.34, H 4.21; found: C 59.55, H 4.31.

NMR (δ/ppm, $CDCl_3$): **^{1}H** (500 MHz) 7.68 (d, $^3J_{HH}$ = 8.8 Hz, 2H, OCCHC<u>H</u>), 7.45 (pseudo quartet, $^3J_{HH}$ = 8.3 Hz, 8H, *p*-C_6H_4), 7.10 (d, $^4J_{HH}$ = 2.4 Hz, 2H, OCC<u>H</u>C), 7.08 (dd, $^3J_{HH}$ = 8.8 Hz, $^4J_{HH}$ = 2.5 Hz, 2H, OCC<u>H</u>CH), 5.16 (s, 4H, OC<u>H</u>$_2$), 4.52 (s, 4H, BrC<u>H</u>$_2$); **^{13}C {^{1}H}** (125 MHz) 157.4 (s, O<u>C</u>CH), 137.7, 137.4 (2 × s, <u>C</u>CH_2, <u>C</u>'C'H'$_2$), 135.9 (s, CH<u>C</u>CCH), 129.5 (s, CH_2C<u>C</u>H), 129.4 (s, naphthyl CH), 128.0 (s, 'C'H$_2$'C'<u>C</u>'H), 124.8 (s, CHC<u>C</u>CH), 116.7, 106.8 (2 × s, naphthyl CH), 69.7 (s, O<u>C</u>H_2), 33.3 (s, Br<u>C</u>H_2).

2,7-bis(3-bromomethylbenzyloxy)naphthalene (2f). A round bottom flask was charged with acetone solutions (80 mL total) of 2,7-dihydroxynaphthalene (2.006 g, 13.92 mmol) and 1,3-bis(bromomethyl)benzene (8.897 g, 37.55 mmol) and fitted with a

condenser. Then K_2CO_3 (4.324 g, 31.29 mmol) was added with stirring. The mixture was refluxed in the dark. After 3 d, the solvent was removed by rotary evaporation. Water (250 mL) was added. The residue was extracted with CH_2Cl_2 (200 mL). The extract was washed with aqueous NaOH (2 × 100 mL, 10% w/v) and brine (2 × 100 mL) and dried ($MgSO_4$). The solvent was removed by rotary evaporation. The residue was chromatographed (silica gel, 4.5 × 29 cm, packed in hexanes, eluted with a CH_2Cl_2/hexanes gradient). The solvent was removed from the product containing fractions (assayed by TLC, eluent 1:2 v/v CH_2Cl_2/hexanes) by rotary evaporation to give **2f** as a white solid (1.042 g, 1.98 mmol, 14%), mp 122-123 °C. Anal. calcd. (%) for $C_{26}H_{22}Br_2O_2$ (526.27): C 59.34, H 4.21, Br 30.37; found: C 59.07, H 4.14, Br 30.30.

NMR (δ/ppm, $CDCl_3$): **^{1}H** (500 MHz) 7.69 (d, $^3J_{HH}$ = 8.9 Hz, 2H, OCCHC<u>H</u>), 7.53 (s, 2H, BrCH_2CC<u>H</u>C), 7.43-7.37 (2 × overlapping m, 6H, CC<u>H</u>C<u>H</u>C<u>H</u>C), 7.12 (d, $^4J_{HH}$ = 2.5 Hz, 2H, OCC<u>H</u>C), 7.09 (dd, $^3J_{HH}$ = 8.9 Hz, $^4J_{HH}$ = 2.5 Hz, 2H, OCC<u>H</u>CH), 5.16 (s, 4H, OC<u>H_2</u>), 4.53 (s, 4H, BrC<u>H_2</u>); **^{13}C{^{1}H}** (125 MHz) 157.4 (s, O<u>C</u>CH), 138.3, 137.8 (2 × s, <u>C</u>CH_2, <u>C</u>'C'H'$_2$),[s3] 135.9 (s, CH<u>C</u>CCH),[s3] 129.4, 129.3, 128.8, 128.2, 127.7 (5 × s, aryl), 124.8 (s, CH<u>C</u>CCH),[s3] 116.7, 106.8 (2 × s, aryl), 69.7 (s, O<u>C</u>H_2), 33.5 (s, Br<u>C</u>H_2).

MS (m/z, ESI$^+$): 566 ([**2f** + 40]$^+$, 33%).[s4]

(2,9-(1,10-phenanthrolinediyl))(4-$C_6H_4O(CH_2)_6O)_2$(1,3-C_6H_4) (3a).[s5,s6] A round bottom flask was charged with solutions of **2a** (0.967 g, 2.65 mmol)[s1] and **1** (1.158 g, 2.654 mmol) in DMSO (250 mL each) that had been neutralized as reported earlier.[s7] Then a solution of K_2CO_3 (5.136 g, 37.16 mmol) in H_2O (5 mL) was added with stirring. The mixture was stirred at 65 °C. After 19 h, the solvent was removed by rotary evaporation. Water was added and the mixture was extracted with CH_2Cl_2. The extract was washed with water and dried ($MgSO_4$). The solvent was removed by rotary

evaporation. The residue was chromatographed (silica gel, 4.5 × 22 cm, packed in CH_2Cl_2 and eluted with a MeOH/CH_2Cl_2 gradient 0:100 → 0.3:99.7). The solvent was removed from the product containing fractions (assayed by TLC) by rotary evaporation to give **3a** as a white solid (1.007 g, 1.576 mmol, 59%) that was stored in the dark (moderately light sensitive).

NMR (δ/ppm, $CDCl_3$): **^{1}H** (500 MHz) 8.45 (d, $^3J_{HH}$ = 8.5 Hz, 4H, H_o),[s8] 8.26 (d, $^3J_{HH}$ = 8.4 Hz, 2H, H_4 or H_7),[s8] 8.08 (d, $^3J_{HH}$ = 8.4 Hz, 2H, H_3 or H_8),[s8] 7.74 (s, 2H, H_5 or H_6),[s8] 7.18 (t, $^3J_{HH}$ = 8.1 Hz, 1H, OCCHC<u>H</u> of *m*-C_6H_4), 7.12 (d, $^3J_{HH}$ = 8.5 Hz, 4H, H_m),[s8] 6.56 (t, $^4J_{HH}$ = 2.2 Hz, 1H, OCC<u>H</u>CO), 6.52 (d, $^3J_{HH}$ = 8.2 Hz, 2H, OCC<u>H</u>CH of *m*-C_6H_4), 4.11 (t, $^3J_{HH}$ = 6.9 Hz, 4H, OCH_2), 4.01 (t, $^3J_{HH}$ = 6.1 Hz, 4H, O'C'H_2), 1.93-1.85 (m, 8H, $OCH_2C\underline{H}_2$, O'C'H_2C'$\underline{H}_2$), 1.61-1.59 (m, 8H, $OCH_2CH_2C\underline{H}_2$, O'C'$H_2C'H_2C'\underline{H}_2$); **^{13}C{^{1}H}** (125 MHz) 160.58, 160.57, 156.4, 146.1, 136.9, 132.1, 130.0 (7 × s), 129.1 (s, CH of *p*-C_6H_4), 127.6, 125.7, 119.3 (3 × s), 114.9 (s, CH of *p*-C_6H_4), 107.0 (s), 101.2 (s, OC<u>C</u>HCO), 68.2, 67.9 (2 × s, O<u>C</u>H_2, O'<u>C</u>'H_2), 29.7, 29.2 (2 × s, $OCH_2\underline{C}H_2$, O'C'H_2<u>C</u>'H_2), 26.13, 26.08 (2 × s, $OCH_2CH_2\underline{C}H_2$, O'C'$H_2C'H_2$<u>C</u>'$H_2$).

(3a)CuI (4a).[s5] A solution of CuI (0.296 g, 1.55 mmol) in CH_3CN (30 mL) was added to a solution of **1** (0.992 g, 1.55 mmol) in CH_2Cl_2 (70 mL) in a Schlenk flask. The mixture was stirred in the dark. After 2.5 h, the mixture was heated to 38 °C and the solvent removed by rotary evaporation. The residue was recrystallized from hot CH_2Cl_2 (refrigerator storage). After 3 d, the precipitate was isolated by filtration to give **4a** as a dark orange crystalline solid (1.021 g, 1.231 mmol, 79%).

NMR (δ/ppm, $CDCl_3$): **^{1}H** (500 MHz) 8.41 (d, $^3J_{HH}$ = 8.2 Hz, 2H), 8.11 (overlapping d, $^3J_{HH}$ = 7.5 Hz, 4H), 8.05 (overlapping d, $^3J_{HH}$ = 8.4 Hz, 2H), 7.85 (s, 2H, H_5 or H_6),[s8] 7.15 (overlapping t, $^3J_{HH}$ = 8.1 Hz, 1H, OCCHC<u>H</u> of *m*-C_6H_4), 7.10 (overlapping d, $^3J_{HH}$ = 8.4 Hz, 4H), 6.54 (s, 1H, OCC<u>H</u>CO), 6.49 (d, $^3J_{HH}$ = 8.1 Hz,

2H, OCC<u>H</u>CH of *m*-C_6H_4), 4.10 (t, $^3J_{HH}$ = 7.0 Hz, 4H, OCH_2), 4.03-3.84 (br, 4H, O'C'H_2), 1.91 (br m, 4H, $OCH_2C\underline{H}_2$), 1.82 (br, 4H, O'C'H_2C'$\underline{H}_2$), 1.56 (br, 8H, $OCH_2CH_2C\underline{H}_2$, O'C'$H_2C'H_2C'\underline{H}_2$); **$^{13}C\{^1H\}$** (125 MHz) 161.0, 160.5, 158.4, 144.0, 137.8, 131.3, 130.2 (7 × s), 129.6 (s, CH of *p*-C_6H_4), 127.3, 125.7, 124.4 (3 × s), 115.0 (s, CH of *p*-C_6H_4), 107.0 (s), 100.8 (s, OC<u>C</u>HCO), 68.1, 67.8 (2 × s, O<u>C</u>H_2, O'<u>C</u>'H_2), 29.6, 28.8 (2 × s, $OCH_2\underline{C}H_2$, O'C'H_2<u>C</u>'H_2), 25.8, 25.7 (2 × s, $OCH_2CH_2\underline{C}H_2$, O'C'$H_2C'H_2$<u>C</u>'$H_2$).

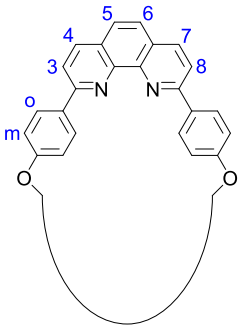

Figure A.1. Atom numbering or lettering used in the ^{1}H NMR assignments of 2,9-diaryl-1,10-phenanthrolines.

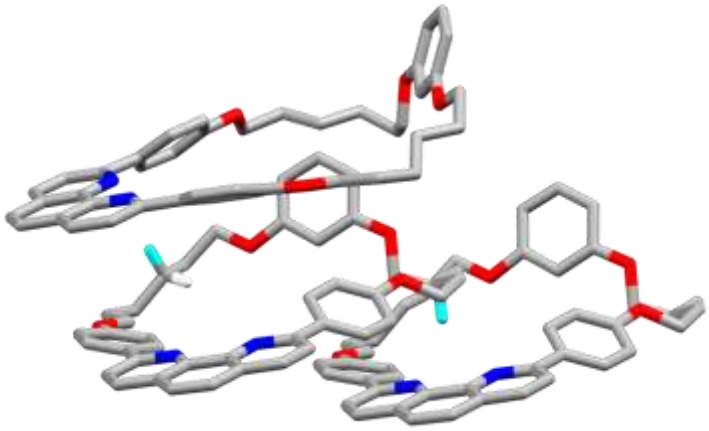

	distance [Å]	angle [°]
C22H22A···N1	2.689	143.51
C22H22A···N2	2.566	152.64
C32H32A···N1	2.901	132.94
C32H32A···N1	2.462	148.41

Figure A.2. Weak intermolecular phenanthroline N···HC interactions in crystalline **3a**.

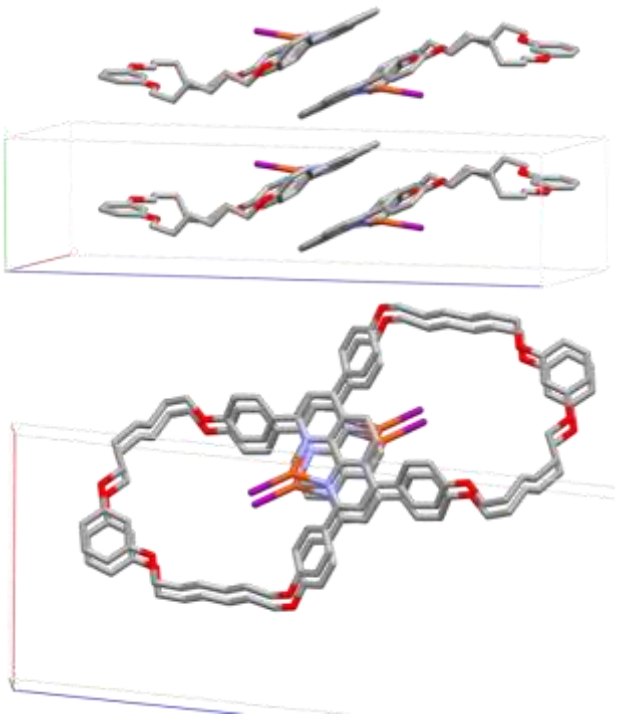

Figure A.3. Views of the lattice of **4a** showing phenanthroline π-π interactions with stacking distances of 3.559-3.734 Å.

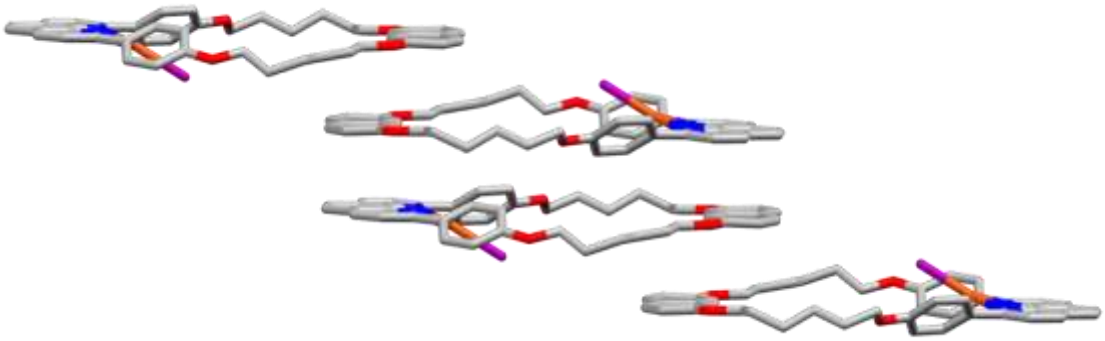

Figure A.4. Views of the lattice of **4b** showing phenanthroline/dihydroxynaphthalene π-π interactions with stacking distances of 3.424-3.702 Å.

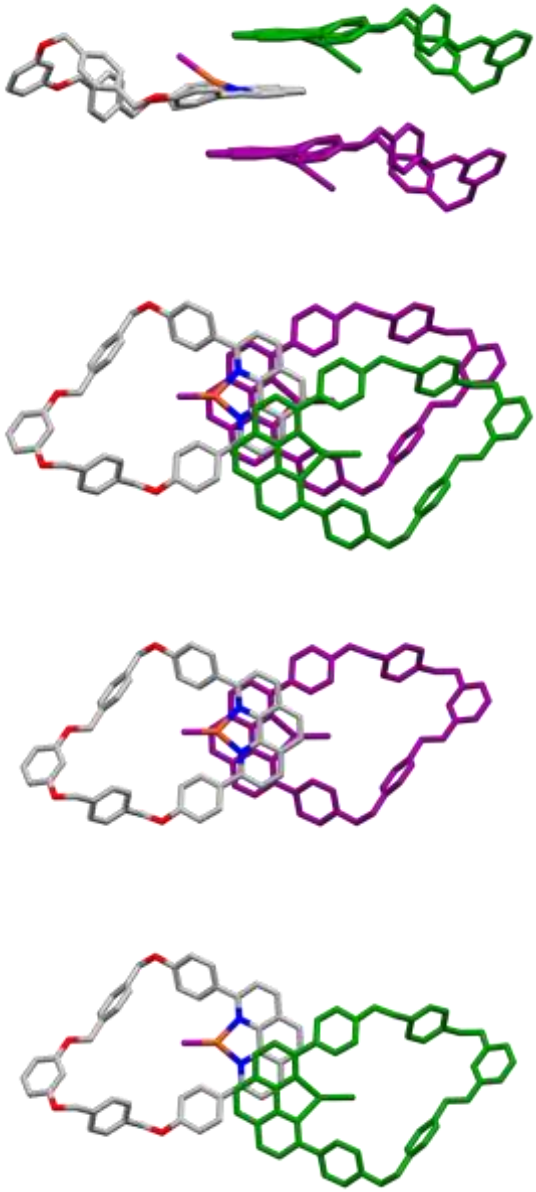

Figure A.5. Views of the lattice of **4c** showing phenanthroline π-π interactions with stacking distances of 3.408-3.516 Å.

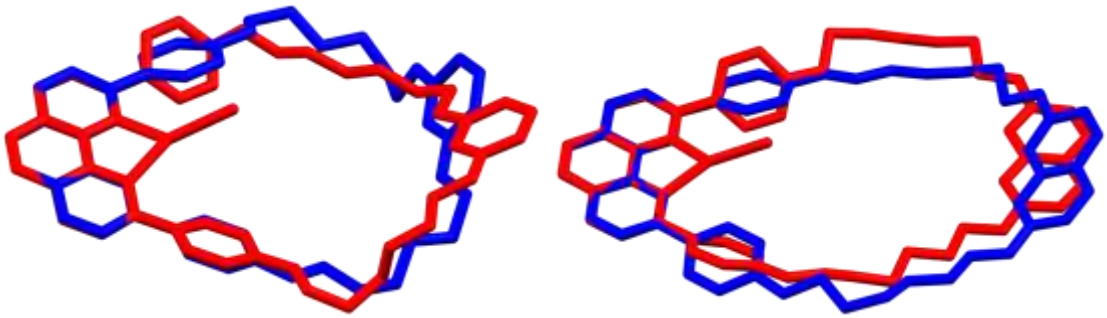

Figure A.6. Overlays of the crystal structures of macrocycles (blue) and their CuI complexes (red): left, **3a** and **4a**; right, **3b** and **4b**.

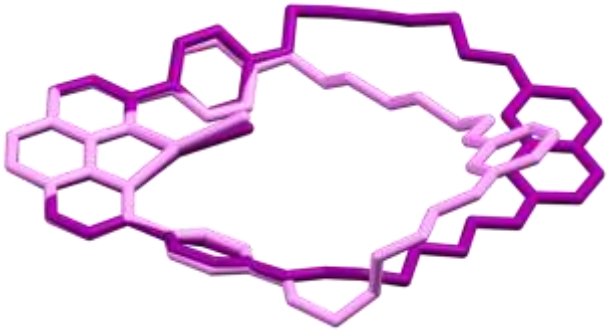

Figure A.7. Overlay of the crystal structures of the CuI complexes **4a** (pale purple) and **4b** (dark purple).

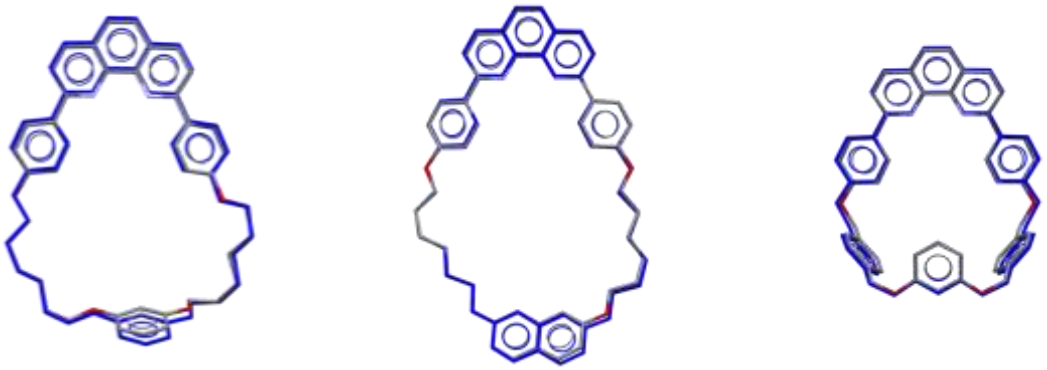

Figure A.8. Overlays of the crystal structures (colored as in Figure 2) and optimized DFT geometries (blue) of **3a** (left), **3b** (middle) and **3c** (right).

Figure A.9. Overlays of the crystal structures (colored as in Figure 3) and optimized DFT geometries (red) of **4a** (left), **4b** (middle) and **4c** (right).

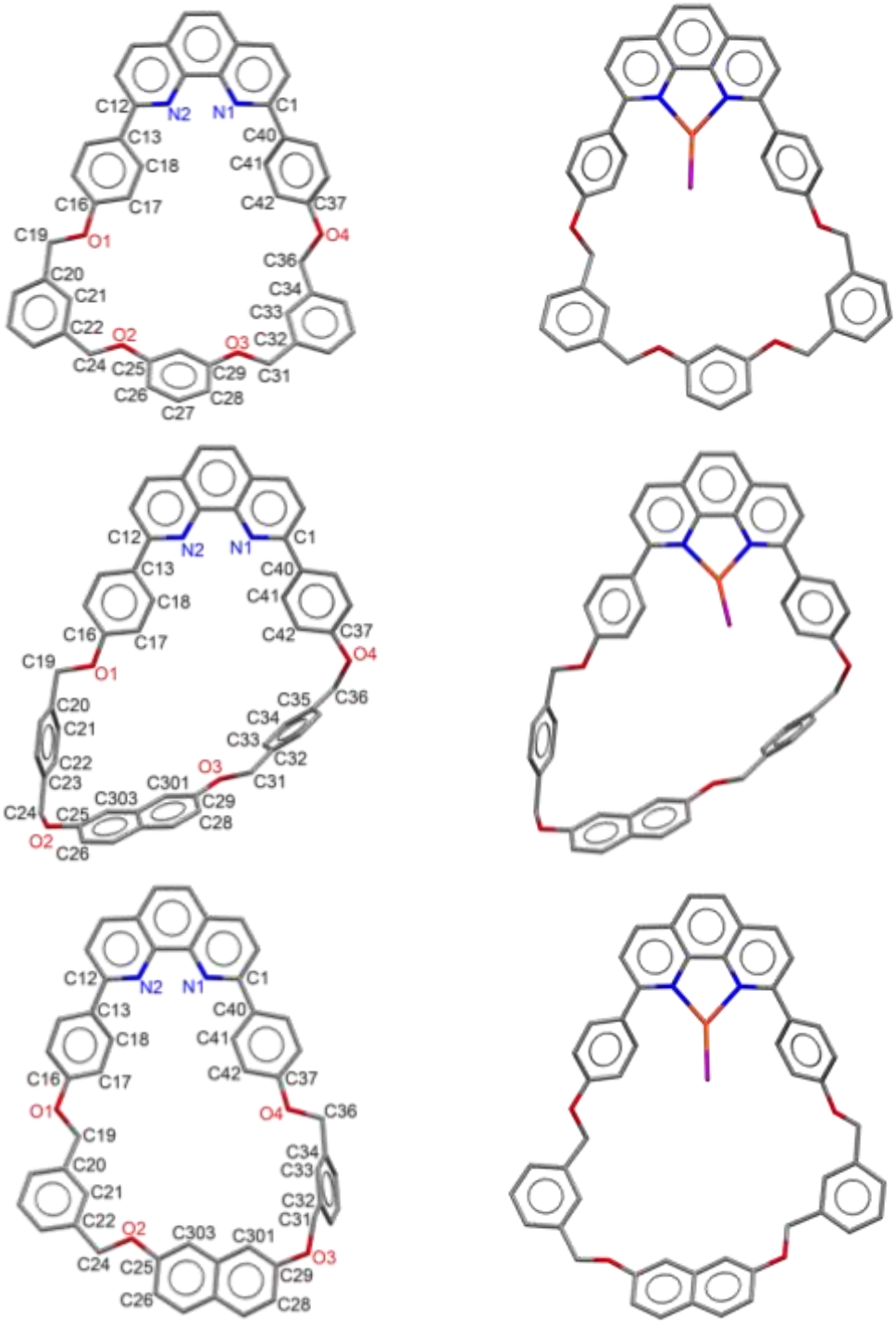

Figure A.10. Views of the optimized DFT geometries of **3d** (top left), **3e** (middle left), **3f** (bottom left), **4d** (top right), **4e** (middle right), and **4f** (bottom right).

Table A.1. Selected computed distances [Å] and angles [°] for **3a-f** and **4a-f**.[a]

	3a	**3b**	**3c**	**3d**	**3e**	**3f**
O1···O4	10.248	11.042	10.841	9.687	10.474	9.487
O2···O3	4.842	7.417	4.726	4.724	7.321	7.338
N1···O3	11.307	13.439	10.344	10.304	10.021	12.412
N2···O2	10.975	12.815	10.344	10.167	13.096	10.824
N1···C_{distal}[d]	11.449	12.907	9.616 (8.459)	10.968	11.207	11.444
N2···C_{distal}[d]	11.515	12.807	9.616 (8.459)	10.756	11.690	11.278
O1···O3	10.693	12.945	10.377	7.932	7.135	12.140
O2···O4	8.385	11.469	10.377	9.485	14.205	8.429
C17···C42	6.364	6.862	6.626	6.186	6.515	5.946
	4a	**4b**	**4c**	**4d**	**4e**	**4f**
Cu···phen[b]	0.545	0.505	0.571	0.542	0.765	0.490
I···phen[b]	1.813	1.687	1.860	1.918	2.533	1.682
CuIN1N2 vs. phen[c]	26.29	24.36	26.82	28.32	38.41	24.44
O1···O4	11.042	11.101	11.318	10.058	10.876	10.773
O2···O3	4.838	7.435	4.947	4.727	7.331	7.317
N1···O3	10.880	12.752	11.717	10.115	9.884	11.191
N2···O2	11.331	12.373	10.417	10.179	13.017	11.478
N1···C_{distal}[d]	11.691	12.140	11.795	10.752	11.095	11.093
N2···C_{distal}[d]	11.641	12.286	11.335	10.921	11.563	11.182
O1···O3	8.359	13.130	11.694	9.544	7.170	10.664
O2···O4	11.601	10.513	8.598	8.228	14.270	11.033
C17···C42	7.098	7.170	7.122	6.744	7.198	7.091

[a]See Figure A.10 for the atomic numbering. [b]The distance from the $C_{12}N_2$ least squares plane. [c]The angle defined by the CuIN1N2 least squares plane and the $C_{12}N_2$ least squares plane. [d]The carbon atoms distal to N1 and N2 are taken as C29 and C25 (**3a**), C301 and C303 (**3b**), and C25 and C29 (C26 and C28, values in parenthesis) (**3c**), C29 and C25 (**3d**), C301 and C303 (**3e**), and C301 and C303 (**3f**), respectively; the analogous atoms are employed for **4d-f**.

A.2 References

(s1) Ogawa, T.; Kishimoto, T.; Kobayashi, K.; Ono, N. *J. Chem. Soc., Perkin Trans. 1* **1998**, 529-538.

(s2) Watarai, N.; Kawasaki, H.; Azumaya, I.; Yamasaki, R.; Saito, S. *Heterocycles* **2009**, *79*, 531-548.

(s3) These signals were assigned based on the relative intensities.

(s4) $[\mathbf{2f} + 40]^+$ is tentatively assigned as $[\mathbf{2f} + K + 1]^+$.

(s5) Saito, S.; Nakazono, K.; Takahashi, E. *J. Org. Chem.* **2006**, *71*, 7477-7480.

(s6) Sahnoune, H; Baranová, Z.; Bhuvanesh, N.; Gladysz, J. A.; Halet, J.-F. *Organometallics* **2013**, *32*, 6360-6367.

(s7) Dietrich-Buchecker, C.; Sauvage, J.-P. *Tetrahedron* **1990**, *46*, 503-512.

(s8) These ^{1}H NMR assignments are based upon those given in reference s7. For the numbering or labeling of certain atoms, see Figure A.1.

APPENDIX B

B.1 Experimental, Part 2 for Section 3

***trans*-(C_6F_5)(*p*-tol_3P)$_2$Pt(C≡C)$_3$H (7).**[s9] A Schlenk flask was charged with **8a** (0.502 g, 0.434 mmol) and THF (140 mL). Then *n*-Bu_4N^+ F^- (1.0 M in THF/5 wt% H_2O, 0.087 mL, 0.087 mmol) was added with stirring. After 15 min, the mixture was poured into cold water (80 mL). The sample was extracted with cold CH_2Cl_2 (3 × 50 mL). The combined extracts were dried ($MgSO_4$). The solvent was removed by rotary evaporation at 0 °C. The yellow residue was extracted with cold hexanes (3 × 10 mL). The combined extracts were passed through a silica gel plug (4.5 × 10 cm, packed in hexanes); these fractions were discarded. The yellow residue was then extracted with cold CH_2Cl_2 (5 mL) and transferred onto the same plug. The plug was eluted with a CH_2Cl_2/hexanes gradient (1:9 → 1:1 v/v). The pale yellow fractions were collected and the solvent was removed by rotary evaporation at 0 °C to give **7** as a white solid (0.356 g, 0.340 mmol, 79%), which was stored at –34 °C. Complex **7** became brown within a few minutes at room temperature but was stable for several weeks at –34 °C.

NMR (δ/ppm, $CDCl_3$):[s9] **^{1}H** (500 MHz) 7.47 (m, 12 H, *o* to P), 7.12 (d, 12 H, $^3J_{HH}$ = 7.7 Hz, *m* to P), 2.36 (s, 18 H, CH_3), 1.83 (s, 1H, ≡CH); **^{13}C{^{1}H}** (125 MHz) 141.0 (s, *p* to P), 134.4 (t, $^2J_{CP}$ = 6.4 Hz, *o* to P), 128.8 (t, $^3J_{CP}$ = 5.6 Hz, *m* to P), 127.2 (t, $^1J_{CP}$ = 30.3 Hz, *i* to P), 70.5, 63.9, 55.3 (3 × s, PtC≡CC≡<u>CC</u>≡<u>C</u>H),[s10] 21.5 (s, CH_3); **^{19}F** (470 MHz) –116.14 to –116.22 (m, $^3J_{FPt}$ = 291.3 Hz, 2F, *o* to Pt),[s11] –163.54 to –163.86 (m, 2F, *m* to Pt), –164.13 (t, $^3J_{FF}$ = 19.4 Hz, 1F, *p* to Pt); **^{31}P{^{1}H}** (202 MHz) 17.96 (s, $^1J_{PPt}$ = 2634 Hz).[s11]

***trans*-(C_6F_5)(*p*-tol_3P)$_2$Pt(C≡C)$_4$SiMe$_3$ (11b)** (**C**; third route, Scheme 3.6). A three necked round bottom flask was charged with **8a**[s9] (0.302 g, 0.261 mmol) and

acetone (52 mL), and fitted with a dry ice condenser. Then *n*-Bu_4N^+ F^- (1.0 M in THF/5 wt% H_2O, 0.060 mL, 0.060 mmol) was added to the pale yellow solution with stirring. After 10 min, $ClSiMe_3$ (0.035 mL, 0.28 mmol) was added. The reaction was monitored by TLC (silica, 1:2 v/v CH_2Cl_2/hexanes). The three necked flask was transferred to a 60 °C oil bath, and O_2 was aspirated through the mixture. After 5 min, $HC{\equiv}CSiMe_3$ (0.72 mL, 5.2 mmol) was added, and then the CuCl/TMEDA adduct (0.40 M in acetone; 1.7 mL, 0.65 mmol) in portions over 40 min. The sample was stirred overnight at room temperature. Then hexanes (50 mL) was added to the bluish-green mixture, which was passed through an alumina plug (3 × 10 cm, packed with 1:1 v/v acetone/hexanes). The plug was eluted with 1:1 v/v acetone/hexanes until the eluate was colorless (monitored by TLC for **11b**). The solvent was removed from the yellow eluate by rotary evaporation. The residue was chromatographed on a silica gel column (3 × 28 cm, packed in hexanes, eluted with a CH_2Cl_2/ hexanes gradient). Complex **11b** eluted with 15:85 v/v CH_2Cl_2/hexanes, and a second yellow band containing **9** eluted with 40:60 v/v CH_2Cl_2/hexanes. The solvent was removed from the first band by rotary evaporation and oil pump vacuum to give **11b** as a yellow solid (0.043 g, 0.038 mmol, 14%).

***trans,trans*-$(C_6F_5)(p\text{-}tol_3P)_2Pt(C{\equiv}C)_6Pt(Pp\text{-}tol_3)_2(C_6F_5)$ (9).**[s9] A three necked round bottom flask was charged with **8b** (0.008 g, 0.007 mmol) and THF (1 mL) and fitted with a dry ice condenser. Then K_2CO_3 (0.004 g, 0.03 mmol) and MeOH (0.5 mL) were added with stirring (the desilylation was monitored by TLC: silica, 2:1 v/v CH_2Cl_2/hexanes). Then O_2 was aspirated through the mixture. The flask was placed in a 40 °C oil bath. The CuCl/TMEDA adduct (0.40 M in acetone; 0.8 mL, 0.3 mmol) and acetone (1 mL) were added with stirring. After 3 h, the solvent was removed by rotary evaporation. The residue was extracted with hexanes (3 × 1 mL). The extract was filtered through an alumina plug (0.7 × 4 cm, packed in hexanes) and discarded. The

residue was then extracted with benzene (3 × 1 mL). This extract was passed through the same plug, which was rinsed with additional benzene. The solvent was removed from the yellow filtrate by rotary evaporation and oil pump vacuum to give **9** as a yellow solid (0.007 g, 0.003 mmol, 91%).

NMR (δ/ppm, $CDCl_3$):[s9] **^{1}H** (500 MHz) 7.44 (m, 24H, *o* to P), 7.11 (d, $^3J_{HH}$ = 7.9 Hz, 24H, *m* to P), 2.35 (s, 36H, CH_3); **^{31}P{^{1}H}** (202 MHz) 17.94 (s, $^1J_{PPt}$ = 2619 Hz).[s11]

Table B.1. Crystallographic data for **8a**[a] and **8b**.

	8a[a]	**8b**
empirical formula	$C_{60}H_{57}F_5P_2PtSi$	$C_{57}H_{51}F_5P_2PtSi$
formula weight	1158.22	1116.09
temperature [K]	173(2)	110.0
wavelength [Å]	0.71073	1.54178
diffractometer	Nonius KappaCCD	Bruker D8 GADDS
crystal system	Triclinic	Triclinic
space group	*P-1*	*P-1*
unit cell dimensions		
a [Å]	12.9303(2)	12.7418(6)
b [Å]	13.2663(2)	12.8650(5)
c [Å]	15.8682(2)	15.8271(7)
α [°]	87.9570(10)	91.813(3)
β [°]	88.2170(10)	90.657(3)
γ [°]	89.3000(10)	93.537(3)
volume [$Å^3$]	2718.77(7)	2588.0(2)
Z	2	2
ρ_{calcd} [Mg/m^3]	1.415	1.432
μ [mm^{-1}]	2.715	6.320
F (000)		1120
crystal size [mm^3]	0.30 × 0.30 × 0.10	0.16 × 0.08 × 0.02
range for data collection	1.28 to 27.46	2.793 to 60.855
index ranges	$-16 \le h \le 16$	$-13 \le h \le 14$
	$-17 \le k \le 17$	$-14 \le k \le 14$
	$-18 \le l \le 20$	$-17 \le l \le 17$
reflections collected	22881	61027
independent reflections	12290 [R(int)=0.0245]	7665 [R(int) = 0.0493]
max. and min. transmission		0.7519 and 0.4882
data / restraints / parameters	12290 / 0 / 622	7665 / 0 / 604
goodness-of-fit on F^2	1.121	1.098
final R indices [I>2σ(I)]	R1 = 0.0260	R1 = 0.0224
	wR2 = 0.0619	wR2 = 0.0573
R indices (all data)	R1 = 0.0355	R1 = 0.0249
	wR2 = 0.0756	wR2 = 0.0584
largest diff. peak & hole [$eÅ^{-3}$]	0.614	0.905 and -1.032

[a] Mohr, W.; Peters, T. B.; Bohling, J. C.; Hampel, F.; Arif, A. M.; Gladysz, J. A. *C. R. Chimie* **2002**, *5*, 111-118.

Table B.2. Key crystallographic distances [Å] and angles [°] for new and previously reported platinum trialkylsilylhexatriynyl complexes **8a**[a] and **8b**.

	8a[a]	**8b**
Pt-C1	1.985(3)	2.003(3)
C1≡C2	1.226(4)	1.201(4)
C2-C3	1.362(4)	1.366(5)
C3≡C4	1.210(5)	1.220(5)
C4-C5	1.367(5)	1.367(5)
C5≡C6	1.206(5)	1.205(5)
C6-Si	1.843(3)	1.840(4)
Pt-P1	2.3111(7)	2.3074(7)
Pt-P2	2.2994(7)	2.3019(7)
Pt-C_{ipso}[b]	2.068(3)	2.065(3)
av. C_{sp}-C_{sp}	1.365	1.367
av. C_{sp}≡C_{sp}	1.214	1.209
Pt···Si	10.147	10.120
Sum of bond lengths Pt to Si	10.199	10.202
P1-Pt-P2	174.14	174.30(2)
C1-Pt-P1	88.31	89.08(8)
C1-Pt-P2	88.36	89.38(8)
C1-Pt-C_{ipso}	179.37	179.56(11)
C_{ipso}-Pt-P1	91.99	91.26(8)
C_{ipso}-Pt-P2	91.30	90.31(8)
Pt-C1-C2	178.8(3)	179.7(3)
C1-C2-C3	175.7(3)	177.7(3)
C2-C3-C4	177.3(4)	176.9(4)
C3-C4-C5	174.9(4)	174.6(4)
C4-C5-C6	178.7(4)	176.9(4)
C5-C6-Si	178.8(4)	173.8(3)
av. C_{sp}-C_{sp}-C_{sp}	177.4	176.6
π stacking[c]	3.594-3.724	3.502-3.676
angle stacking[d]	159.65	161.30
C_{sp}···C_{sp}[e]	5.909 (C2···C4)	5.596 (C2···C3)

[a] Mohr, W.; Peters, T. B.; Bohling, J. C.; Hampel, F.; Arif, A. M.; Gladysz, J. A. *C. R. Chimie* **2002**, 5, 111-118. [b] C_{ipso} is the ligating C_6F_5 carbon atom. [c] Distances between centroids of the C_6F_5 and C_6H_4R rings (see Figure B.2). [d] Angle of centroids of the three rings in *c* (see Figure B.2). [e] The shortest carbon-carbon distance between parallel sp chains in the crystal lattice.

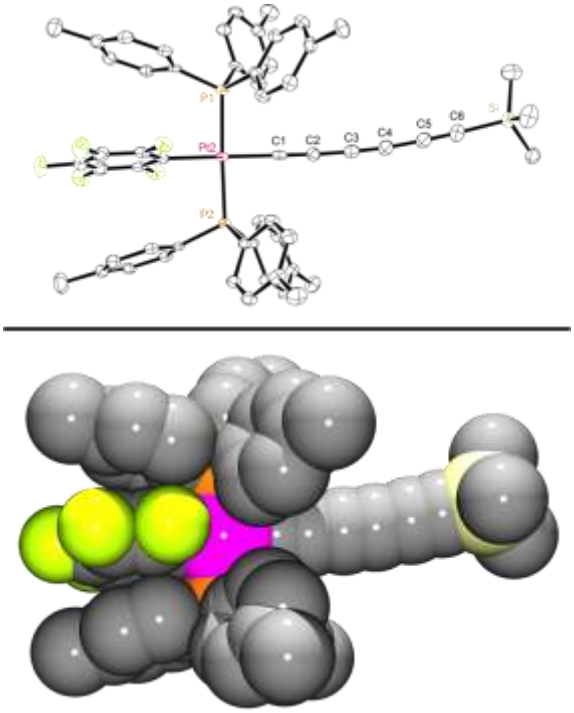

Figure B.1. Thermal ellipsoid plot (50% probability; top) and space filling representation (bottom) of the molecular structure of **8b**.

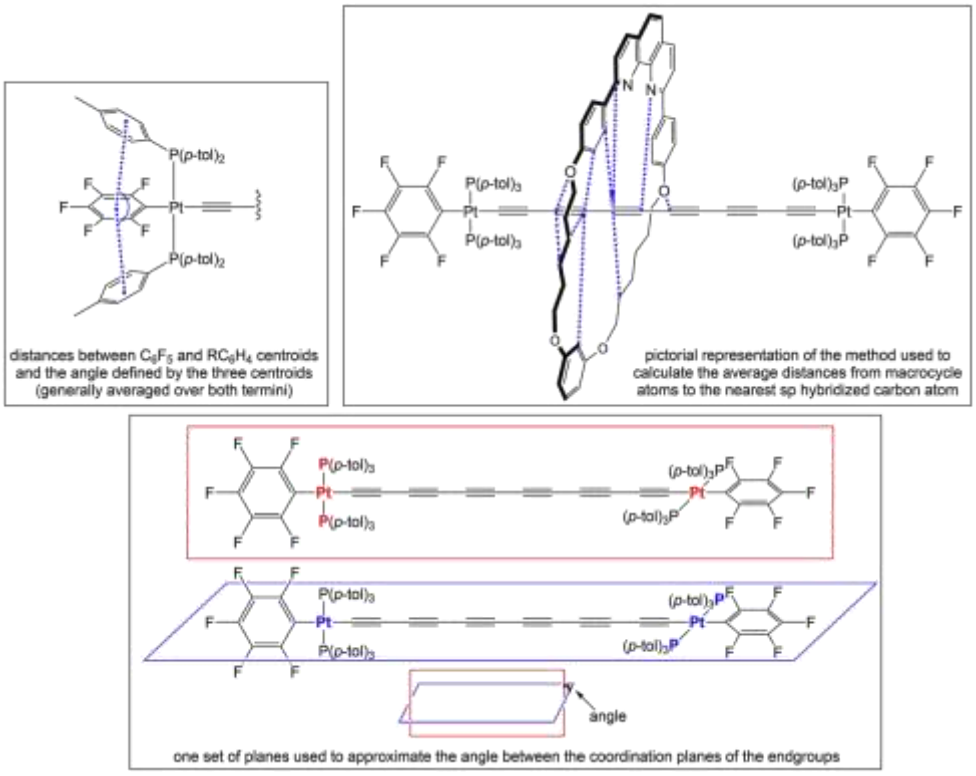

Figure B.2. Representations of selected crystallographic parameters from Tables 3.5 and B.2.

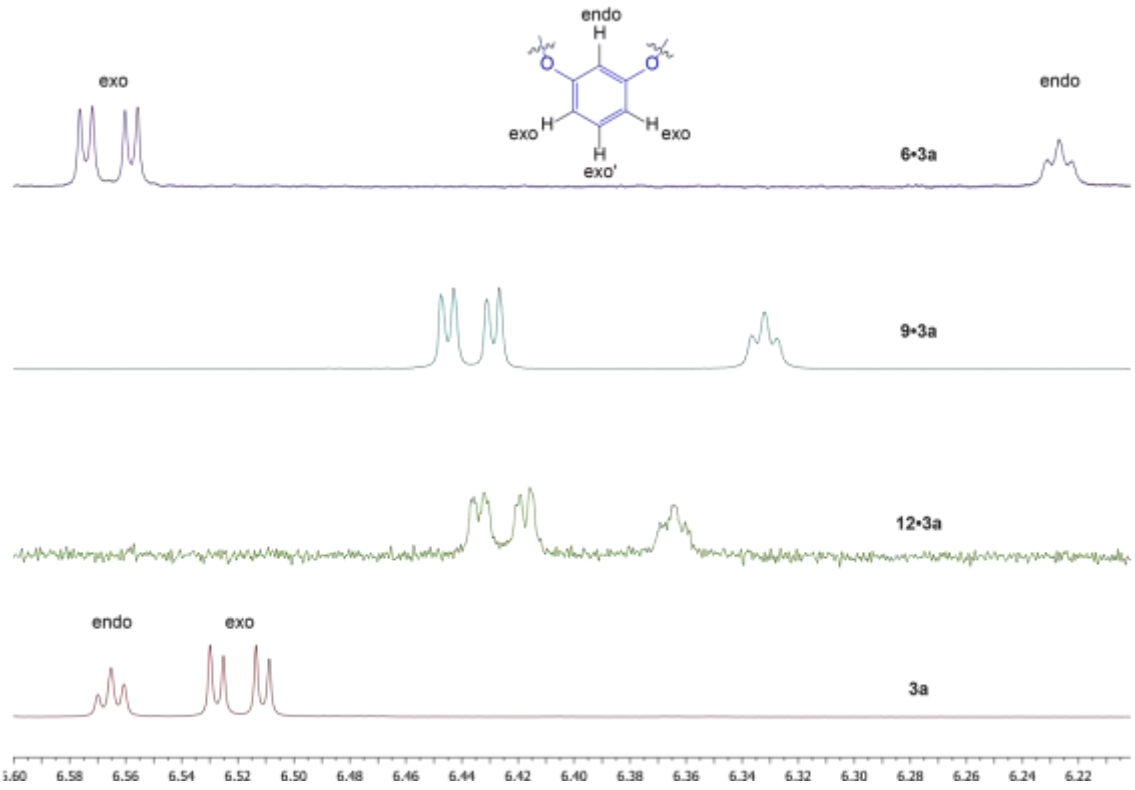

Figure B.3. ^{1}H NMR spectra of the resorcinol ether region of macrocycle **3a** and the rotaxanes **6·3a**, **9·3a**, and **12·3a**.

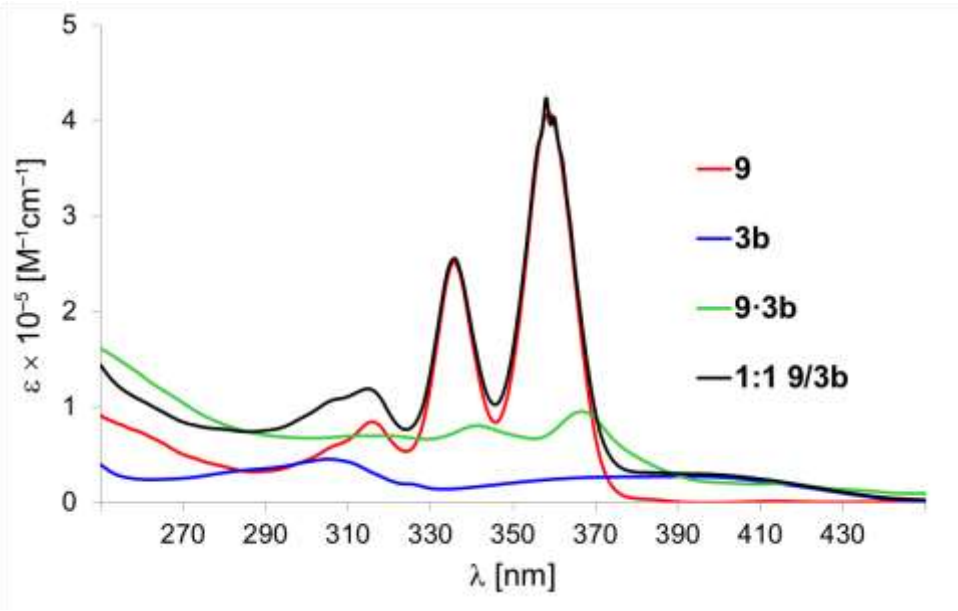

Figure B.4. UV-visible spectra of rotaxane **9·3b**, its macrocycle (**3b**) and axle (**9**) components, and 1:1 mixture thereof (in CH_2Cl_2).

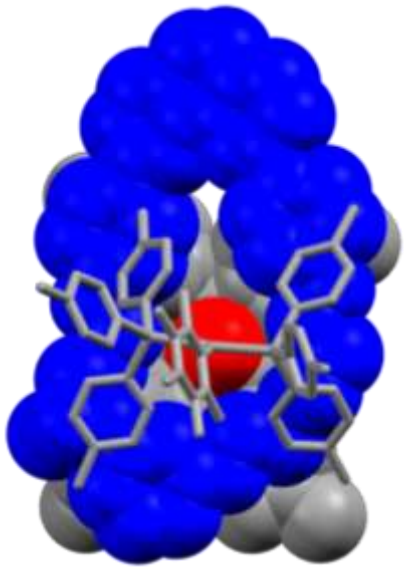

Figure B.5. End-on view of the molecular structure of **9·3a** illustrating the size of the axle endgroup (gray, space filling) behind the macrocycle (blue, space filling), with a wire frame representation of the opposite endgroup in front (red = dodecahexaynediyl moiety).

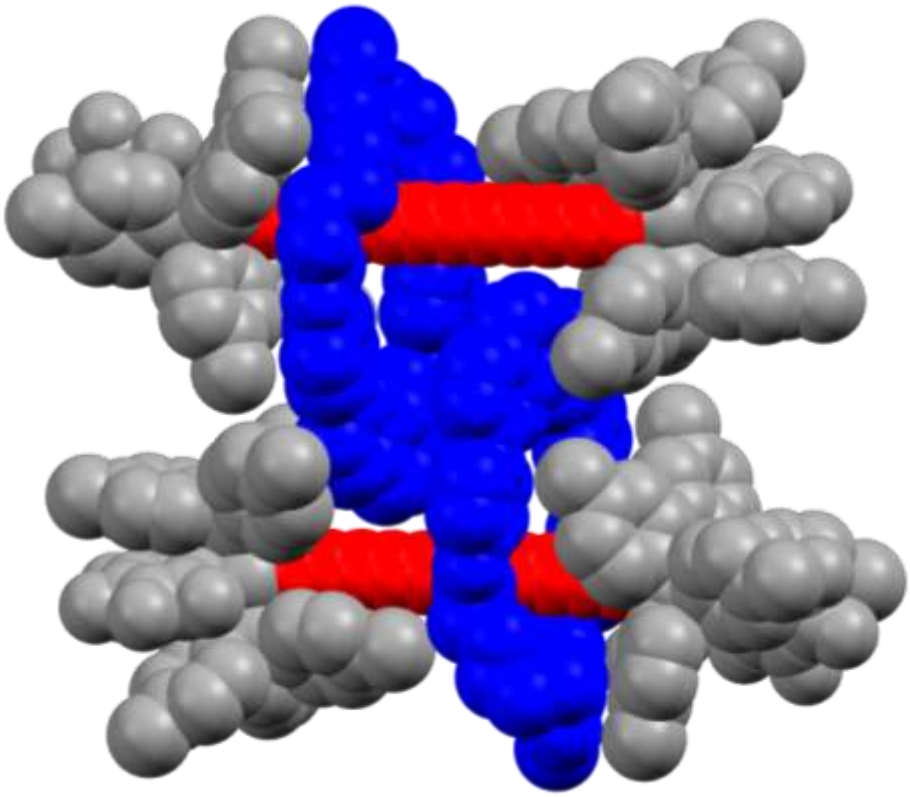

Figure B.6. The two molecules of **9·3a** in the unit cell (blue, macrocycles; grey, axle endgroups; red, dodecahexaynediyl moieties).

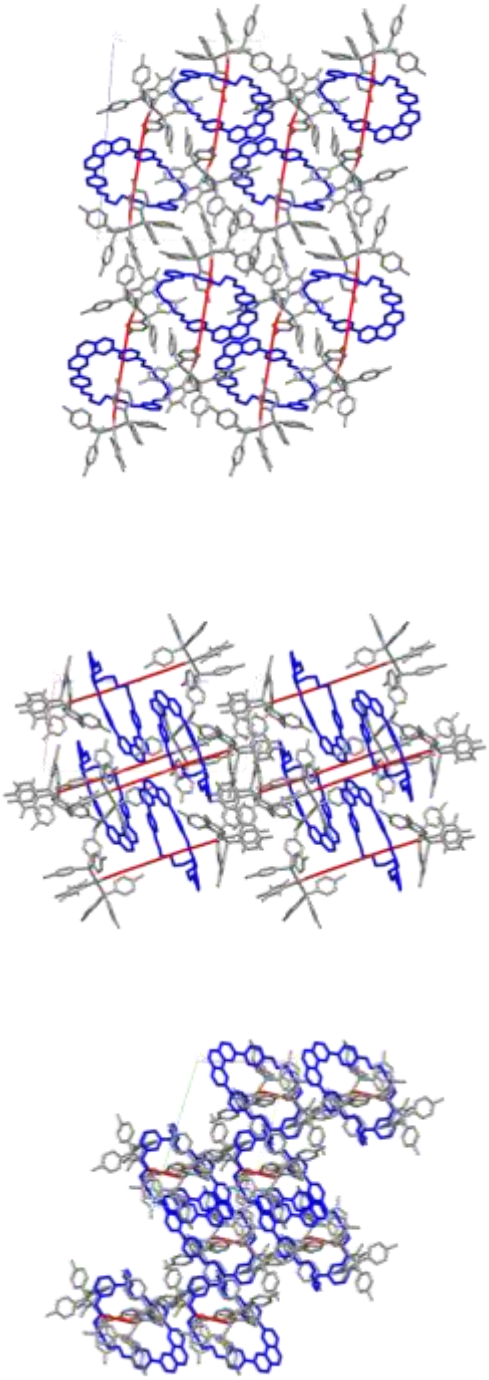

Figure B.7. Views of the packing of **9·3a** in four unit cells of the crystal lattice (blue, macrocycles; grey, axle endgroups; red, dodecahexaynediyl moieties).

B.2 References

(s9) Previous synthesis and characterization of **3** and **5**: Mohr, W.; Stahl, J.; Hampel, F.; Gladysz, J. A. *Chem. Eur. J.* **2003**, *9*, 3324-3340.

(s10) Some of the sp carbon signals were not observed. Assignments were made by analogy to related complexes.

(s11) This coupling represents a satellite (d, ^{195}Pt = 33.8%), and is not reflected in the peak multiplicity given.